

# **RESPONSE OF COUPLED FRICTIONAL CONTACTS TO CYCLIC LOADING**

by

Young Ju Ahn

A dissertation submitted in partial fulfillment  
of the requirements for the degree of  
Doctor of Philosophy  
(Mechanical Engineering)  
in The University of Michigan  
2009

Doctoral Committee:

Professor James R. Barber, Chair  
Professor Radoslaw L. Michalowski  
Professor Noel C. Perkins  
Professor Nicolas Triantafyllidis  
Professor Alan S. Wineman

© Young Ju Ahn  

---

All Rights Reserved  
2009

*To my both parents, wife, and two daughters*

## ACKNOWLEDGEMENTS

I wish to express my gratitude to Professor James R. Barber, the chairman of my doctoral committee and my advisor, for his guidance and insightful suggestions. I am also grateful to the members of my doctoral committee, Professor Radoslaw Michalowski, Professor Noel Perkins, Professor Nicolas Triantafyllidis, and Professor Alan Wineman, for their comments and suggestions. I am also grateful for the opportunity to work with Professor Galip A. Ulsoy.

The advice, knowledge, and experience of Dr. Donghee Lee, Dr. Ho Choi and Dr. Hyung-Ju Kim are gratefully acknowledged. I owe a debt of their sincere friendship to Jinuk Kim, Jeongseok Kim, Kwanghyun Park, Youngseok Oh, and Seunghwan Keum. I also thank Michael Wisenberg who has served as a communication partner.

Thanks to my family for their endless love and support. Especially thanks to my wife, Yang Hee Kim, and to my lovely two daughters, Se Eun and Kate Bomin Ahn for their patience and assistance

Finally, I wishes to thank the Electric Power National Scholarship Program of the Korean Ministry of Commerce, Industry and Energy (MOCIE) for financial support.

# TABLE OF CONTENTS

<b>DEDICATION</b> . . . . .	<b>ii</b>
<b>ACKNOWLEDGEMENTS</b> . . . . .	<b>iii</b>
<b>LIST OF FIGURES</b> . . . . .	<b>vii</b>
<b>CHAPTER</b>	
<b>I. Introduction</b> . . . . .	<b>1</b>
1.1 Motivation . . . . .	1
1.2 Analytical Method in Frictional Contact Problems . . . . .	2
1.2.1 Uncoupled Problems with Similar Materials . . . . .	6
1.2.2 Coupled Problems with Dissimilar Materials . . . . .	8
1.3 Frictional Response to Cyclic Loading: Shakedown, Cyclic Slip and Ratchetting . . . . .	10
1.4 Receding Contact . . . . .	15
1.5 Dissertation Overview . . . . .	18
<b>II. Time Evolution Solution Algorithm to Quasi-static Contact Problems with Friction</b> . . . . .	<b>20</b>
2.1 Introduction . . . . .	20
2.2 Problem Description . . . . .	21
2.3 The Coulomb Friction Law . . . . .	22
2.3.1 Solution Procedure . . . . .	23
2.3.2 Solution Algorithm . . . . .	24
<b>III. Response of Frictional Receding Contact Problems to Cyclic Loading</b>	<b>28</b>
3.1 Introduction . . . . .	28
3.1.1 Coulomb Friction . . . . .	29
3.1.2 Unloading . . . . .	29
3.2 Problem Description . . . . .	31
3.3 Results . . . . .	31
3.3.1 Unloading . . . . .	32

3.3.2	Oscillatory Loading . . . . .	34
3.4	Conclusions . . . . .	37
<b>IV. Shakedown of Coupled Two-dimensional Discrete Frictional Systems</b>		<b>40</b>
4.1	Introduction . . . . .	40
4.2	Critical Coefficient of Friction . . . . .	42
4.3	The Two-node System in Reaction Space . . . . .	43
4.3.1	Effect of Slip Displacement . . . . .	43
4.3.2	Wedging . . . . .	45
4.3.3	Existence of a Safe Shakedown State . . . . .	46
4.3.4	Safe shakedown state at the critical limit . . . . .	49
4.3.5	Numerical simulation result at the critical limit value . . . . .	53
4.4	The two-node system in $v_1, v_2$ space . . . . .	55
4.4.1	Admissible regions in $v_1, v_2$ space . . . . .	56
4.4.2	Wedging . . . . .	57
4.4.3	Transient evolution of the system . . . . .	59
4.4.4	Periodic loading . . . . .	61
4.4.5	Limiting values of the loading parameter $\lambda$ . . . . .	64
4.4.6	Separation . . . . .	65
4.5	Conclusions . . . . .	66
<b>V. Shakedown Bounds of Coupled Multi-Node Discrete Frictional Systems</b>		<b>67</b>
5.1	Introduction . . . . .	67
5.2	Procedure for Determining the Lower Bound ( $\lambda^{\min}$ ) . . . . .	67
5.3	Solution Method for Determining the Upper Bound ( $\lambda^{\max}$ ) . . . . .	72
5.3.1	A Two-node System . . . . .	76
5.3.2	Numerical Results . . . . .	76
5.4	Numerical Example for an $N$ -node System . . . . .	78
5.4.1	Problem Description . . . . .	78
5.4.2	Numerical Result . . . . .	78
5.5	Conclusions . . . . .	81
<b>VI. Discontinuities for Elastic Quasi-static Evolution Problem</b>		<b>83</b>
6.1	Introduction . . . . .	83
6.2	The two-node system . . . . .	84
6.2.1	Single node discontinuities in $v_1, v_2$ space . . . . .	84
6.2.2	Both node discontinuities in $v_1, v_2$ space . . . . .	85
6.3	Perturbation analysis involving viscous damping . . . . .	88
6.3.1	Both nodes separated at discontinuity point . . . . .	90
6.3.2	One node separated at discontinuity point . . . . .	90
6.4	Numerical example . . . . .	95

6.5	Conclusions . . . . .	99
<b>VII.</b>	<b>Conclusions and Future Work . . . . .</b>	<b>100</b>
7.1	Conclusions . . . . .	100
7.2	Future Work . . . . .	103
7.2.1	Final State Prediction in Multi-node system . . . . .	103
7.2.2	Uniqueness of the Limit Cycle . . . . .	103
<b>APPENDIX</b>	<b>. . . . .</b>	<b>105</b>
<b>BIBLIOGRAPHY</b>	<b>. . . . .</b>	<b>115</b>

## LIST OF FIGURES

### Figure

1.1	Coulomb’s friction law with the coefficient of friction, $f$ . $P$ and $Q$ represent the normal and tangential forces, respectively, and $\dot{v}$ is the velocity in the tangential direction. . . . .	3
1.2	Normal contact between two similar bodies . . . . .	4
1.3	Cattaneo and Mindlin’s problem . . . . .	5
1.4	Stress regimes for the uniaxial-stress model of a thin tube whose yield stress $\sigma_Y$ : $\sigma_P$ and $\sigma_T$ represent internal pressure stress and maximum value of elastic thermal stress. $R_1$ and $R_2$ show ratchetting, $S_1$ and $S_2$ show shakedown after the first half-cycle, $P$ shows plastic cycling, $E$ shows elastic behavior, respectively . . . . .	13
1.5	Two rectangular elastic blocks compressed by a normal force: (a) unloaded and (b) loaded configuration . . . . .	16
1.6	Pin in a circular hole compressed by a normal force, $P$ : (a) unloaded and (b) loaded configuration . . . . .	17
2.1	A rectangular elastic block pressed against a rigid plane surface. . . . .	21
2.2	Solution Algorithm . . . . .	26
3.1	A rectangular elastic block pressed against a rigid plane surface. . . . .	31
3.2	Normalized contact traction distributions during the initial loading. Numbers in parentheses refer to the four states defined in Section 2.3 . . . . .	32
3.3	Evolution of stick, slip and separation regions during unloading . . . . .	33
3.4	Normalized contact traction distributions during unloading . . . . .	34

3.5	Evolution of the stick, slip and separation regions during the ninth cycle of (a) unloading and (b) reloading . . . . .	36
3.6	Incremental slip $\Delta v_i$ per cycle at a representative node as a function of cycle number $N$ . . . . .	37
3.7	Evolution of the stick, slip and separation regions during (a) unloading and (b) reloading in the steady cyclic state. The dashed line in Fig. 3.7(a) indicates points which reach the limiting friction condition but which do not actually slip . . . . .	38
3.8	Evolution of the energy dissipated in friction per loading cycle as a proportion of that during the first cycle. . . . .	39
4.1	Reaction space . . . . .	44
4.2	Oscillating external load loops on the two nodal diagrams . . . . .	46
4.3	Moving the loop for node 1 into the position where it is tangential to both slip lines . . . . .	47
4.4	A safe shakedown state . . . . .	48
4.5	Configuration in which gets to a safe shakedown state . . . . .	49
4.6	Moving the loop at each node into the position where it is tangential to both slip lines . . . . .	50
4.7	Moving the loop for node 1 into the position where it is tangential to both slip lines . . . . .	51
4.8	Moving the loop for node 1 into the position where it is tangential to both slip lines . . . . .	52
4.9	A shakedown state at the maximum load factor, $\lambda^c$ . . . . .	53
4.10	The transient external load loops followed by the oscillating external load loops at both nodes . . . . .	55
4.11	Intersection of the admissible regions (values of $v_1, v_2$ ) that satisfy constraints I,II,III,IV. . . . .	57
4.12	Configurations of the constraints leading to an admissible region that is (a) a triangle or (b) a region open to infinity . . . . .	58

4.13	Motion of the instantaneous operating point $P$ due to the advance of constraints IV. . . . .	60
4.14	Cyclic slip limit cycle in the case where the safe shakedown region is triangular. . . . .	62
4.15	Progression of the operating point towards the safe shakedown region (SD) due to motion of constraints for two different nodes. . . . .	63
5.1	Configuration of extremal points in the given reaction loop consisting of $m$ discrete values at node $j$ . . . . .	70
5.2	Configurations of load loops on the two nodal reaction force diagrams. . . . .	73
5.3	Configurations of shakedown state on the two nodal reaction force diagrams. . . . .	74
5.4	Configurations of the constraints leading to a safe shakedown region that is at (a) $\lambda < \lambda^{\min}$ , (b) $\lambda = \lambda^{\min}$ , (c) $\lambda^{\min} < \lambda < \lambda^{\max}$ , and (d) $\lambda = \lambda^{\max}$ . . . . .	77
5.5	Configuration of a elastic block contacting on a rigid plane surface. . . . .	79
5.6	Configuration of the finite element mesh of a contact surface. . . . .	79
5.7	Configuration of reaction forces at (a) node 1 and (b) node 9 due to the time-varying external loading $p(t)$ : two dots denote maximum and minimum extreme points, respectively. . . . .	80
5.8	Slip displacement distributions along the contact surface during the 10 <sup>th</sup> loading cycle at the upper shakedown limit ( $\lambda = \lambda^{\max}$ ): (a) the safe shakedown vector $\mathbf{v}$ is used as initial conditions and (b) arbitrary initial conditions except $\mathbf{v}$ are used. . . . .	82
6.1	Motion of the instantaneous operating point $P$ due to the advance of constraints I. . . . .	85
6.2	Configurations of the constraints leading to an admissible region that is a region open to infinity. . . . .	86
6.3	Four possible pairs in both node discontinuity. . . . .	87
6.4	Configuration for two-node discontinuity in the pair II and III. . . . .	96

6.5	The admissible regions for $a_1$ and $a_2$ that satisfy initial conditions. . . .	98
A.1	The one-point model . . . . .	106
A.2	The $F_1 - F_2$ diagram . . . . .	108
A.3	Loading scenario leading to forward slip . . . . .	109
A.4	Loading scenario leading to shakedown . . . . .	110
A.5	$F_1 - F_2$ diagram for $f > f_{cr}$ . . . . .	111
A.6	Separation-stick cycle . . . . .	113
A.7	Cyclic slip scenario . . . . .	114

# CHAPTER I

## Introduction

### 1.1 Motivation

Frictional contact problems arise in many applications of mechanical or civil engineering. These are often subjected to a substantial mean load and a superposed oscillatory load with a small amplitude. For example, the contact interface between a turbine blade and the blade disk in an aero engine is subjected to a large constant load due to centrifugal action, but also experiences time-varying cyclic load due to vibration and turbulence in the gas flow (Murthy *et al.* 2004). Other similar situations are found in many different areas: for example, bolted joints in machine tools (Bercyński and Gutowski 2006, Law *et al.* 2006), engine conrod bush systems in the automotive industry (Antoni *et al.* 2007), and the contact of bodies with rough surfaces (Bureau *et al.* 2003, Walsh 2003), interactions of granular material and soils (Zhang and Makse 2005, Holt *et al.* 2005, Leurser and Dvorkin 2006), and so on.

Under those cyclic loads, the interface of components experiences periodic reversed relative motion and might fail (Lovrich and Neu 2006, Nowell *et al.* 2006). However, the frictional slip that occurs during the first few cycles might set up a state of residual stress that inhibits or reduces slip in subsequent cycles. Therefore, it is worthwhile to predict what loading conditions will make a system experience those different long term

behaviors.

In order to explore these challenging questions, we will restrict attention to the simplest case where the bodies are two-dimensional and sliding occurs within the plane.

## 1.2 Analytical Method in Frictional Contact Problems

We will review the state of the art in analytical solutions of contact mechanics with special attention to local friction phenomena. In general, contact problems can be categorized into those without friction and those with friction at the contact interfaces, and these are also subdivided into *static* or *quasi-static problems* and *dynamic problems*. Assuming that the applied forces vary slowly with time, quasi-static problems are those in which the inertia effects are negligible, whereas dynamic problems are those in which the inertia effect plays an important role. The inertia is generally important only when the loading time scale (e.g. the period of cyclic loading) is comparable with the time it takes for an elastic wave to traverse the body.

At first, we will analyze the tractions induced in frictional contact and their influence on the contact normal distribution. As a simple model of friction, *Coulomb's law* (Coulomb, 1785), which applies to sliding contact of two rigid bodies, is widely used. It defines the state of *stick* or *slip* depending on the following relationship between the applied tangential force,  $Q$ , and the normal force,  $P$ ,

$$\begin{aligned} \textit{stick} & : |Q| < fP ; & \dot{v} = 0 \\ \textit{slip} & : Q = \begin{cases} -fP ; & \dot{v} > 0 \\ +fP ; & \dot{v} < 0 \end{cases} \end{aligned} \tag{1.1}$$

where  $\dot{v}$  is the velocity in the tangential direction, and  $f$  is the coefficient of friction, respectively.

Fig. 1.1(a) shows the relationship between the reaction force and the velocity in the

tangential direction. Since the tangential reaction force  $Q$  acts in the opposite direction to that of the slip direction, the *forward* ( $\dot{v} > 0$ ) and *backward* ( $\dot{v} < 0$ ) slip make the tangential reaction force negative and positive, respectively, as shown in Eq. (1.1). If a single rigid body makes contact with a rigid support governed by Coulomb's law, as shown in Fig. 1.1(b), *sliding* will occur only if the tangential friction force,  $Q$ , reach the limiting value,  $fP$ . Otherwise, the body remains in a state of *stick* with no relative tangential motion.

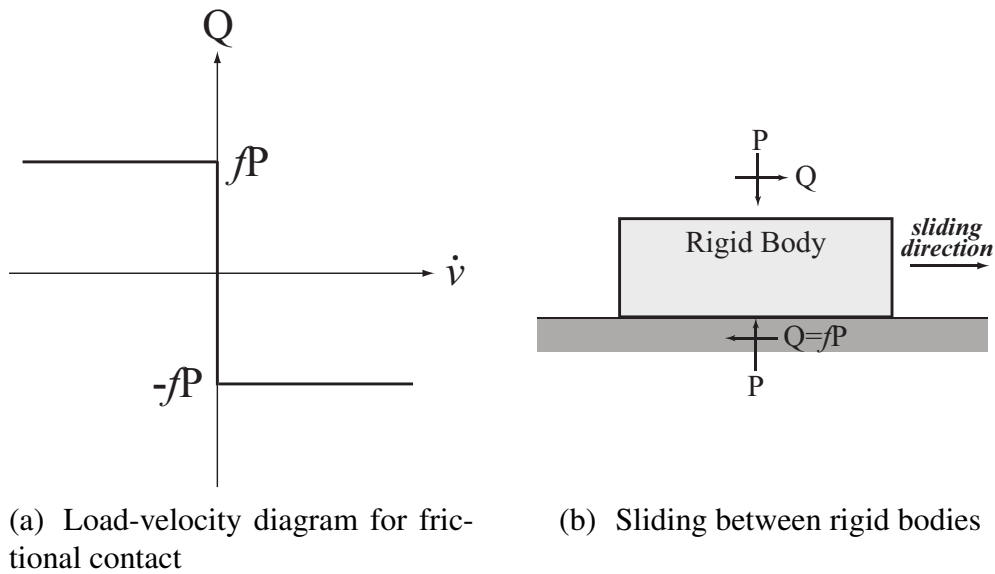


Figure 1.1: Coulomb's friction law with the coefficient of friction,  $f$ .  $P$  and  $Q$  represent the normal and tangential forces, respectively, and  $\dot{v}$  is the velocity in the tangential direction.

Now, we will apply Coulomb's law to the analysis of frictional elastic contacts. Suppose that two elastically similar bodies are pressed together with their axis parallel, as shown in Fig. 1.2. As pressure is applied, deformation must occur so that a mutual contact pressure develops and the surfaces' points are compressed. However, because system is symmetry, the normal tractions do not produce relative tangential displacements, and there is no tendency for the bodies to slip. This means that no frictional tangential tractions arise, and the solution to the problem, which is known as the Hertz solution (Hertz, 1882), is the

same whether the surfaces have friction or are well lubricated, i.e. no friction.

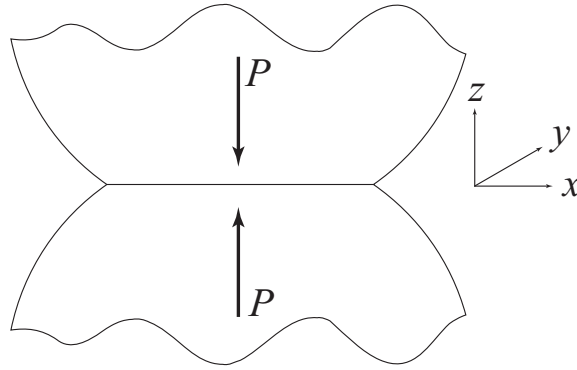


Figure 1.2: Normal contact between two similar bodies

If now a tangential force sufficient to cause *gross sliding* is applied (i.e.  $Q = fP$ ), shear tractions that are everywhere limited by the coefficient of friction,  $f$ , arise, i.e.,

$$|q(x, y)| = fp(x, y), \quad (1.2)$$

where the shear and normal tractions,  $q(x)$  and  $p(x)$ , are functions of the contact point  $x$  and  $y$ , and the normal traction is positive if compressive. The presence of the shearing tractions will cause a normal displacement of the contacting surfaces. However, since the shear tractions act in opposite directions over the surface of the two bodies, surface contact points will move in the normal direction by the same amount so that the contact pressure distribution remains unchanged.

We now apply a shearing force that is less than the limiting value (i.e.  $Q < fP$ ). In this case, the contact area consists of a mixture of stick and slip zones, as shown in Fig. 1.3(a). Such a contact is said to be in a state of *micro-slip* since the slip amount in the slip zones is limited because of the elastic strains of the body at the interface. Within the slip zones, Eq. (1.2) still applies, whereas the shearing traction of the stick zones must be less than the limiting values, i.e.,

$$|q(x, y)| < fp(x, y). \quad (1.3)$$

It will be noted that the shearing tractions on each body are equal in magnitude but opposite in direction, so that the normal surface displacements induced in each body are the same. Hence, the effects of normal and shear tractions are entirely independent and may be analyzed separately.

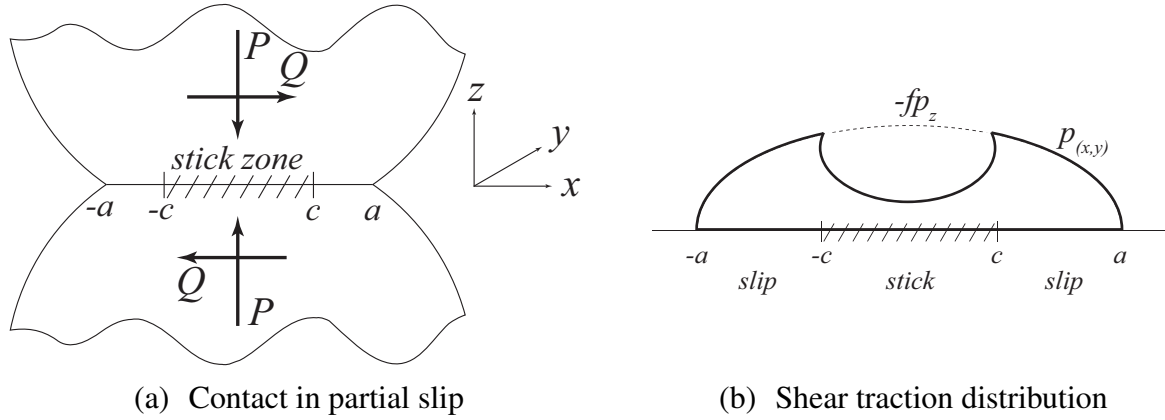


Figure 1.3: Cattaneo and Mindlin's problem

This type of contact problem is referred to as an '*uncoupled contact problem*'. If the contact problem is uncoupled, Dundurs' constant (Dundurs, 1969)

$$\beta = \frac{\left(\frac{1-2\nu_1}{\mu_1} - \frac{1-2\nu_2}{\mu_2}\right)}{2\left(\frac{1-\nu_1}{\mu_1} + \frac{1-\nu_2}{\mu_2}\right)}, \quad (1.4)$$

is zero, where  $\mu_i, \nu_i, i = 1, 2$  are the modulus of rigidity and Poisson's ratio, respectively, for the two materials. The following four cases satisfy the uncoupled condition (Barber, 2002, §12.7);

- (i) The contact is frictionless.
- (ii) The materials are similar ( $\nu_1 = \nu_2, \mu_1 = \mu_2$ ).
- (iii) Both materials are incompressible ( $\nu_1 = \nu_2 = 0.5, \mu_1 \neq \mu_2$ ).
- (iv) One body is rigid ( $\mu_2 \rightarrow \infty$ ) and the other is incompressible ( $\nu_1 = 0.5$ ).

### 1.2.1 Uncoupled Problems with Similar Materials

Here, we will confine our attention to contacts between elastically similar materials. In this case, Dundurs's constant in Eq. 1.4 will be zero.

Let us consider that two elastically similar cylinders are pressed together by a normal force ( $P$ ) and then subjected to a monotonically increasing tangential force ( $Q$ ), as shown in Fig. 1.3. Further, a tangential force is less than the limiting frictional value ( $Q < fP$ ). Such a contact problem was first solved by Cattaneo (1938) and later independently by Mindlin (1949). They showed that slip would occur in an elliptical annulus to the edge of contact area and that the resulting frictional traction distribution would be the difference between the traction distribution at limiting friction and an opposing self-similar distribution in the central ellipse.

Mindlin and Deresiewicz (1953) extended Mindlin's analysis to the more general situation of spherical surfaces subjected to an oscillating force that acts obliquely at an arbitrary angle  $\alpha$  to the normal. They showed that due to the presence of slip and its associated energy dissipation, the changes in tractions and displacements depend on the entire past history of loading and the instantaneous relative rates of change of the normal and tangential forces as well as the initial state of loading.

Micro-slip under oscillatory tangential forces have been experimentally observed by many researchers. Mindlin *et al.* (1952), Johnson (1955), and Courtney-Pratt and Eisner (1957) measured the tangential micro-slip amount that occurs in friction experiments using metallic surfaces, and their results supported the validity of Mindlin's theory. Johnson (1961) also experimentally investigated Mindlin and Deresiewicz's results with the contact between a hard steel sphere and a plane that is subjected to compressive normal force and superposed oscillating oblique force at an arbitrary angle  $\alpha$  to the normal. He showed that slip does not occur if the line of action of the oscillating force lies within the

friction cone, and at greater angles of obliquity, oscillating slip takes place in an annular region at the edge of the contact circle with a consequent dissipation of energy. The energy dissipation and resulting surface damage increase rapidly with the angle of obliquity, reaching a maximum when the force is purely tangential.

As shown in Johnson's experimental observation, oscillating micro-slip at the localized interface of two surfaces produces the surface damage referred to as *fretting*, which can lead to *fretting failure* of the components by fatigue. These are closely associated with the loading history of the applied normal and tangential forces, as shown by Cattaneo (1938), Mindlin and Deresiewicz (1953). The effect of loading history was also examined by Dundurs and Comninou in a series of educational problems ( Dundurs and Comninou 1981, 1983, Comninou and Dundurs 1982). Their conclusions showed that incremental problems in which the normal( $P$ ) and tangential( $Q$ ) forces are increased (or decreased) by small increments  $\Delta P$  and  $\Delta Q$ , will involve the state of stick throughout the instantaneous contact area as long as

$$|\Delta Q| < f\Delta P \quad (1.5)$$

where  $f$  is the coefficient of friction. If the force is truly static, it is not possible to distinguish the existence of slip from that of stick with limiting frictions since the shear tractions are the same and no slip takes place until the load is increased or decreased.

In fretting contact, the tangential loading is cycled between limits. Hills *et al.* (1993, §4.3) considered the development of shear tractions and stick zone during cyclic tangential loading for similar materials. They show that even when the load has been completely removed after reaching the maximum limit of the tangential loading, self-equilibrating shear tractions still persist at the interface. This illustrates that the traction distribution depends on the history of loading. Thus, we cannot necessarily exploit superposition in determining the stress state.

A significant generalization of Cattaneo and Mindlin's problem was discovered independently by Jäger (1997) and Ciavarella (1998). They showed that contact problems can be analyzed as one of two normal indentation cases, specifically the actual normal contact problem, and a corrective normal contact problem for a reduced load that provides the shear correction in the stick zone. Thus, as the tangential force is increased at constant normal force, the stick zone shrinks, passing monotonically through the same sequence of areas as the normal contact area passed through during the normal loading process. These results can be used to predict the size of the slip zone in conditions of fretting fatigue (Hills and Nowell, 1994; Szolwinski and Farris, 1996). Jäger and Ciavarella's theorem was extended to the wear process in fretting of plane contact that is subjected to oscillating tangential forces (Ciavarella and Hills, 1999). They showed that the wear operates only in the region of initial micro-slip, and that wear must always proceed so as to give a steady state of full adhesion.

### **1.2.2 Coupled Problems with Dissimilar Materials**

When the contacting bodies are elastically dissimilar (if  $\beta \neq 0$  in Eq. 1.4) and subjected only to a purely normal loading, it is possible to generate shear tractions because of different tangential displacements at the interface. Therefore, the problem is fully coupled in the sense that a normal force induces relative tangential displacement in addition to relative normal displacement. Correspondingly, an applied tangential force will produce relative displacements in both tangential and normal directions. Hence, the surface pressure distribution will differ from the corresponding elastically similar contact. However, for practical material combinations and realistic coefficients of friction, the difference in pressure distribution is likely to be very small.

This type of problem was first studied by Goodman (1962) for the normally loaded fric-

tional contact of two rough spheres. In his analysis, he assumed complete adhesion and neglected the influence of the tangential traction on the Hertz distribution of normal pressure. The complete solution to this problem was found incrementally by Mossakovskii (1963) and Spence (1968, 1973). Spence's solution concentrates on a rigid, flat-ended punch, and uses an iterative scheme to develop the coupled solution. He showed that the indentation of an elastic half-space by a power law punch with Coulomb friction is *self-similar* and hence that the extent of the central adhesion zone maintains a constant ratio to the extent of the contact area.

Furthermore, Spence (1975) also investigated the normally loaded contact problem for the loading and subsequent unloading of a rigid flat cylindrical punch indenting an elastic half space. The solution showed that the center of the stick region is surrounded by an annulus of slip and that the radius of the stick region is the same for all bodies whose profiles are of polynomial form, including a flat-ended rigid punch. Once the radius is specified, the frictional traction and the normal pressure can be evaluated numerically. For the unloading procedure after monotonic loading, his solution also showed that slip must take place at the edge of the contact circle in the direction opposite to that during the loading. Thus, it showed that the state of contact stress depends on the history of the applied loading.

Turner (1979) derived a variation formulation for the problem of contact between a rigid cylindrical indenter and elastic half-space. Using the variational formulation, numerical solutions are obtained to the problems of frictionless contact, adhesive contact, and frictional loading, for which there are known analytical solutions, as well as to the frictional unloading problem, for which there is no previous known solution, and then comparisons are made with experimental data and predictions from physical considerations

Tangential loading of dissimilar elastic bodies has been considered by several investigators. Spence (1986) considered the two-dimensional contact problem of a monotonically loaded indenter under an inclined load that produced both normal and shear components. Keer *et al.* (1984) had investigated three-dimensional monotonic normal and tangential loading of dissimilar bodies. Keer and Farris (1987) considered the two-dimensional contact problem of a cyclically loaded indenter on an elastic half plane, including the interaction of the normal and shear stress. However, the indenter was of non-uniform profile, so it is not readily possible to quantify the effect of elastic dissimilarity on the stress distributions and locations of micro-slip. Their analysis was extended by Hanson *et al.* (1989) in order to model an actual fretting fatigue experimental situation and to estimate the energy dissipation under cyclic tangential loading. Nowell *et al.* (1988) investigated normal and cyclic tangential loading of dissimilar elastic cylinders. They accounted for full interaction in analyzing normal and subsequent monotonic tangential loading. The corresponding axisymmetric problem was treated by Munisamy *et al.* (1994).

### **1.3 Frictional Response to Cyclic Loading: Shakedown, Cyclic Slip and Ratchetting**

The response of elastic bodies in frictional contact has many similarities with that of bodies governed by an elastic-plastic constitutive law. For example, as applied loads increase, both systems show elastic response until the loads reach critical limiting values. Once the loads reach the limiting values, frictional slip or plastic deformation (yield) occurs and the amount of slip (or plastic strain) can be indefinite without increase in stress. And also both processes involve energy dissipation and show history dependence of the applied loads.

Furthermore, both systems also show similar long-term behaviors to cyclic loading: assuming that elastic-plastic bodies are subjected to cyclic loading, they show *incremental collapse (ratcheting)*, in which large permanent strains are acquired through the accumulation of small increments occurring with each cycle of repeated loading; *cyclic plasticity*, in which the plastic strains show the same pattern after many cycles as after the first cycle with no net accumulation of plastic deformation; or *plastic shakedown*, in which the plastic strains show only for the first few cycles and then perfectly elastic response shows as a result of the residual stresses.

Similarly, assuming that elastic bodies with frictional interfaces are subjected to a cyclic loading, the long-term behavior of the frictional system might lead to the following corresponding physical phenomena known as *ratcheting*, *cyclic slip* or *frictional shakedown*. Ratcheting occurs when a micro-slip shows in a different contact area for each loading cycle and accumulates over all of the cycles, eventually showing a rigid body motion and repeating the previous cycle. Cyclic slip occurs when a micro-slip shows repeated, identical patterns between two limit values for every loading cycle with no net slip accumulation. Shakedown occurs when a micro-slip shows at the interface only for the first few loading cycles, and then stick conditions apply throughout the contact area as a result of beneficial residual stresses that prevent further slips.

These corresponding behaviors lead to the possibility that some of the results arising in plasticity theory might be applied to friction problems, especially when a contact undergoes cyclic loading. From the practical point of view, one way to prevent fretting fatigue, which is closely associated with steady state slip, is to increase the normal contact pressure, but another is to encourage slip to occur during the first few cycles of loading, so that the system will shake down without further slip. Merwin and Johnson (1963) investigated the similar problem of shakedown due to subsurface plastic deformation in a half

plane subjected to surface loads. Comninou and Barber (1983) established the shakedown limit for the frictional problem of an elastic layer pressed against an elastic half-plane and subjected to a tangential force varying periodically in time. Their solution showed no slip, slip in first cycle only, or slip in steady state, depending on the ratio between tangential force and normal force.

Bree (1967) considered elastic-plastic behavior of thin tubes in the design of nuclear reactor fuel elements, which are subjected to internal gas pressure and intermittent high-heat fluxes. He showed that the plastic strains produced may cause ratchetting or plastic cycling as the temperature gradients occur across the tube wall cycles because of start-up or shutdown of the reactor. Fig. 1.4, known as the *Bree diagram*, depicts the strain behavior depending on the stress regimes at a point consisting of  $\sigma_P$  (internal pressure stress) and  $\sigma_T$  (maximum value of elastic thermal stress). Similar behavior is observed in the frictional problem. For example, Churchman *et al.* (2006) recently explored this question in more detail in the context of a simple two-node discrete elastic system. They identified loading regimes in which the long term behavior includes shakedown, cyclic slip, and frictional ratchetting, and presented these in the form of the Bree diagram.

Furthermore, several authors (Saez *et al.* 2003; Churchman *et al.* 2006) investigated whether *Melan's theorem* (1936) for classical plasticity might apply to a frictional contact problem in order to predict whether shakedown occurs. The classic Melan's theorem is the shakedown theorem in plasticity, and it states that "if any time-independent distribution of residual stresses can be found which, together with the elastic stresses due to the load, constitute a system of stresses within the elastic limit, then the system will shake down." The corresponding frictional equivalent of Melan's theorem might be stated in the following way: "if a state of residual stress associated with frictional slip that would be sufficient to inhibit further slip can be identified throughout a periodic loading cycle, then

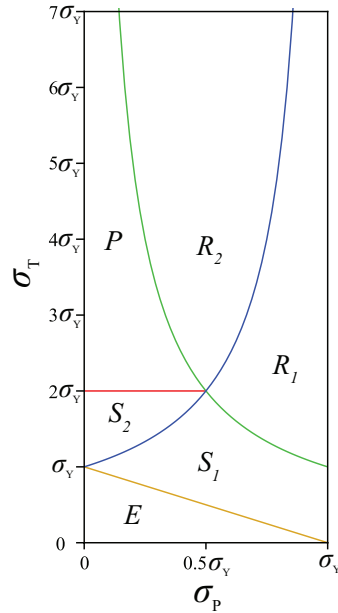


Figure 1.4: Stress regimes for the uniaxial-stress model of a thin tube whose yield stress  $\sigma_Y$ :  $\sigma_P$  and  $\sigma_T$  represent internal pressure stress and maximum value of elastic thermal stress.  $R_1$  and  $R_2$  show ratchetting,  $S_1$  and  $S_2$  show shakedown after the first half-cycle,  $P$  shows plastic cycling,  $E$  shows elastic behavior, respectively

the system will in fact shake down”.

However, the proof of Melan in plasticity depends on associativity; hence the proof cannot be applied to frictional systems. This is due to the *non-associative* character of the friction law, which says that the slip will occur in the direction of a tangent of the contact surface and not in the normal direction to the slip surface. In contrast, the shakedown theorem in plasticity requires the flow rule to be *associative*, in which plastic strain should occur in the direction of the outward normal of the yield surface. Therefore, there is no reason to expect Melan’s theorem to apply to a general coupled system.

Björkman and Klarbring (1987) constructed the solution of a linear programming method that determined the upper bound to the shakedown limit. It is similar to that given by Maier (1969), whose theorem allows the upper and lower limit to the shakedown

for a non-associated elastic-plastic material. However, their results in frictional systems showed considerably higher values than those obtained from direct quasi-static solutions, so Melan's theorem cannot be valid. Nonetheless, in many example problems (Fredriksson and Rydholm 1981, Churchman *et al.*, 2006; Antoni *et al.* 2007) that have been solved incrementally, it has been found that the actual limiting load for shakedown appears to obey Melan's theorem. Fredriksson and Rydholm argued that if the normal traction at the interface is constant and prescribed, the flow rule essentially becomes associative in the sense that its dependence of flow on pressure merely alters the effective yield criterion and the permitted slip within the plane does satisfy the condition that it must align with the direction of maximum tangential traction. This requires both that there be no coupling between tangential displacements and normal tractions and that the periodic component of the applied load does not generate a corresponding variation in normal traction. The conditions specified above are also met in the simple example model given by Churchman *et al.* (2006). In this model, the normal force remains constant, as in a fretting fatigue experiment, and hence the slip displacements retain associativity with respect to the time-varying reactions, thus meeting the conditions for Melan's theorem to apply. Similar considerations apply to the 'Tresca' friction law used by Antoni *et al.* (2007) in their study of ratchetting of a bushing in a connecting rod end. Furthermore, a frictional Melan's theorem has been established for both discrete (Klabring *et al.*, 2007) and continuous (Barber *et al.*, 2008) systems, which can explain why Melan's theorem holds for the above cases. Klabring *et al.* (2007) established definitive rules for the conditions that must be met by a discrete frictional system subjected only to the restriction that the contact be complete. They proved that shakedown is possible only (i) for systems with no coupling between relative tangential displacements at the interface and the corresponding normal contact tractions and (ii) for certain two-dimensional problems in which the friction coefficient at

each node is less than a certain critical value.

Even though Klabring *et. al* (2007) showed how counter-examples can be constructed for all systems coupling, such systems may experience either shakedown or cyclic slip depending on the initial loading conditions. Therefore, there is still a possibility that a reduced form of Melan's theorem might apply to such systems under suitable restrictions on the loading history.

Before introducing a more general system, it is instructive to consider the simple two-dimensional one-point model contact problem described in Appendix A. Chapter 4 and 5 present a developed form of the theorem and a proof of its validity for a coupled system.

## 1.4 Receding Contact

Problems involving the contact of two separate bodies pressed against each other have been widely studied. Although in the majority of cases the contact area increases after the application of the load, there are others where the final contact area is smaller than the original. For example, Fig. 1.5(a) shows a thin, flat elastic block resting on an extended substrate and a normal force applied at the center. If the block is sufficiently long compared with its height, separation occurs near the outer edges of the nominal contact area as shown in Fig. 1.5(b). This result was first predicted by Filon (1903), based on the fact that a single rectangular block loaded by two equal and opposite forces would experience a tensile stress near the edges. Later Coker and Filon (1957) showed by photoelastic studies that the contact semi-width is approximately 1.35 times the block thickness.

Problems of this class, in which the contact area  $\Gamma_C$  under load is included within the contact area  $\Gamma_0$  in the unloaded state ( $\Gamma_C \in \Gamma_0$ ) were described as *receding contact problems* by Dundurs and Stippes (1970). The concept is further explored in Tsai *et al.* (1974) and Dundurs (1975).

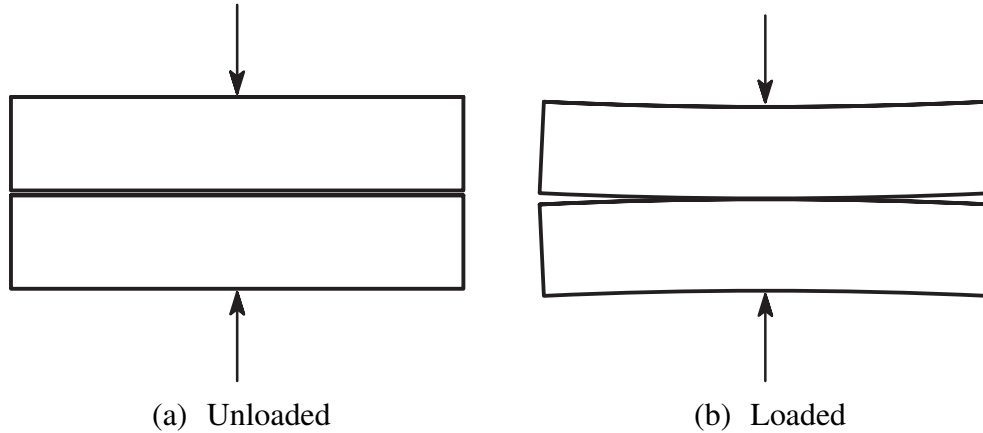


Figure 1.5: Two rectangular elastic blocks compressed by a normal force: (a) unloaded and (b) loaded configuration

The receding contact has been analytically studied by many researchers. Keer *et al.* (1972) investigated the smooth receding contact problem between an elastic layer and a half-space under the assumption of plane stress, plane strain and axisymmetric conditions. Gladwell (1976) solved the same problem by treating the layer as a simple beam in bending. Ratwani and Erdogan (1973) considered the plane smooth contact problem for an elastic layer lying on an elastic half-space with an applied compressive load through a frictionless rigid stamp. Civelek and Erdogan (1974) investigated the general axisymmetric double frictionless contact problem for an elastic layer pressed against a half-space by an elastic stamp under the assumption that the three materials have different elastic properties. Gecit (1986) studied the frictionless contact problem of a semi-infinite cylinder compressed against a half-space. Birinch and Erdol (2001) solved the frictionless contact problem between a flat-ended or rounded rigid stamp and two elastic layers. Comez *et al.* (2004) investigated the plane double receding frictionless contact problem for a loaded rigid stamp in contact with two different elastic layers. El-Borgi *et al.* (2006) considered the plane problem of a frictionless receding contact between an elastic functionally graded layer and a homogeneous half-space, when the two bodies are pressed together.

Kahya (2007) investigated a frictionless receding contact problem between an anisotropic elastic layer and an anisotropic elastic half plane, when the two bodies are pressed together by means of a rigid circular stamp.

The numerical studies on this type of contact problems were based either on the finite element method (Chan and Tuba, 1971; Jing and Liao, 1990; Kauzlarich and Greenwood, 2001) or on the boundary element method (Garrido *et al.*, 1994; Paris *et al.*, 1995; Garrido and Lorenzana, 1998).

Further, receding contact problems necessarily fall into the category of *conforming* contacts in which the initial area of contact is a significant over an appreciable area of the contacting bodies, since an extended contact area  $\Gamma_C$  must exist if a load is to be transmitted and hence  $\Gamma_0$  must also be extended *a fortiori*. For example, a frictionless perfectly fitting pin in a hole will initially touch around the whole of its circumference, but when it is loaded perpendicular to its axis, a gap will appear between the pin and the hole on the unloaded side, as shown in Fig. 1.6.

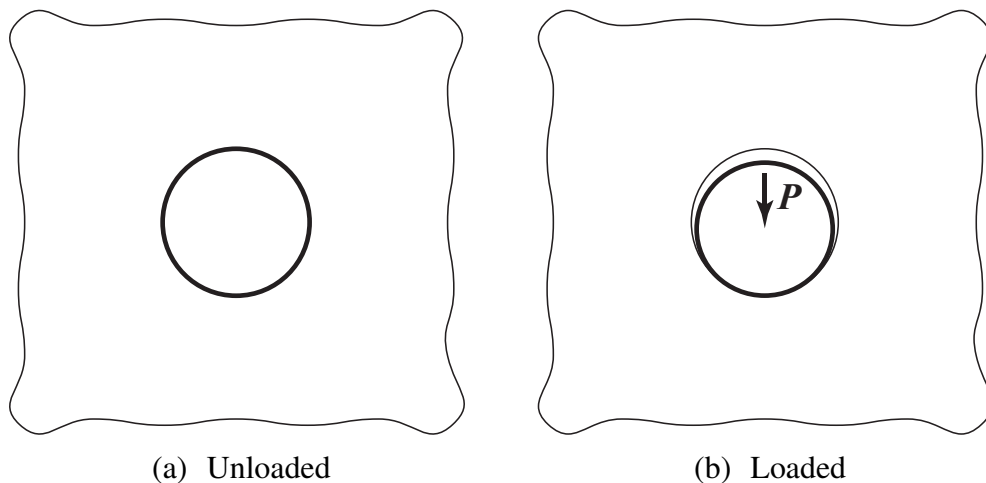


Figure 1.6: Pin in a circular hole compressed by a normal force,  $P$  : (a) unloaded and (b) loaded configuration

This problem was solved by Persson (1964), Goodman and Keer (1965), and Mostofi and Gohar (1980). Persson solved the case where the materials of the pin and matrix are

identical and the results are described by Johnson (1985). This analysis was extended to the case of dissimilar elastic materials by Ciavarella and Decuzzi (2001).

The influence of interfacial friction on the contact between a pin and an almost conforming hole is considered by Hou and Hills (2002). They proposed a numerically efficient method for handling the problem, and the solution showed the presence of regions of micro-slip. Ciavarella et al. (2006) demonstrated that similar results obtained by Dundurs and Stippes (1970) in frictionless contact, apply in the presence of Coulomb friction, in which case the extent of the stick and slip zones and the local direction of sliding are independent of load as long as the loading is monotonic in time.

In Chapter 3, we will look at the response of a receding contact problem that is subjected to a combination of mean and oscillating loads, and examine whether the slip zones remain unchanged throughout the loading and unloading phases.

## 1.5 Dissertation Overview

**Chapter II** devises a time incremental algorithm to study a frictional contact problem subjected to cyclic loading. Using the algorithm, a series of simulations is performed to investigate the influence of friction coefficients and external loading magnitudes on the steady state of the frictional system.

**Chapter III** investigates the response of a receding contact problem to a combination of mean and oscillating loads with the incremental program. We will verify that the slip and separation zones remain unchanged throughout the first loading phase, but thereafter all the zone boundaries vary during both loading and unloading periods.

**Chapter IV** deals with situations in which periodic loading scenarios can be devised that lead to either shakedown or cyclic slip for coupled systems. We will consider this question in the context of a simple two-dimensional coupled discrete system comprising

two contact nodes.

**Chapter V** describes an automated procedure for determining the lower shakedown limit for a multi-node contact system. Further, we propose an optimization method that defines the upper shakedown limit above which the system cannot shake down.

**Chapter VI** develops an analytical method to predict friction-induced instability in the context of a simple two-dimensional coupled discrete system comprising two contact nodes. In particular, we will determine that there is a unique solution and demonstrate how to find it without using a transient dynamic approach.

**Chapter VII** reviews the findings and contributions of this dissertation and proposes future research topics.

## CHAPTER II

# Time Evolution Solution Algorithm to Quasi-static Contact Problems with Friction

### 2.1 Introduction

If an elastic system is subjected to external loads that vary slowly in comparison with the period of the lowest natural frequency, it is usually possible to predict its behavior using a quasi-static analysis in which the mass of the system is neglected and the structure is assumed to pass through a sequence of equilibrium states. However, if friction exists at the contact interface, Coulomb friction law must also be considered. Furthermore, if the system with the frictional interface experiences time-varying cyclic loads which tend to produce micro-slip in some contact areas but not all of the contact interface, it is very important to identify the behavior of the contact interface since erosion of the surface and a failure known as fretting fatigue are closely related to it. Therefore, we need to develop a numerical algorithm capable of tracking the behavior of a system with frictional interfaces

For this purpose, we will develop an algorithm to solve the quasi-static contact problem subjected to oscillating external load. First, to address the time-evolution program, we will model an elastic rectangle contacting a rigid support in ABAQUS, and then extract the stiffness matrix coupling tangential slip displacements to normal contact forces in ABAQUS. Second, we will develop a separate numerical algorithm for Coulomb's friction

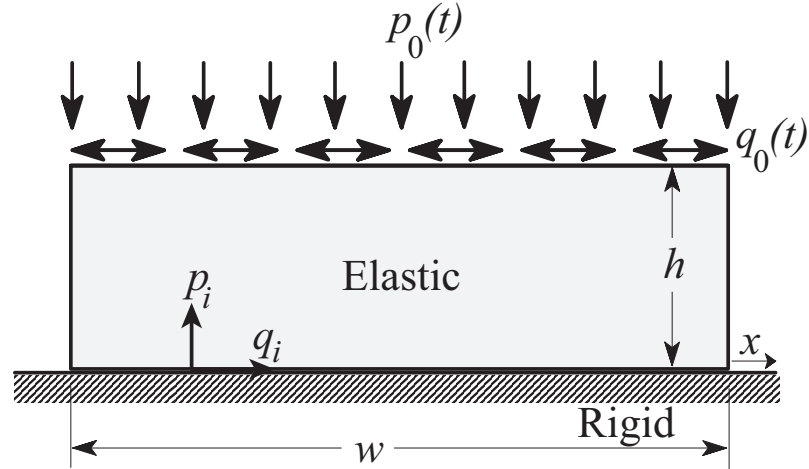


Figure 2.1: A rectangular elastic block pressed against a rigid plane surface.

problem using iteration and inequalities.

## 2.2 Problem Description

We shall consider the two-dimensional problem illustrated in Fig. 2.1, in which a rectangular elastic body of height  $h$  and width  $w$  is pressed against a rigid plane surface by time-varying loadings,  $p_0(t)$  and  $q_0(t)$ , exerted over the upper surface.

Coulomb friction boundary conditions are assumed at the interface between the block and the plane with friction coefficient,  $f$ . We assume that the loading is sufficiently slow for the quasi-static analysis to be appropriate, in which case time,  $t$ , appears only as an evolutionary parameter describing the sequence of the loading.

The deformation of the block is analyzed by the finite element method and in particular the contact surface is defined by a set of  $N$  nodes,  $i = 1, 2, \dots, N$ . The normal and tangential nodal reaction forces acting on the block will be denoted by

$$\mathbf{r}_i = [q_i, p_i]^T \quad (2.1)$$

where,  $q_i, p_i$  are respectively the tangential and normal reactions at node  $i$  and we adopt

the convention that compressive normal reactions are positive and  $q_i$  is positive in the positive  $x$ -direction, as shown in Fig. 2.1. The corresponding vertical and horizontal nodal displacements are denoted by

$$\mathbf{u}_i = [v_i, w_i]^T \quad (2.2)$$

where, a positive value of normal displacement  $w_i$  corresponds to a gap between the elastic body and the obstacle.

### 2.3 The Coulomb Friction Law

At any time  $t$ , the Coulomb friction law for node  $i$  must be in one of the four states:-

- (1) *Stick*: The node is in contact and there is no relative motion, so

$$w_i = 0; \quad \dot{v}_i = 0. \quad (2.3)$$

For this state to hold, the normal reaction must be compressive and the tangential reaction must satisfy the Coulomb friction inequality, giving

$$p_i > 0; \quad -fp_i \leq q_i \leq fp_i. \quad (2.4)$$

- (2) *Separation*: The node is not in contact, so the reaction forces are both zero, giving

$$p_i = q_i = 0. \quad (2.5)$$

For this to hold, the gap between the block and the plane surface must be non-negative, which requires

$$w_i \geq 0. \quad (2.6)$$

(3) *Forward slip*: The node is in contact and slipping to the right, so

$$w_i = 0; \quad \dot{v}_i > 0. \quad (2.7)$$

The normal contact reaction must be compressive and the Coulomb friction law implies that  $q_i$  opposes the motion, giving

$$p_i > 0; \quad q_i = -fp_i. \quad (2.8)$$

(4) *Backward slip*: The node is in contact and slipping to the left, so

$$w_i = 0; \quad \dot{v}_i < 0; \quad p_i > 0; \quad \text{and} \quad q_i = fp_i. \quad (2.9)$$

### 2.3.1 Solution Procedure

As in Klarbring et al. (2007), we can employ a standard static condensation procedure to eliminate displacements at interior nodes of the discretized elastic body and hence write the reactions in the form

$$\mathbf{r} = \mathbf{r}^w + \boldsymbol{\kappa} \mathbf{u}, \quad (2.10)$$

where

$$\mathbf{q} = [q_j]^T, \quad \mathbf{p} = [p_j]^T, \quad \mathbf{v} = [v_j]^T, \quad \mathbf{w} = [w_j]^T, \quad \mathbf{r} = [\mathbf{q}^T, \mathbf{p}^T]^T, \quad \mathbf{u} = [\mathbf{v}^T, \mathbf{w}^T]^T.$$

$\mathbf{r}_i^w$  are the reactions that would be generated by the external forces if all the nodal displacements were constrained to be zero, i.e. if the contact nodes were welded to the obstacle, and  $\boldsymbol{\kappa}$  is the contact stiffness matrix which we take to be symmetric and positive definite. Using Eqs. (2.1) and (2.2), we can partition  $\boldsymbol{\kappa}$  into three sub-matrices  $\mathbf{A}$ ,  $\mathbf{B}$ ,  $\mathbf{C}$ , such that

$$\begin{aligned} q_j &= q_j^w + A_{ji}v_i + B_{ij}w_i \\ p_j &= p_j^w + B_{ji}v_i + C_{ji}w_i \end{aligned} \quad (2.11)$$

where  $\mathbf{A}$ ,  $\mathbf{C}$  are symmetric and positive definite.  $\mathbf{B}$  represents the coupling between tangential displacements and normal reactions which is not subject to these restrictions, but

they obey the relation

$$\mathbf{B} = \mathbf{B}^T \quad (2.12)$$

The solution of the transient loading problem under any transient loading,  $p_0(t)$  and  $q_0(t)$ , can then be stated and solved in terms of the variables defined in Eq. (2.10), making use of the state equations (2.3-2.9).

The problem is solved at a series of time increments  $t_j$  in which case the stick condition  $\dot{v}_i = 0$  in Eq. (2.3) translates to the condition

$$v_i(t_{j+1}) = v_i(t_j) \quad (2.13)$$

and the frictional inequalities  $\dot{v}_i > 0$  in Eq. (2.7) and  $\dot{v}_i < 0$  in Eq. (2.9) translate to

$$v_i(t_{j+1}) > v_i(t_j) \quad \text{and} \quad v_i(t_{j+1}) < v_i(t_j) \quad (2.14)$$

respectively. Thus, if the state of the system is completely known at time  $t_j$ , Eqs. (2.3-2.9) provide a set of conditions sufficient to determine the state at time  $t_{j+1}$ .

### 2.3.2 Solution Algorithm

The numerical solution is obtained by a Gauss-Seidel procedure whereby the displacements at each node are updated one by one, assuming that those at other nodes remain unchanged (Atkinson 1989, Nakamura 1996). The slip at node  $i$  can be written as follows:

$$u_i^{(m+1)} = \frac{1}{\kappa_{ii}} \left\{ r_i - r_i^w - \sum_{j=1}^{i-1} \kappa_{ij} u_j^{(m+1)} - \sum_{j=i+1}^n \kappa_{ij} u_j^m \right\}, \quad i = 1, 2, \dots, N \quad (2.15)$$

where, superscript  $m(\geq 0)$  is the iteration number and initial guesses  $u_i^{(0)}$  are assumed to be assigned. In this scheme,  $u_j$  for  $j \neq i$  are assumed to be known, and also  $u_j$  for  $j < i$  uses updated values obtained by previous iteration, which can help increase the convergence rate.

At each time step, the algorithm cycles through the entire set of contact nodes several times until the governing equations at all nodes are satisfied to within a set tolerance. A block diagram of the algorithm is given in Fig. 2.2. For the update procedure, the state (stick, forward slip, backward slip or separation) at the node in question is assumed to be that for the previous iteration. The corresponding equations are then solved and the appropriate inequalities are checked. If the inequalities are not satisfied, the state assumption is changed and the node is solved again.

We should remark at this point that the system ‘memory’ is entirely contained in the instantaneously locked-in displacements in the stick regions and this memory is acquired at times when any node makes the transition from slip or separation to stick. Such a transition may actually be indicated at a time between  $t_j$  and  $t_{j+1}$  and hence the accuracy of the stored displacements depends on the time step (or more strictly the loading increment) being small enough for this to have a negligible effect on the solution. When the transition occurs from separation to stick, a better approximation is achieved by first identifying the position of the node predicted under the zero traction assumption. If there is to be a transition to contact, this will involve a negative gap. By assuming a linear trajectory from the previous position of the node, we can estimate the point of first contact and use this for the tangential nodal displacement at the newly stuck node.

The iteration at each time step is terminated when the changes  $\Delta v_i, \Delta w_i$  in the displacements  $v_i, w_i$  at all slipping and separated nodes during the last iteration are less than a given proportion of the corresponding displacement. In other words, when  $\varepsilon < \varepsilon_0$ , where

$$\varepsilon = \max_{v_i, w_i} \left( \frac{\Delta v_i}{v_i}, \frac{\Delta w_i}{w_i} \right). \quad (2.16)$$

The implementation of time incremental evolution program is summarized as follows:

- (i) Assume previous state at node  $i$ .

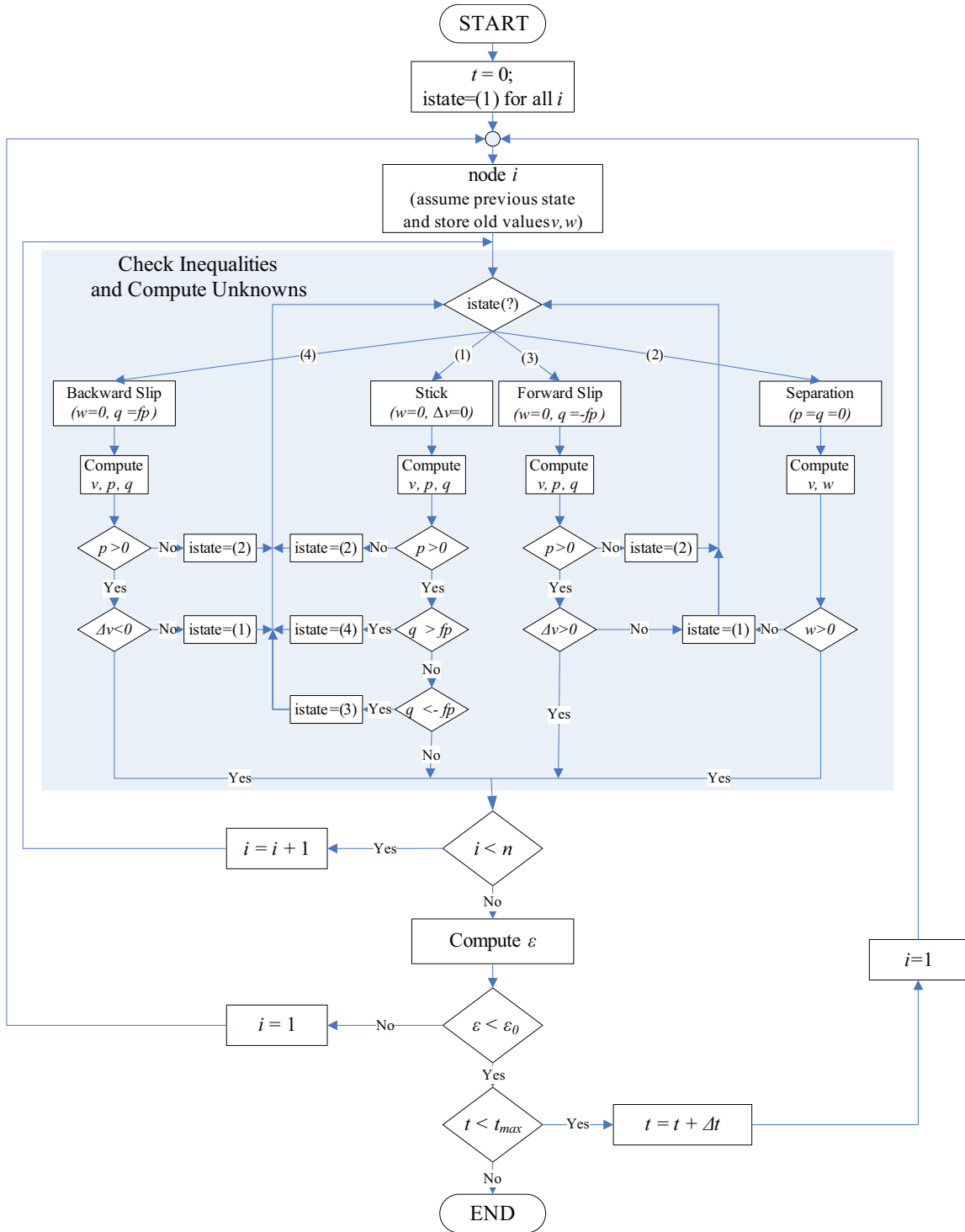


Figure 2.2: Solution Algorithm

- (ii) Store the latest values as  $v_0$  at node  $i$ .
- (iii) Calculate unknowns at node  $i$ .
- (iv) Check inequality at node  $i$ .
- (v) Change the state at node  $i$  if any inequality is violated.
- (vi) Repeat Step (iii)-(v) until the inequality is satisfied.
- (vii) Update tolerance ( $\varepsilon = |v^{new} - v^{old}|$ ) at node  $i$ .
- (viii) Go on to node  $i + 1$  and repeat the same procedure.
- (ix) Check the error tolerance ( $\varepsilon < \varepsilon_0$ ) after cycling through all the nodes  $i = 1 \sim N$ .
- (x) Start again at node  $i$  and repeat the same procedures until the tolerances are satisfied.
- (xi) Go on to the next time step and repeat the same procedures.

As a test example, we will consider a receding contact problem in Chapter III, which is subjected to oscillating loading.

## CHAPTER III

# Response of Frictional Receding Contact Problems to Cyclic Loading

### 3.1 Introduction

The background of the receding contact problem was discussed in Section 1.4. Problems of this class, in which the contact area  $\Gamma_C$  under load is included within the contact area  $\Gamma_0$  in the unloaded state ( $\Gamma_C \in \Gamma_0$ ) were described by Dundurs and Stippes (1970). They possess the interesting characteristic that the stress and displacement fields are linearly proportional to the applied loads, despite the fact that the problem definition includes the unilateral contact inequalities. In particular, the extent of the contact area  $\Gamma_C$  is independent of the load — it immediately jumps to the loaded value as soon as an infinitesimal load is applied and remains at that value on subsequent increased loading.

The proof of this result is very simple (Dundurs, 1970). Suppose the stresses  $\boldsymbol{\sigma}$ , displacements  $\boldsymbol{u}$  and the contact area  $\Gamma_C$  are known for any particular load  $P$ . In particular, this implies that the normal tractions  $\tau_n$  are compressive throughout  $\Gamma_C$  and that the gap is positive throughout  $\Gamma_0 - \Gamma_C$ . Now postulate that the corresponding solution for a load  $\lambda P$  is  $\lambda\boldsymbol{\sigma}$ ,  $\lambda\boldsymbol{u}$ ,  $\Gamma_C$ , where  $\lambda$  is a scalar multiplier. Clearly this solution satisfies all the governing equations of the problem and if the normal tractions  $\tau_n$  are compressive, so also will be  $\lambda\tau_n$  as long as  $\lambda > 0$ . Similarly, if the gap derived from  $\boldsymbol{u}$  is positive, that derived from

$\lambda \mathbf{u}$  will also be positive. Thus, the inequalities are also satisfied and the initial postulate is confirmed.

### 3.1.1 Coulomb Friction

The same argument can be applied to problems involving Coulomb friction as long as the loading is monotonic in time. In this case  $\Gamma_C$  must be subdivided into a slip region  $\Gamma_S$  and a stick region  $\Gamma_C - \Gamma_S$ . In  $\Gamma_S$ , we have the additional condition

$$\boldsymbol{\tau}_s = -\frac{f \dot{\mathbf{u}} \tau_n}{|\dot{\mathbf{u}}|}, \quad (3.1)$$

where  $f$  is the coefficient of friction and the dot denotes differentiation with respect to time  $t$ . This condition states that the tangential traction  $\boldsymbol{\tau}_s$  (which is a vector in the contact plane in a three-dimensional problem) must oppose the instantaneous sliding velocity  $\dot{\mathbf{u}}$ . In the stick region  $\Gamma_C - \Gamma_S$ , we have

$$\dot{\mathbf{u}} = 0; |\boldsymbol{\tau}_s| < f \tau_n \quad (3.2)$$

Suppose that the load is given by  $\lambda(t)P$  and we postulate that the corresponding displacements and tractions can be written in the form  $\lambda(t)\mathbf{u}$ ,  $\lambda(t)\boldsymbol{\tau}$  respectively, where  $\mathbf{u}$ ,  $\boldsymbol{\tau}$  and  $\Gamma_C, \Gamma_S$  are independent of time. If these expressions are substituted into the governing equations and inequalities, the factor  $\lambda(t)$  will cancel in all except Eq. (3.1), which reduces to

$$\boldsymbol{\tau}_s = -\frac{f \dot{\lambda} \mathbf{u} \tau_n}{|\dot{\lambda}| |\mathbf{u}|}, \quad (3.3)$$

It follows that the initial postulate is confirmed as long as  $\dot{\lambda}$  retains the same sign and hence that the loading is monotonic in time.

### 3.1.2 Unloading

If the loading is non-monotonic, the previous results imply that the extent of the stick, slip and separation regions will generally differ from those during loading. This behavior

is illustrated by the solution due to Spence (1973) and Turner (1979) for the loading and subsequent unloading of a rigid at cylindrical punch indenting an elastic half space. No separation occurs in this problem, but during loading ( $\dot{P} > 0$ ), radially-inward slip occurs in an annular slip zone surrounding a central stick zone whose radius is independent of the load  $P$ , depending only on Poisson's ratio for the half space (Spence 1973). When the load reaches a maximum value and starts to decrease, a more complex pattern of stick and slip zones is developed. Initially, the central stick zone shrinks with decreasing load and a surrounding annulus of stick is developed at the edge. Then an outer annulus of reversed slip develops, eventually spreading inwards across the entire contact region (Turner 1979).

An important case of frictional loading and unloading is that in which a contact is subjected to a combination of mean and oscillating load. Under these conditions, the long term behavior might involve *shakedown* (Klarbring *et al.* 2007) (no slip after an initial transient), *cyclic slip* (where there is completely reversed microslip in some regions), or *ratchetting*, where the stress cycle repeats itself, but where a rigid-body displacement accumulates during each loading cycle (Mugadu *et al.* 2004). Cyclic slip is of concern in practical applications because the microslip, which typically occurs in a region adjacent to the edge of the contact area, can lead to failure due to fretting fatigue (Nowell *et al.* 2006).

In the present chapter, we shall use the numerical algorithm of Chapter II to examine the response of a receding contact problem to a combination of mean and oscillating loads. We shall verify that the slip and separation zones remain unchanged throughout the first loading phase, but thereafter all the zone boundaries vary during both loading and unloading periods. Eventually a steady periodic state is achieved.

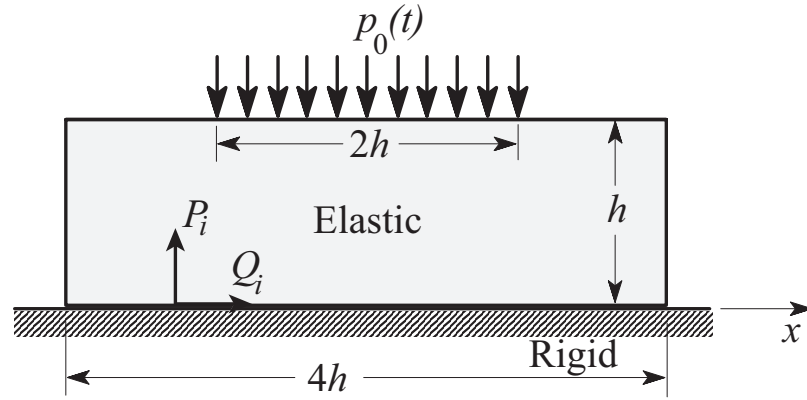


Figure 3.1: A rectangular elastic block pressed against a rigid plane surface.

### 3.2 Problem Description

We consider the two-dimensional problem illustrated in Fig. 3.1, in which a rectangular elastic body of height  $h$  and width  $4h$  is pressed against a rigid plane surface by a uniform time-varying pressure  $p_0(t)$  exerted over a central strip of width  $2h$  on the upper surface. This example shares many of the features of the receding contact problems discussed by previous authors. However, in contrast to Filon's problem of Fig. 1.5, the contact interface is not a plane of symmetry, implying that we should expect coupling between normal and tangential effects. Coulomb friction boundary conditions are assumed at the interface between the block and the plane, with friction coefficient  $f$ . We assume that the loading is sufficiently slow for the quasi-static analysis to be appropriate, in which case time  $t$  appears only as an evolutionary parameter describing the sequence of the loading.

### 3.3 Results

Results were obtained for the case where the external load  $p_0(t)$  initially increases with time to a maximum value  $p_0^{max}$ , after which it is monotonically reduced to zero. The coefficient of friction was taken to be  $f = 0.35$  and Poisson's ratio  $\nu = 0.3$ .

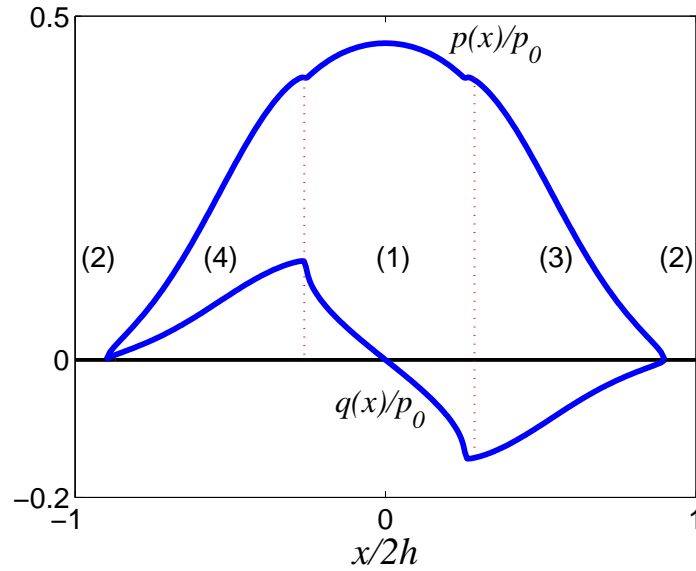


Figure 3.2: Normalized contact traction distributions during the initial loading. Numbers in parentheses refer to the four states defined in Section 2.3

During the initial loading phase, separation occurs at the edges of the block and the contact area comprises a central stick zone flanked by regions of forward and backward slip. The extent of these zones remains constant throughout the loading phase and the normal and shear tractions retain the same form and increase proportionally with the load, as predicted in § 3.1.1. Fig. 3.2 shows the distributions of normal traction  $p(x)$  and shear traction  $q(x)$ , normalized by the instantaneous value of  $p_0(t)$ .

### 3.3.1 Unloading

When the load starts to decrease from its maximum value, the immediate effect is for a stick zone to be developed at the edges of the contact, but two interior slip regions remain. Fig. 3.3 shows the evolution of the stick, slip and separation regions during the unloading process. As in Turner's indentation problem (Turner 1979), regions of slip are developed at the edge of the contact area opposite in sign to the slip that occurred during loading, whilst the interior slip regions extend inwards at the expense of the central stick

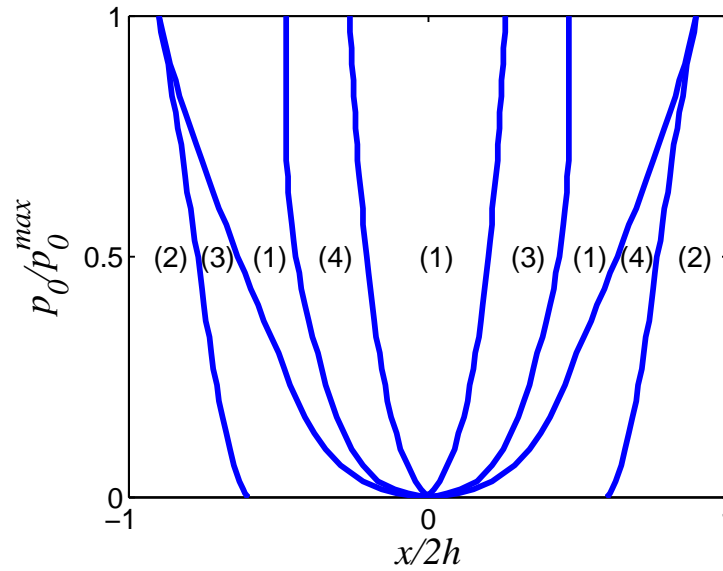


Figure 3.3: Evolution of stick, slip and separation regions during unloading

region. Notice that the five central zones (stick/forward slip/stick/backward slip/stick) all tend to zero near the end of the unloading process. This is necessary since if we track the state at a point that is stuck during loading and that experiences forward slip during unloading, it must eventually also experience a period of backward slip, since at complete unloading the total slip displacement must revert to zero. A new feature in this problem is that the total contact area itself decreases monotonically relative to the fully loaded state (the two separation regions extend). This continues until the instant of complete unloading when the gap at all points in the separation zone goes to zero. Notice also that the inner boundaries of the two outer stick zones (1) in Fig. 3.2 move inwards during unloading, implying that the stick zone is ‘advancing’ and hence that the instantaneous state depends on the complete history of unloading and not merely on the instantaneous load (Hills *et al.*, 1996). Fig. 3.4 shows the normalized traction distributions at  $p_0(t) = p_0^{max}/3$  during the unloading process.

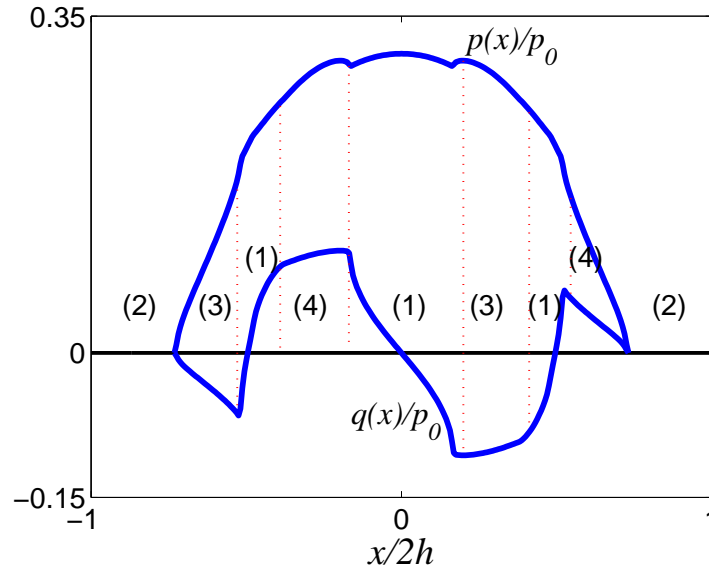


Figure 3.4: Normalized contact traction distributions during unloading

### 3.3.2 Oscillatory Loading

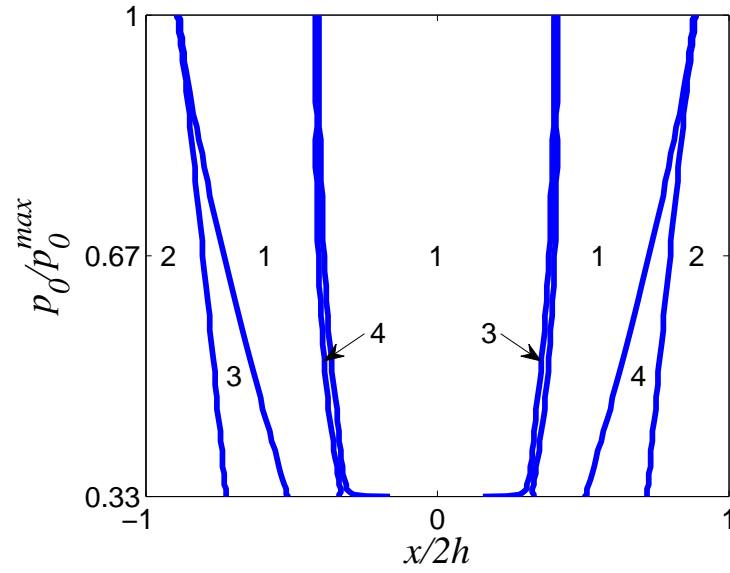
We next consider the case where the load is first increased to the maximum value  $p_0^{max}$ , after which it oscillates in the range  $p_0^{max} > p_0(t) > p_0^{max}/3$ . Other values for the minimum load were also examined and found to give qualitatively similar results. The first loading and unloading cycle is of course similar to that presented in Section 3.3.1 and the traction distribution when the load is first reduced to  $p_0^{max}/3$  is given by Fig. 3.4 as before. However, during the reloading phase, the tractions and the extent of the stick, slip and separation zones follow a new scenario and the cycle continues to evolve over subsequent cycles. This contrasts with previous studies of frictional systems subject to oscillatory loading, where the steady cyclic state is generally reached after only a few cycles (Karuppanan and Hills, 2008).

Figs. 3.5 show the evolution of the slip, stick and separation regions during the unloading and reloading phases respectively after nine cycles of loading. The extent of the separation zone varies during the cycle and points near the edge of the contact area expe-

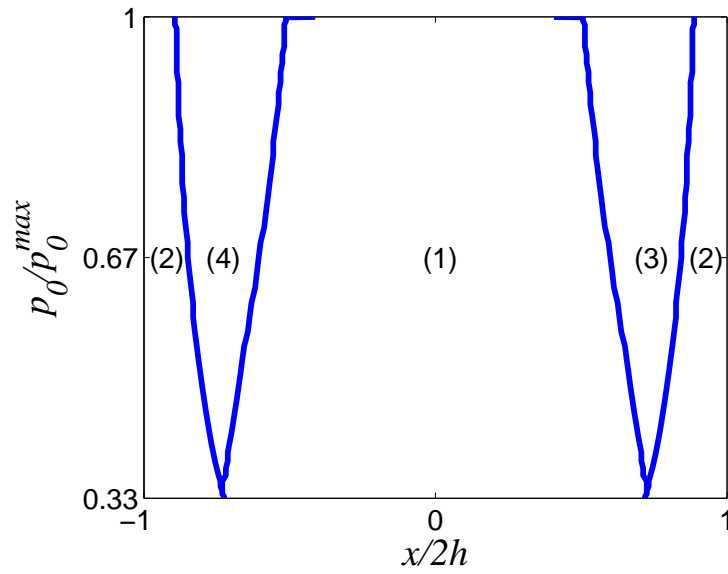
rience cyclic slip. Notice in particular that during unloading, the three stick regions (1) are separated by small regions of slip, indicated by arrows in Fig. 3.5(a). These regions remain stuck during reloading and this is a clear indication that the steady state has not yet been reached, since the magnitude of the accumulated slip displacement  $v_i$  in these regions continues to increase monotonically with each cycle. However, the increment  $\Delta v_i$  in slip displacement per cycle decreases with the number of cycles elapsed  $N$ . Results for a representative node are shown in Fig. 3.6 and show that  $\Delta v_i \sim N^{-3.1}$ . Eventually  $\Delta v_i$  falls within the tolerance of the numerical algorithm, but if this trend were assumed to continue indefinitely (given arbitrarily high levels of numerical precision), the increments  $\Delta v_i$  would have a finite sum representing a steady-state that is approached monotonically and asymptotically.

The evolution of slip, stick and separation regions during unloading and reloading in the final steady state is shown in Figs. 3.7. The dashed line in Fig. 3.7(a) denotes a range of points that achieve the limiting friction condition  $|Q| = fP$  at some point during the cycle, but at which no slip actually occurs. This phenomenon was also noted by Dini and Hills (1996).

The extent of the cyclic slip zones in the steady state is smaller than in the earlier phases of loading, showing that some degree of shakedown has occurred. This effect is quantified in Fig. 3.8 where we present the evolution of the normalized energy dissipation per cycle, which is a parameter that is expected to correlate with fretting damage. The energy dissipation per cycle decreases monotonically with each cycle and it seems likely that this would be true for all frictional systems, though the present authors are unaware of a proof of this result. The steady-state energy dissipation is approximately 56% of that during the first loading cycle.



(a) Unloading



(b) Reloading

Figure 3.5: Evolution of the stick, slip and separation regions during the ninth cycle of (a) unloading and (b) reloading

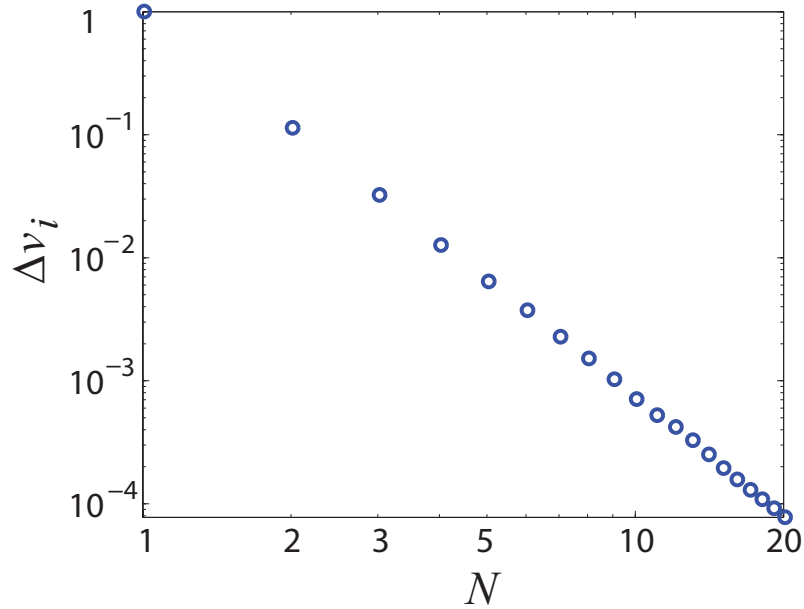
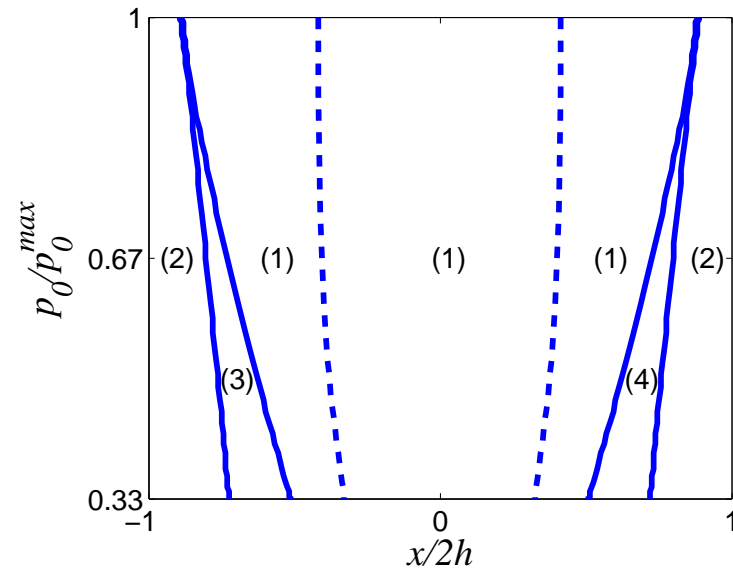


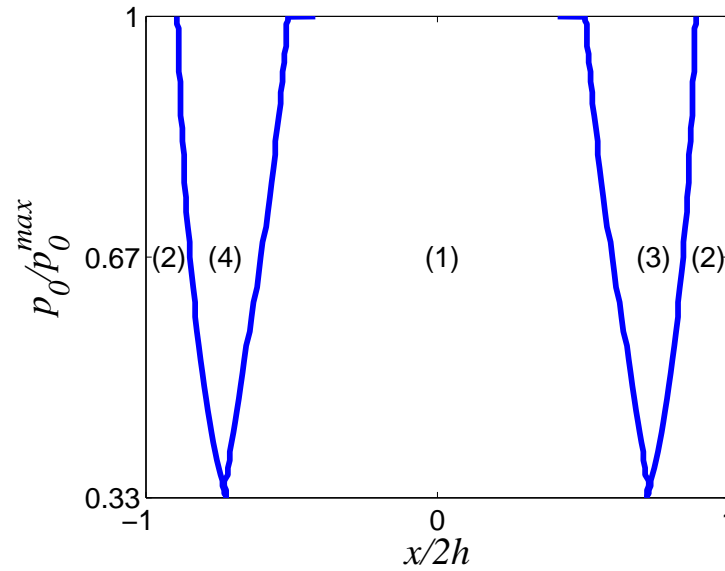
Figure 3.6: Incremental slip  $\Delta v_i$  per cycle at a representative node as a function of cycle number  $N$ .

### 3.4 Conclusions

Dundurs' results for receding contact problems can be extended to problems involving Coulomb friction, but only as long as the loading is monotonic. During unloading, changes occur in the extent of both separation and slip zones. We have illustrated this behavior for the case of an elastic block pressed against a frictional rigid plane. In particular, we find that if the load is periodic in time, the system approaches a steady periodic state relatively slowly and in this final state there is continuous variation of the contact area, with the minimum (i.e. the maximum amount of separation) occurring at the minimum applied load. The system exhibits some degree of shakedown in the sense that the energy dissipation decreases monotonically with each successive cycle.



(a) Unloading



(b) Reloading

Figure 3.7: Evolution of the stick, slip and separation regions during (a) unloading and (b) reloading in the steady cyclic state. The dashed line in Fig. 3.7(a) indicates points which reach the limiting friction condition but which do not actually slip

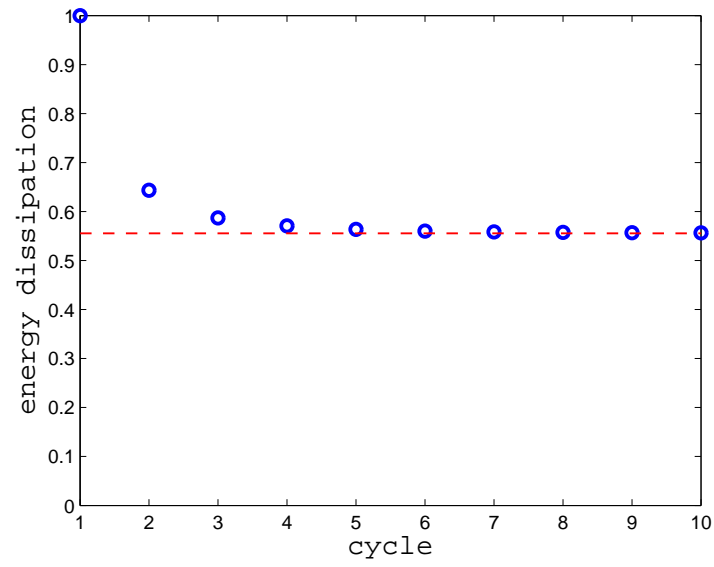


Figure 3.8: Evolution of the energy dissipated in friction per loading cycle as a proportion of that during the first cycle.

## CHAPTER IV

# Shakedown of Coupled Two-dimensional Discrete Frictional Systems

### 4.1 Introduction

The frictional shakedown was introduced in Section 1.3. Elastic systems with frictional interfaces subjected to periodic loading are often found to shake down in the sense that frictional slip ceases after the first few loading cycles. The similarities in behavior between such systems and monolithic bodies with elastic-plastic constitutive behavior make various authors to investigate that Melan's theorem (1936) might apply to them. This question was investigated in two previous papers in the context of discrete (Klarbring *et al.*, 2007) and continuous (Barber *et al.*, 2008) systems, respectively. A necessary condition for shakedown to occur in a discrete system is that there exist at least one vector of nodal slip displacements (the 'safe shakedown vector') such that the resulting time-varying nodal reactions satisfy the condition  $|q_i| < fp_i$  at all nodes  $i$  throughout the loading cycle. The frictional Melan's theorem, if true, would then imply that this was also a sufficient condition for shakedown.

Klarbring *et al.*, (2007) were able to establish such a theorem for two- and three-dimensional discrete systems that are uncoupled, meaning that changes in nodal slip displacements do not influence the normal contact tractions  $p_i$ . In this proof, shakedown was

defined such that any slip that occurred during the initial cycles of loading caused the instantaneous slip displacements to approach the safe shakedown state monotonically in the sense of a certain norm. A similar result was established for continuous systems by Barber *et al.*, (2008). Klarbring *et al.*, (2007) also identified a class of two-dimensional systems with a degeneracy in the stiffness matrix, for which the theorem could be established if the friction coefficient  $f$  was less than a certain critical value. For all other discrete coupled systems, they showed that counter-examples could be identified — i.e. particular loading scenarios such that, depending on the initial conditions, the system may experience either shakedown or cyclic slip.

These counter-examples often require rather contrived loading. For example, we have explored the problem of a rectangular elastic block in contact with a rigid plane surface and found that failure to reach the optimal safe shakedown state occurred only when the mean load induced large normal reactions at nodes near both edges of the block. Therefore, there is reason to hope that a reduced form of Melan's theorem might still apply to such systems under suitable restrictions on the loading history.

In this chapter, we shall examine this question in the context of a simple two-dimensional coupled discrete system, comprising two contact nodes. In particular, we shall demonstrate that by considering the range of permissible slip displacements at the two nodes, it is possible to determine a lower bound on the amplitude of the cyclic load below which the system will always shake down, regardless of the initial transient, and an upper bound above which it cannot shake down. The methodology introduced is also capable of extension to more general multi-node systems.

## 4.2 Critical Coefficient of Friction

The case where there is only one contact node was first introduced by Klarbring (1990) to illustrate and elucidate the anomalous behavior of frictional systems when the coefficient of friction is large (see Appendix A). In the present notation, if

$$f > f_c \equiv \frac{A_{11}}{|B_{11}|}, \quad (4.1)$$

conditions (2.3-2.9) may fail to define a unique quasi-static evolution for the single-node system under a given loading history. Uniqueness can be restored by using an elastodynamic formulation (Cho and Barber, 1998), but dynamic instabilities are then predicted (Martins et al., 1995, Adams, 1996), resulting in rapid transitions from one state to another at certain points in the evolution. In the limit of low mass, where we would expect to recover the quasi-static solution, this translates into ‘*displacement jumps*’ — i.e. a loss of continuity of nodal displacements under continuously varying loads (Cho and Barber, 1998, Martins et al., 1994).

The coefficient  $f_c$  plays a pivotal role in determining the behavior of the single-node system. It is the sole eigenvalue in Hild’s eigenvalue problem (Hassani et al., 2003) and it was shown in (Klarbring et al., 2007) that Melan’s theorem applies to this system if and only if  $f < f_c$ . Also, the single-node system is capable of becoming ‘*wedged*’ if and only if  $f > f_c$ , meaning that it can sustain a deformed configuration in the absence of external loads (Barber and Hild, 2006). By contrast, if  $f < f_c$ , it always returns to the undeformed configuration when the external loads are removed.

For multi-node systems, the behavior is more complex (Andersson and Klarbring, 2001). Hassani *et al.* (2003) establish some relations between the uniqueness of solution and the eigenvalue problem. Also, the solution is always nonunique if the system is capable of wedging (Andersson, 2008). In this case, we can always generate scenar-

ios in which discontinuous displacement jumps occur. For example, suppose the system is wedged and tangential external loads are then gradually applied until all the wedged nodes just exceed the limiting friction condition in Eq. (2.4) in the direction tending to reduce the wedging displacements. Relaxation due to incremental slip now causes a larger change in the normal force than is required to stay on the slip constraint and the system will accelerate (actually towards a state involving separation) with no further change in external forces. In effect, slip motion in the opposite direction to that required to establish the wedged state is dynamically unstable, as demonstrated by Cho and Barber (1998) for the single-node system. However, for multi-node systems we shall show that wedging is a sufficient but not a necessary condition for the transient evolution to be discontinuous. Notice also that multi-node systems can exhibit many different wedging modes.

For the most part, we shall restrict attention in the present Chapter to coefficients of friction that are low enough for wedging to be impossible and for the quasi-static evolution to be continuous and unique.

### 4.3 The Two-node System in Reaction Space

The following graphical construction will be introduced to represent the history of the reaction forces instead of that of the applied forces used by Cho and Barber (1998). The allowable domains for reaction forces comprise simply the stick sector  $ABC$  with forward slip and backward slip being the two lines  $AB, AC$  and separation corresponding to the apex  $A$ , as shown in Fig. 4.1.

#### 4.3.1 Effect of Slip Displacement

Consider a system comprising just two contact nodes,  $i = 1, 2$  and suppose that at some point in the loading cycle both nodes are in contact, so that  $w_1 = w_2 = 0$  and Eq. (2.11)

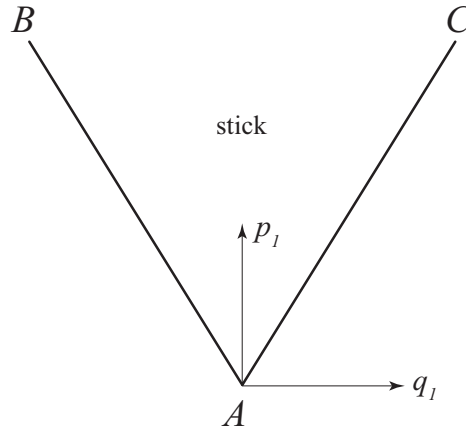


Figure 4.1: Reaction space

reduces to

$$\begin{aligned} q_j &= q_j^w + A_{ji}v_i, \\ p_j &= p_j^w + B_{ji}v_i. \end{aligned} \quad (4.2)$$

The points corresponding to  $p_i^w, q_i^w$  will generally be known, but the actual operating point in the diagram will be modified by the terms including the unknown slip displacements  $v_1, v_2$  at the two nodes. These unknowns constitute two degrees of freedom, from which the four reactions  $p_1, q_1, p_2, q_2$  are determined. Thus, if any two of these are known (say  $p_1, q_1$ ) and we assume that both nodes are in contact with a rigid support, the remaining unknowns  $p_2, q_2$  can be calculated from Eq. (4.2). Writing

$$\begin{aligned} q_j^* &= q_j - q_j^w = A_{ji}v_i, \\ p_j^* &= p_j - p_j^w = B_{ji}v_i. \end{aligned} \quad (4.3)$$

we have

$$\begin{aligned} q_1^* &= q_1 - q_1^w = A_{11}v_1 + A_{12}v_2, \\ p_1^* &= p_1 - p_1^w = B_{11}v_1 + B_{12}v_2, \\ q_2^* &= q_2 - q_2^w = A_{21}v_1 + A_{22}v_2, \\ p_2^* &= p_2 - p_2^w = B_{21}v_1 + B_{22}v_2. \end{aligned} \quad (4.4)$$

which can be written in matrix form as

$$\begin{aligned} \mathbf{r}_1^* &= \mathbf{r}_1 - \mathbf{r}_1^w = \mathbf{L}_1\mathbf{v}, \\ \mathbf{r}_2^* &= \mathbf{r}_2 - \mathbf{r}_2^w = \mathbf{L}_2\mathbf{v}. \end{aligned} \quad (4.5)$$

where

$$\mathbf{r}_i = \begin{Bmatrix} q_i \\ p_i \end{Bmatrix}; \quad \mathbf{r}_i^* = \begin{Bmatrix} q_i^* \\ p_i^* \end{Bmatrix}; \quad \mathbf{L}_1 = \begin{bmatrix} A_{11} & A_{12} \\ B_{11} & B_{12} \end{bmatrix}; \quad \mathbf{L}_2 = \begin{bmatrix} A_{21} & A_{22} \\ B_{21} & B_{22} \end{bmatrix}. \quad (4.6)$$

Inverting the first term of Eq. (4.5), we have

$$\mathbf{v} = \mathbf{L}_1^{-1} \mathbf{r}_1^* \quad (4.7)$$

and hence

$$\mathbf{r}_2^* = \mathbf{M} \mathbf{r}_1^*, \quad (4.8)$$

where

$$\mathbf{M} = \mathbf{L}_2 \mathbf{L}_1^{-1}. \quad (4.9)$$

Eq. (4.8) defines the motion of the operating point for node 2 in terms of the motion of the corresponding point for node 1 as a result of slip displacements. The properties of the matrix  $\mathbf{M}$  will be shown to be critical for the qualitative behavior of the two-node system.

### 4.3.2 Wedging

To illustrate the wedging, consider the problem of wedging, in which the external forces  $\mathbf{r}^w$  are zero and  $\mathbf{r} = \mathbf{r}^*$ . For the system to be wedged, it is necessary for both  $\mathbf{r}_1^*$  and  $\mathbf{r}_2^*$  to lie within their corresponding stick sectors. The magnitude of the tractions is arbitrary in this case, since if  $\mathbf{r}$  defines a wedged state, so does  $\lambda \mathbf{r}$  where  $\lambda$  is a scalar multiplier. Thus, the quantity that determines whether wedging is possible is the direction of the traction, which we can define as an angle  $\theta_i$  where

$$\cos(\theta_i) = \frac{p_i^*}{|\mathbf{r}_i^*|}; \quad \sin(\theta_i) = \frac{q_i^*}{|\mathbf{r}_i^*|}. \quad (4.10)$$

Eqs. (4.8) and (4.10) define a one-to-one relationship between  $\theta_1$  and  $\theta_2$  which we can write as

$$\theta_2 = g(\theta_1). \quad (4.11)$$

If this relationship is used to map the stick sector in the node 1 diagram ( $-\arctan(f) < \theta_1 < \arctan(f)$ ) into the node 2 diagram, the condition for wedging is that the mapped sector should overlap with the stick sector,  $-\arctan(f) < \theta_2 < \arctan(f)$ .

### 4.3.3 Existence of a Safe Shakedown State

Suppose that an oscillating external load is applied so that the vectors  $\mathbf{r}_1^w$  and  $\mathbf{r}_2^w$  track out known load loops on the two nodal reaction diagrams, as illustrated in Fig. 4.2.

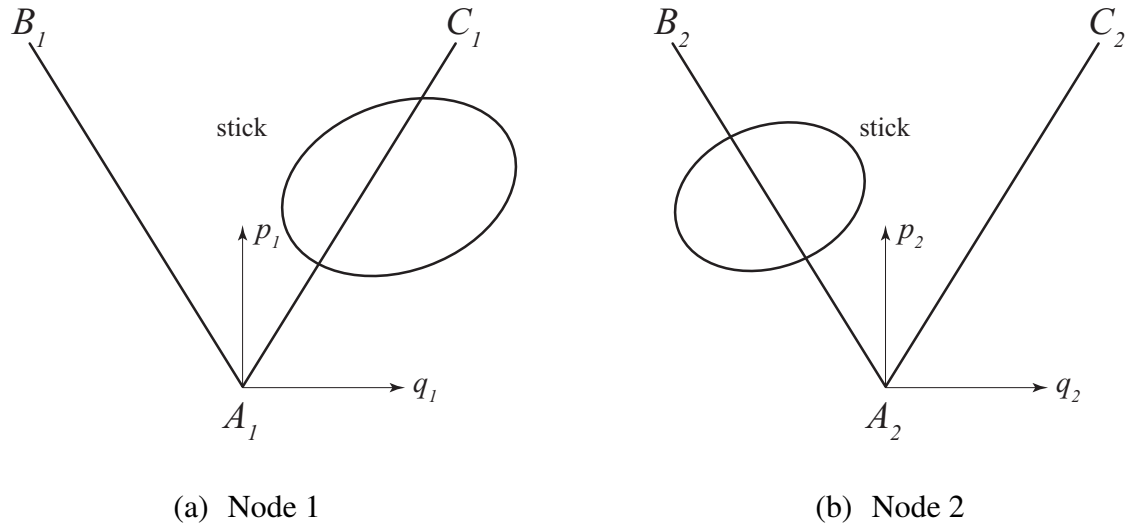


Figure 4.2: Oscillating external load loops on the two nodal diagrams

We wish to determine whether there exists a safe shakedown state  $\tilde{\mathbf{v}}$  such that

$$\begin{aligned} \mathbf{r}_1(t) &= \mathbf{r}_1^w(t) + \mathbf{L}_1 \tilde{\mathbf{v}}, \\ \mathbf{r}_2(t) &= \mathbf{r}_2^w(t) + \mathbf{L}_2 \tilde{\mathbf{v}}. \end{aligned} \quad (4.12)$$

define load loops that lie completely within the respective stick sectors. The effect of changing  $\tilde{\mathbf{v}}$  is to cause a rigid-body motion of the load loops in Fig. 4.2, without change in their shape or orientation.

Suppose we choose  $\tilde{\mathbf{v}}$  such as to move the loop for node 1 into the position where it is tangential to both slip lines, as shown in Fig. 4.3(a). If the corresponding motion of the

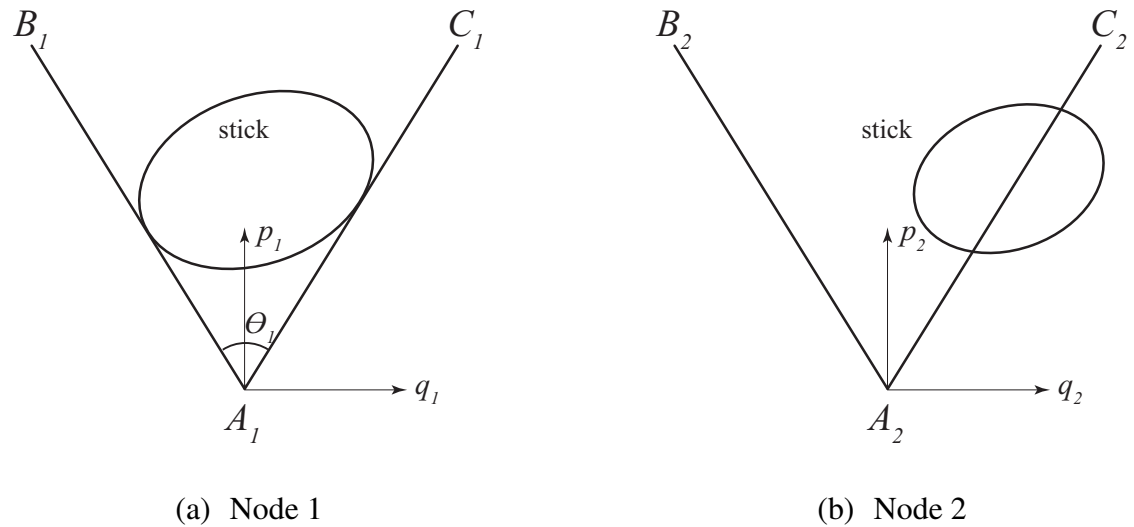


Figure 4.3: Moving the loop for node 1 into the position where it is tangential to both slip lines

loop at node 2 places this inside the stick sector, then we have succeeded in finding a safe shakedown state.

Fig. 4.3(b) illustrates the opposite case, where placing the node 1 loop in the tangent location leaves the loop for node 2 at least partially outside the corresponding stick sector. Suppose we now move the loop at node 1 in a search for a location that will move the loop at node 2 inside the stick sector. If the node 1 loop is to remain inside the sector, we are restricted to moving it in a direction defined by  $-\arctan(f) < \theta_1 < \arctan(f)$ . A safe shakedown state exists if and only if some direction in this range causes a motion of the loop at node 2 that will move it inside the sector.

In Fig. 4.4, we show two limits to the directions of motion at node 2 that will achieve this for a sample initial location. These limits are defined by (i) the slope of the stick sector boundary nearest to the present location of the loop and (ii) the direction in which the loop must move in order to reach the position in which it is tangent to both boundaries of the stick sector. These directions are indicated by the lines  $EF$  and  $ED$  respectively in

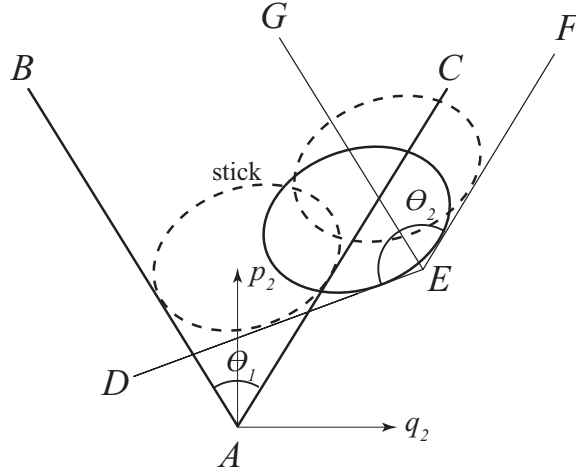


Figure 4.4: A safe shakedown state

Fig. 4.4. It is readily verified that moving the loop on any trajectory that is not contained between these lines will lead to a succession of locations none of which are fully contained in the stick sector and that any trajectory within these lines corresponds to at least one location where the loop is within the sector.

We notice that the sector  $DEF$  includes a sector  $GEF$  that is similar to the original stick sector  $BAC$ . It follows that any system capable of wedging also possesses a safe shakedown state. Of course, this result can also be easily established from first principles. For the system to exclude the possibility of wedging, we have already shown that motion of the loop at node 1 in the sector,  $-\arctan(f) < \theta_1 < \arctan(f)$ , must preclude the corresponding motion at node 2 from the sector,  $-\arctan(f) < \theta_2 < \arctan(f)$ , and hence also from the sector  $GEF$  in Fig. 4.4. Thus, for systems that cannot wedge, the criterion for a safe shakedown state is that the mapping of the sector  $BAC$  at node 1 onto node 2 through Eq. (4.11) must generate a sector which overlaps with the sector  $DEG$ .

The procedure for determining this is clear. We first identify the locations of the two loops that are tangent to both boundaries of their respective slip sectors. We next calculate the location of the loop at node 2 when that at node 1 is in the tangent location. This

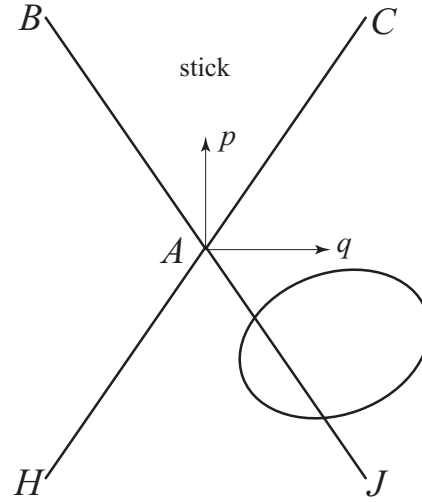


Figure 4.5: Configuration in which gets to a safe shakedown state

result enables us to determine the angles corresponding to the lines  $ED$ ,  $EG$ . Finally, we use Eq. (4.11) to map the stick sector at node 1 onto node 2 and determine whether the resulting sectors overlap.

If the direction  $ED$  itself lies within the sector  $GEF$ , the sector  $DEG$  essentially becomes null and the only directions leading to a safe shakedown state are those in  $GEF$  or equivalently  $BAC$ . In this case, shakedown is possible only if the system is also capable of wedging. This situation corresponds to the situation shown in Fig. 4.5, where moving the load loop at node 1 to the tangent position causes that at node 2 to become totally or partially within the sector  $H AJ$ .

#### 4.3.4 Safe shakedown state at the critical limit

If a safe shakedown state exists, we want to determine the maximum load factor,  $\lambda^{\max}$ , for which shakedown is possible, and also identify the unique shakedown state at  $\lambda^{\max}$ .

We suppose that the system is exposed to periodic external loads that can be expressed in the form

$$\mathbf{r}_i^w(t) = \mathbf{r}_i^0 + \lambda \mathbf{r}_i^1(t), \quad (4.13)$$

where  $r_i^0$  is a mean load that is independent of time  $t$ ,  $r_i^1(t)$  is a periodic load with zero mean value, and  $\lambda$  is a scalar load factor. As we increase the load factor, we can determine whether there is a vector  $\tilde{v}$  to keep both loops inside their stick sectors. If we fail to find the safe shakedown state,  $\tilde{v}$ , the load factor reaches the maximum value. Further, we can assume that the oscillatory part is self-similar because the oscillatory part is multiplied by the positive scalar amount,  $\lambda$ . Therefore, the reaction force for the mean load of each external load moves along the specific center trajectory,  $s$ , as the load factor increases, as shown in Fig. 4.6.

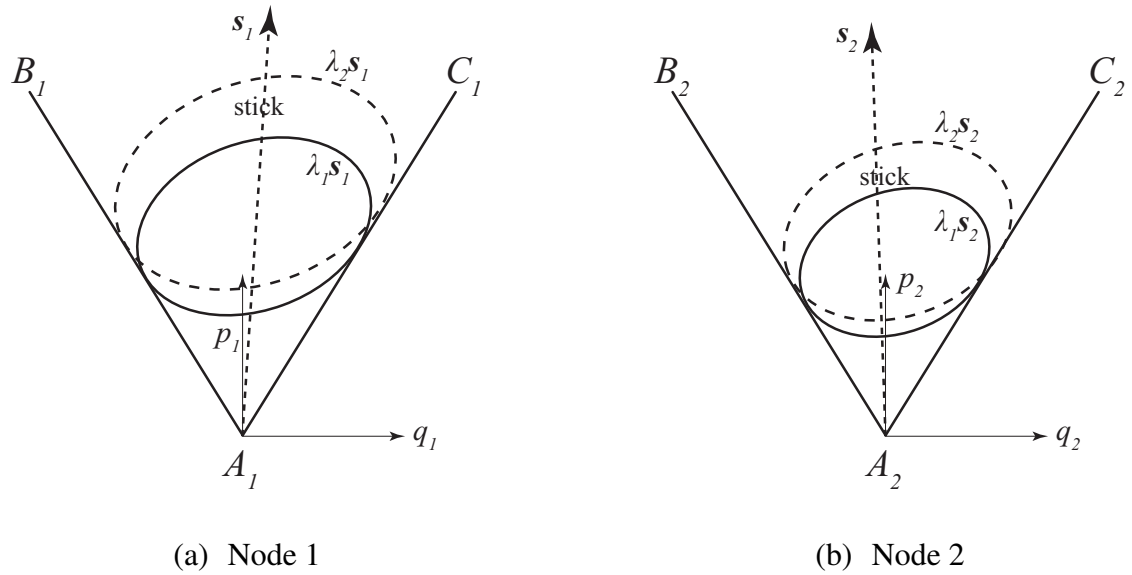


Figure 4.6: Moving the loop at each node into the position where it is tangential to both slip lines

For the general case, we would like to define the vector of the center trajectory of each reaction loop as  $s_i$  at node  $i = 1, 2$ , and the reaction force of the mean load at each node can be written as

$$\begin{aligned} \mathbf{r}_1^m &= \lambda \mathbf{s}_1, \\ \mathbf{r}_2^m &= \lambda \mathbf{s}_2. \end{aligned} \tag{4.14}$$

where,  $\mathbf{r}_i^m (i = 1, 2)$  represents the reaction force at the mean load of the periodic external

loading for each node. Substituting Eq. (4.14) into Eq. (4.8) yields

$$\mathbf{r}_2^m - \mathbf{r}_2^0 = \mathbf{M}(\lambda \mathbf{s}_1 - \mathbf{r}_1^0). \quad (4.15)$$

Eq. (4.15) defines a one-to-one relationship between the load factor,  $\lambda$ , and the reaction force,  $\mathbf{r}_2^m$  at node 2. Therefore, if the load factor,  $\lambda$ , is determined, the corresponding center of the oscillatory loop at node 2 is determined.

Furthermore, by using Eq. (4.15) we can determine the shape of the unique shakedown state at the maximum load factor,  $\lambda^c$ . Suppose that as the loop for node 1 moves between the two slip boundaries,  $(A'_1B'_1)$  and  $(A'_1C'_1)$ , the loop for node 2 is constrained to move between angles produced by two lines,  $(ED')$  and  $(EF')$ , as shown in Fig. 4.7. Using Eqs. (4.10) and (4.11), these one-to-one relationships can be determined.

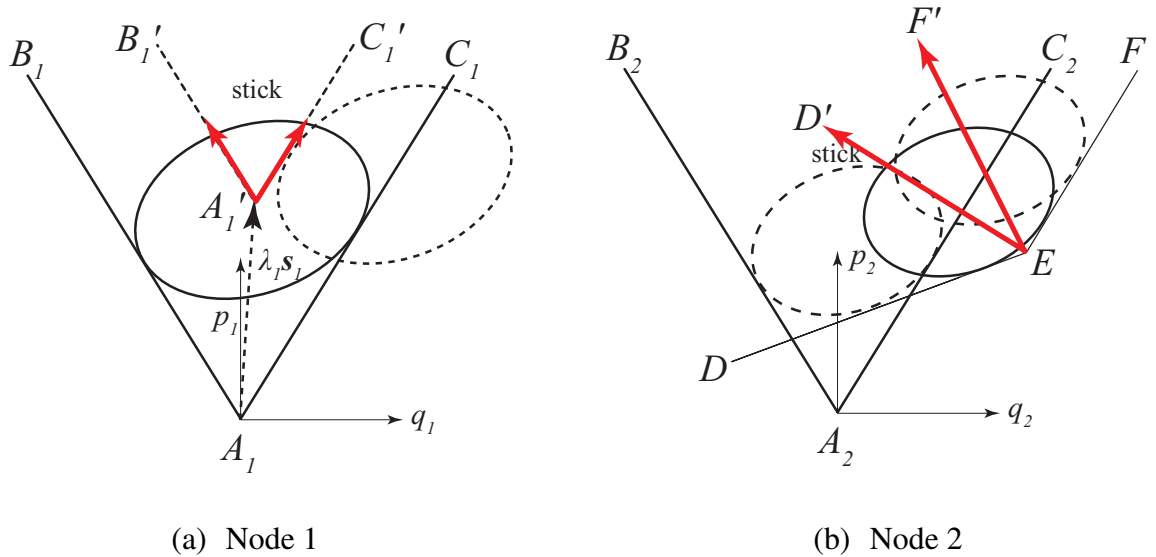


Figure 4.7: Moving the loop for node 1 into the position where it is tangential to both slip lines

Next, if the center of the load loop for node 1 is tangential to both slip lines, and the center for node 2 is located within an inside stick sector,  $(B'_2A'_2C'_2)$ , as shown in Fig. 4.8, we can readily recognize that the loop for node 2 has room to move any direction.

Therefore, we can conclude that the load factor does not reach the maximum value, since there is room to increase the load factor with both loops stuck. On the contrary, we can assume that the loop for node 1 is tangential to both slip boundaries, and the center of the load loop at node 2 lies on the backward slip line. In this case, as the load loop for node 1 moves inside its stick region, the load loop for node 2 can move inward heading for its stick sector. Therefore, we can argue that at the maximum load factor, the two load loops must be tangential to three lines out of the four slip boundary constraints.

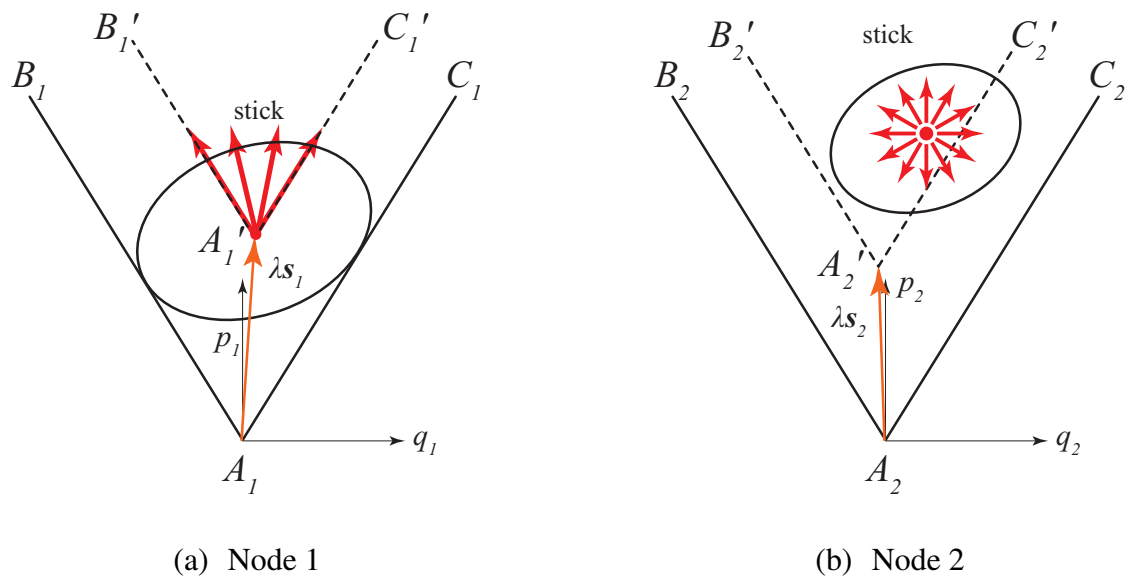


Figure 4.8: Moving the loop for node 1 into the position where it is tangential to both slip lines

If one load loop is tangential to both slip lines and the other loop is located on one of two slip lines, as shown in Fig. 4.9, Shakedown state can be geometrically satisfied with the condition for reaching maximum load factor. Therefore, there should be 4 possible candidates for a two-node system because 4 boundary constraints can make 4 different combinations consisting of 3 equations for each case.

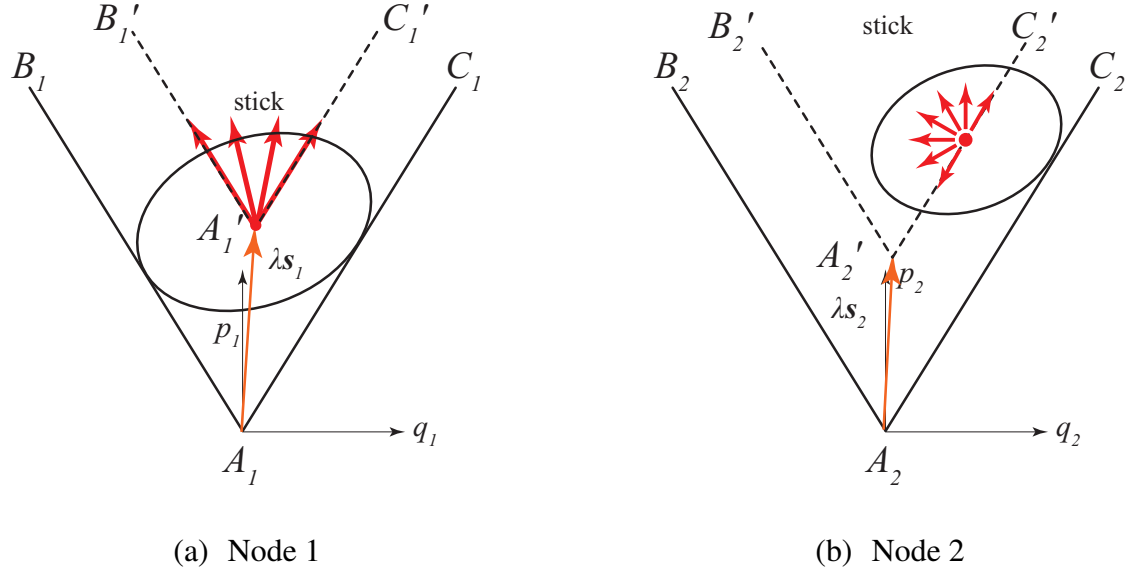


Figure 4.9: A shakedown state at the maximum load factor,  $\lambda^c$

These four equations can be written in the following form,

$$\begin{aligned}
 1) \quad p_1^m &= \frac{1}{f}(q_1^m - \lambda s_{11}) + \lambda s_{12}, \\
 2) \quad p_1^m &= -\frac{1}{f}(q_1^m - \lambda s_{11}) + \lambda s_{12}, \\
 3) \quad p_2^m &= \frac{1}{f}(q_2^m - \lambda s_{21}) + \lambda s_{22}, \\
 4) \quad p_2^m &= -\frac{1}{f}(q_2^m - \lambda s_{21}) + \lambda s_{22},
 \end{aligned} \tag{4.16}$$

where

$$\mathbf{s}_1 = \begin{Bmatrix} s_{11} \\ s_{12} \end{Bmatrix}, \quad \mathbf{s}_2 = \begin{Bmatrix} s_{21} \\ s_{22} \end{Bmatrix}. \tag{4.17}$$

For each case, if we use Eqs. (4.15-4.17), we can calculate the load factor,  $\lambda$ , and the slip displacement,  $\tilde{v}$ . After repeating the same procedure for the other possible cases, we can get four possible load factors allowing a shakedown. Then, we can determine the maximum load factor,  $\lambda^{\max}$ , which must be in the feasible domain.

#### 4.3.5 Numerical simulation result at the critical limit value

Now, we consider whether Melan's theorem, which is introduced in Section 1.3, could apply to the coupled two-dimensional two-node system with only the restriction that the contact is complete. For this, at first, we devise a 4 by 4 positive definite stiffness matrix,

and then suppose that the system is exposed to transient loading part,  $\mathbf{r}_i^{t,w}(t)$ , followed by periodic loading part,  $\mathbf{r}_i^{p,w}(t)$ . That is, the external loading is

$$\mathbf{r}_i^w(t) = \mathbf{r}_i^{t,w}(t) + \mathbf{r}_i^{p,w}(t), \quad (4.18)$$

where

$$\mathbf{r}_i^{p,w}(t) = \mathbf{r}_i^0 + \lambda \mathbf{r}_i^1(t). \quad (4.19)$$

Next, we find the critical loading factor,  $\lambda^{\max}$ , which is defined in Section 4.3.4, such that if  $\lambda$  is greater than  $\lambda^{\max}$ , shakedown is impossible independent of the transient loading part,  $\mathbf{r}_i^{t,w}(t)$ .

Separately, we find the critical loading factor,  $\lambda^T$ , obtained by running the time evolution quasi-static algorithm in Section 2.3.2 with the given external loading  $\mathbf{r}_i^{t,w}(t)$ , such that shakedown occurs.

Finally, we compare the critical loading factor,  $\lambda^{\max}$ , obtained by the theoretical method with the critical loading factor,  $\lambda^T$ , obtained by the time evolution quasi-static algorithm. There may be two possibilities such that i)  $\lambda^T = \lambda^{\max}$ , or ii)  $\lambda^T < \lambda^{\max}$ . The first possibility means that Melan's theorem should apply to the system, while the second possibility means that there is a range where shakedown is possible, but doesn't occur, which can be written as

$$\lambda^T < \lambda < \lambda^{\max}. \quad (4.20)$$

We devised many different external loading scenarios. Fig. 4.10 shows one of these scenarios. Then, we explored the results of the numerical simulation, and compared the two critical loading factors. The results showed that sometimes  $\lambda^T = \lambda^{\max}$  occurs, but it does not always occur.

Since Melan's theorem would say  $\lambda^T = \lambda^{\max}$  always occurs for all  $\mathbf{r}_i^{t,w}(t)$ , all  $\mathbf{r}_i^0$ , and  $\lambda \mathbf{r}_i^1(t)$ , for all systems, Melan's theorem is not true for the coupled system. However, for

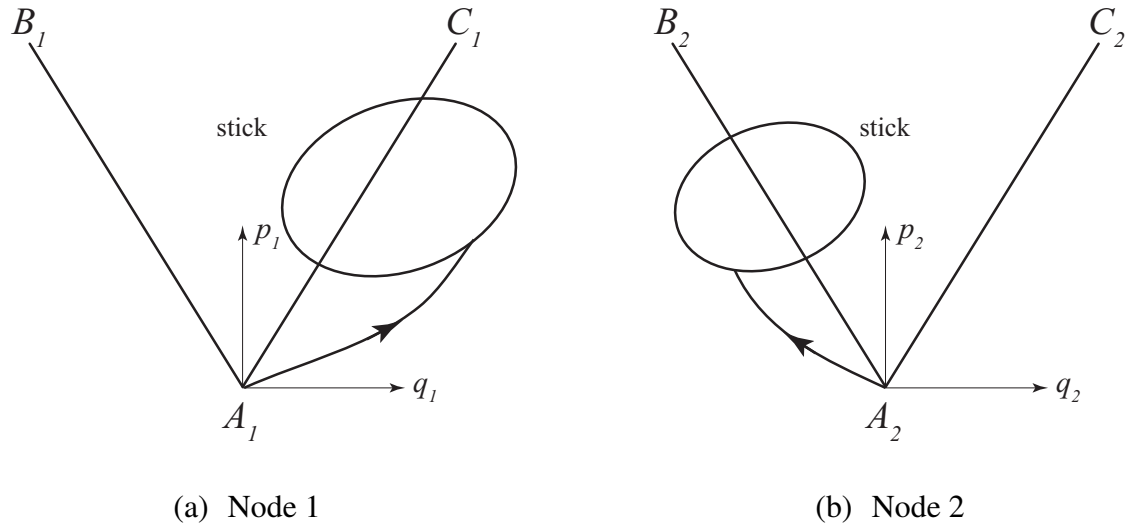


Figure 4.10: The transient external load loops followed by the oscillating external load loops at both nodes

the case  $\lambda^T = \lambda^{\max}$ , we need to study what effect makes it not true, i.e.,  $\lambda^T < \lambda^{\max}$ . These might be (i) the transient external part,  $\mathbf{r}_i^{t,w}(t)$ , or (ii) the periodic external part,  $\mathbf{r}_i^{p,w}(t)$ . Further, there is a possibility that a reduced form of Melan's theorem might still apply to such a coupled system under suitable restrictions on the external loading history.

In the next Section, we will examine this question in more detail by considering the range of permissible slip displacements at the two nodes in  $v_1$  and  $v_2$  space.

#### 4.4 The two-node system in $v_1, v_2$ space

For the state in Eq. (4.2) to be physically admissible for a given loading vector  $\mathbf{r}^w$ , the Coulomb friction law demands that we satisfy the inequality Eq. (2.4) at each of the two nodes  $j = 1, 2$ . Using Eq. (4.2), this implies that

$$fp_j^w - fB_{ji}v_i \leq q_j^w + A_{ji}v_i \leq fp_j^w + fB_{ji}v_i \quad (4.21)$$

and hence

$$\begin{aligned}
 (A_{11} - fB_{11})v_1 + (A_{12} - fB_{12})v_2 &\leq fp_1^w - q_1^w && \text{I} \\
 (A_{11} + fB_{11})v_1 + (A_{12} + fB_{12})v_2 &\geq -fp_1^w - q_1^w && \text{II} \\
 (A_{21} - fB_{21})v_1 + (A_{22} - fB_{22})v_2 &\leq fp_2^w - q_2^w && \text{III} \\
 (A_{21} + fB_{21})v_1 + (A_{22} + fB_{22})v_2 &\geq -fp_2^w - q_2^w && \text{IV}
 \end{aligned} \tag{4.22}$$

#### 4.4.1 Admissible regions in $v_1, v_2$ space

In frictional problems, the ‘memory’ of the system resides in the values of tangential displacements at nodes that are instantaneously stuck. Once a node slips or separates, its condition is determined by an equation and its contribution to the system memory is erased. On the other hand, memory is ‘created’ at nodes which transition from separation or slip to stick (Dundurs and Comninou, 1983). The evolution of the system memory can therefore conveniently be represented graphically in  $v_1, v_2$  space. Each of the four inequalities I,II,III,IV in Eq. (4.22) defines a straight line boundary in this space and excludes the region on one side of the line. The admissible values of  $v_1, v_2$  are defined by the intersection of the admissible regions for each inequality. A typical case is illustrated in Fig. 4.11, where only the central white region is admissible. Notice that since the pairs I,II and III,IV correspond to slip in opposite directions at the same node, they will not intersect except at the critical point where separation occurs at that node. Thus, when a quadrilateral is defined as in Fig. 4.11, I and II will generally represent opposite sides.

The location of the four constraint lines depends on the instantaneous values of  $q_i^w, p_i^w$ , but their slopes depend only on the matrices  $\mathbf{A}, \mathbf{B}$  and the coefficient of friction  $f$ . The admissible region may take various shapes depending on  $\mathbf{r}^w$  and the slopes of the lines. In particular, we may have

(i) A quadrilateral, as in Fig. 4.11.

(ii) A triangle, as in Fig. 4.12(a).

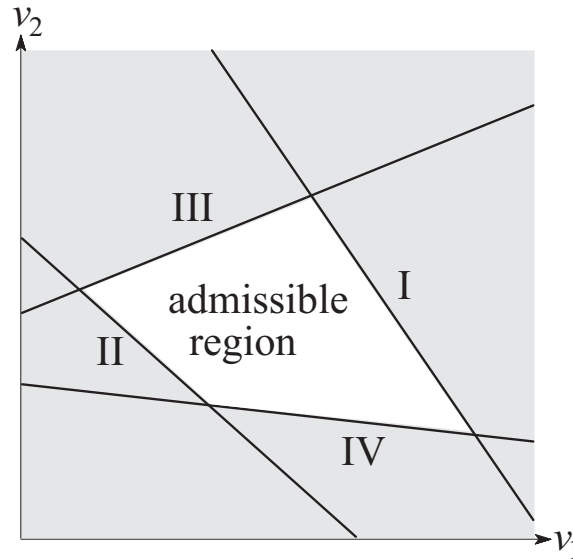


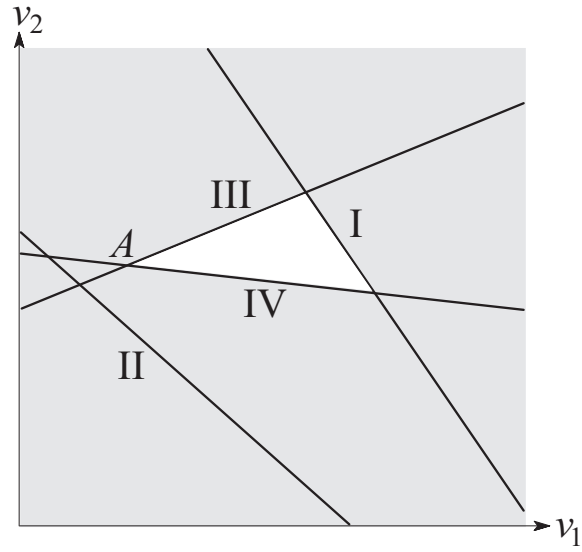
Figure 4.11: Intersection of the admissible regions (values of  $v_1, v_2$ ) that satisfy constraints I,II,III,IV.

- (iii) A region open to the point at infinity and bounded by two, three or four straight line segments (the case of four segments is illustrated in Fig. 4.12(b)).
- (iv) A null space, which implies that our initial assumption of contact at both nodes is false, so one or both of the nodes must separate under the given loads.

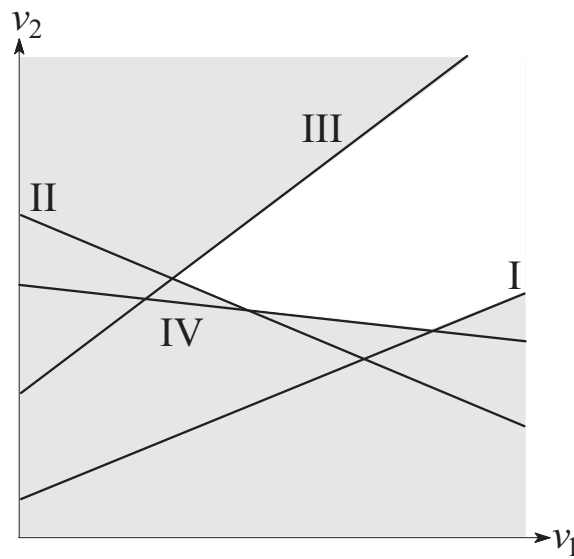
Notice that the vertex  $A$  of the triangle in Fig. 4.12(a) differs from the other two vertices in that it is an intersection between the two constraints for the same node. It follows that this point corresponds to the case where node 2 is on the point of separating. By contrast, the other two vertices correspond to points where both nodes are slipping or on the point of slipping.

#### 4.4.2 Wedging

In the special case where there is no external load ( $\mathbf{r}_i^w = 0$ ), all four constraint lines pass through the origin but have the same slope as under any other value of load. If these slopes are such as to lead to a bounded admissible region, as in Figs. 4.11 and 4.12(a),



(a)



(b)

Figure 4.12: Configurations of the constraints leading to an admissible region that is (a) a triangle or (b) a region open to infinity

this region will then shrink to a point, showing that the system relaxes to a unique position when the external loads are removed. However, under the same relaxation, case (iii) and Fig. 4.12(b) would reduce to a sector open to infinity, showing that the system is capable of becoming wedged, as defined in Section 4.2.

#### 4.4.3 Transient evolution of the system

At each instant during the transient process (and assuming the no-separation condition is satisfied), we must have a figure similar to one of Figs. 4.11 and 4.12, and the instantaneous values of  $v_1, v_2$  define an operating point within or on the boundary of the admissible region. As the external load  $r_i^w(t)$  changes in time, the four boundaries generally move. Slip will occur only when the operating point is on one or more boundaries and when the motion of these boundaries due to the change in load would otherwise cause the operating point to fall outside the new admissible region. Thus, the movement of the operating point can be viewed as a particle in the Figure that is ‘swept’ over the plane by the four moving constraints. Notice however that the motion of the operating point is not generally orthogonal to the corresponding constraint line, but is directed along the appropriate axis. For example, if the instantaneous operating point is at  $P$  in Fig. 4.13 and the constraint line IV advances so as to reduce the admissible region, the motion of  $P$  must be in the direction of the positive  $v_2$  axis as shown ( $\dot{v}_2 > 0$ ). In the same way, advance of constraint III will cause  $P$  to move downwards ( $\dot{v}_2 < 0$ ) and that of constraints I,II cause slip at node 1 in the directions  $\dot{v}_1 < 0, \dot{v}_1 > 0$  respectively.

It is this lack of orthogonality which constitutes the non-associative behavior of the frictional system and we shall see later that it can permit a state of cyclic slip to occur even when a safe shakedown state exists for the given loading. Slip will cause  $P$  to remain on the corresponding constraint line until it reaches an intersection between two constraints

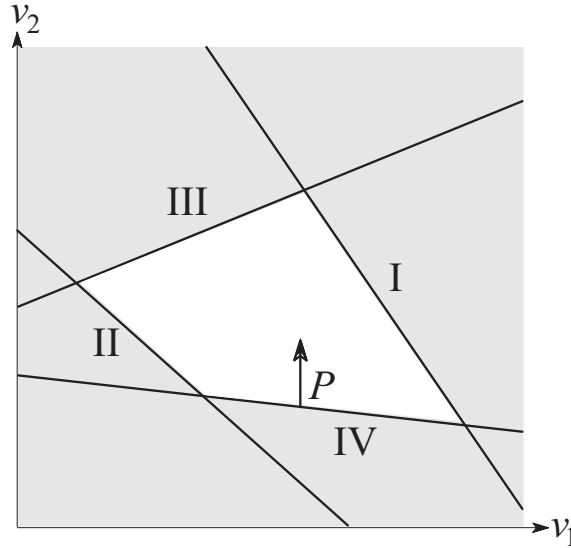


Figure 4.13: Motion of the instantaneous operating point  $P$  due to the advance of constraints IV.

or until the corresponding constraint ‘recedes’ leaving  $P$  strictly within the permissible region. In the former case, slip will also be initiated at the second node and  $P$  will remain in the corresponding corner until one or other of the intersecting constraints recedes.

This evolution mechanism places restrictions on the slopes of the four lines I,II,III,IV and hence on the magnitude of the coefficient of friction. For example, if constraint IV is rotated clockwise until it passes the vertical, it will no longer be able to push  $P$  upwards when it advances. If this condition holds and the other constraints are inactive, there is no admissible state involving both nodes in contact and we anticipate a discontinuous transition to separation at node 2. To avoid this possibility at each of the four constraints, the coefficient of friction must satisfy the condition

$$f < \min \left( \frac{A_{11}}{|B_{11}|}, \frac{A_{22}}{|B_{22}|} \right). \quad (4.23)$$

Comparison with Eq. (4.1) shows that this defines the critical coefficient of friction for a single-node system constructed by anchoring one of the two nodes. A related situation arises if the slope of the lines falls into the category (iii) of Section 4.4.1. In Fig. 4.12(b),

all the constraints satisfy Eq. (4.23) and in particular, advance of I pushes the operating point P to the left ( $\dot{v}_1 < 0$ ) and III pushes it down ( $\dot{v}_2 < 0$ ). However, if as a result of such motion P reaches an intersection between I and III, further advance of either of these constraints leads to an impossible scenario and once again we anticipate that there will be a discontinuous transition to a state involving separation. Of course, this case is also capable of wedging and we have already demonstrated in Section 4.2 that this implies the existence of loading scenarios involving displacement discontinuities.

#### 4.4.4 Periodic loading

We suppose that the system is exposed to periodic external loads, as in Eq. (4.13). The four components of  $\mathbf{r}_i^1(t)$  are independent functions of time, so no restrictions are imposed on the form of the loading cycle. In particular, it is not necessarily sinusoidal and the separate components are not assumed to be in phase. The four constraint lines will now advance and recede in a periodic manner and each will experience a time (generally different for each constraint) at which the region excluded is a maximum. These extreme positions can be defined as

$$\begin{aligned}
 (A_{11} - fB_{11})v_1 + (A_{12} - fB_{12})v_2 &\leq fp_1^0 - q_1^0 + \lambda(fp_1^1 - q_1^1)_{\min} & \text{I}^E \\
 (A_{11} + fB_{11})v_1 + (A_{12} + fB_{12})v_2 &\geq -fp_1^0 - q_1^0 + \lambda(-fp_1^1 - q_1^1)_{\max} & \text{II}^E \\
 (A_{21} - fB_{21})v_1 + (A_{22} - fB_{22})v_2 &\leq fp_2^0 - q_2^0 + \lambda(fp_2^1 - q_2^1)_{\min} & \text{III}^E \\
 (A_{21} + fB_{21})v_1 + (A_{22} + fB_{22})v_2 &\geq -fp_2^0 - q_2^0 + \lambda(-fp_2^1 - q_2^1)_{\max} & \text{IV}^E
 \end{aligned} \tag{4.24}$$

We can plot diagrams similar to Figs. 4.11 and 4.12 corresponding to these maximum excluded regions and any remaining admissible region will now be admissible at all times  $t$  during the loading cycle. If this region is not null, it implies that there exists a safe shakedown state for the system under the given cyclic loading. We shall demonstrate that shakedown always occurs if the safe shakedown region is defined by a quadrilateral, but that if the shakedown region is a triangle, initial conditions can be found in which the long

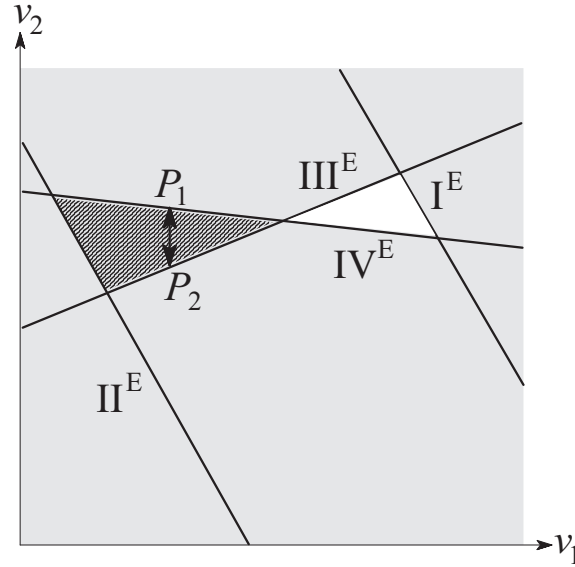


Figure 4.14: Cyclic slip limit cycle in the case where the safe shakedown region is triangular.

term state is cyclic slip.

We consider the latter case first. We suppose that the instantaneous admissible region at all times during the loading cycle is a quadrilateral, so that separation is not possible, but that the safe shakedown region defined by the extremal constraints  $I^E$ ,  $III^E$ ,  $IV^E$  is triangular as shown in Fig. 4.14. This implies that III and IV reach their extreme positions at different times during the cycle. The remaining extremal constraint  $II^E$  is inactive in regard to determining the possibility of shakedown, but it also forms a triangle with constraints  $III^E$ ,  $IV^E$  which we shall call the ‘complementary’ triangle.

Since the instantaneous admissible region is always a quadrilateral *ex hyp.*, there can be no time at which the instantaneous positions of III, IV intersect to the right of  $II^E$  and there must therefore be some instant at which an operating point  $P_1$  on the  $IV^E$  boundary of the complementary triangle is admissible. Suppose we start from this initial condition. At some later time, constraint III advances to its extreme position  $III^E$ , pushing  $P$  down to the point  $P_2$ , as shown in Fig. 4.14. Constraint III now recedes, but IV then advances

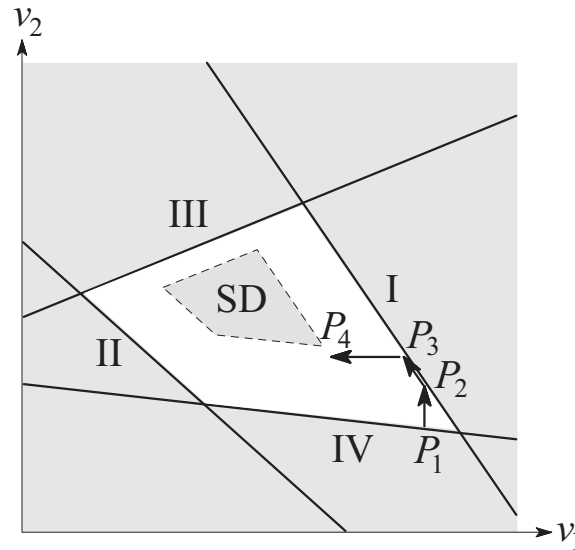


Figure 4.15: Progression of the operating point towards the safe shakedown region (SD) due to motion of constraints for two different nodes.

pushing  $P$  back up to  $P_1$ . This scenario permits indefinite cyclic slip to occur, since the only slip motion permitted on these boundaries involves the displacement  $v_2$  and this does not enable  $P$  to make any progress towards the safe shakedown region. Notice that if instead the friction law were associative, the motion caused by each constraint advancing would be normal to the constraint boundary, resulting in an accumulation of motion of the operating point to the right which would tend asymptotically to the apex of the safe triangle.

This cyclic slip mechanism depends critically on the existence of the complementary triangle, which is a region on the ‘inadmissible’ side of the two constraints corresponding to a single node, but within the region that is admissible throughout the loading cycle in regard to the other node, which therefore remains stuck during the limit cycle. By contrast, consider the motion of the operating point due to the advance and recession of two constraints at different nodes. If constraint IV advances in Fig. 4.15, the operating point  $P_1$  will move up to  $P_2$  at which point slip will also be initiated at node 1. Further

advance of IV will cause  $P$  to remain in the intersection of the two constraints (slipping at both nodes), following the path to  $P_3$ . If IV now recedes and I advances, slip will occur at node 1 only and will move  $P$  to the left to  $P_4$  as shown. On the next loading cycle,  $P$  will move up and then to the left due to the advance of IV and I respectively. This two step pattern will then be repeated, leading to an asymptotic and monotonic approach to the safe shakedown region (labelled SD in Fig. 4.15). Thus, when the two active constraints are associated with different nodes, the same sequence of advancing and receding constraints leads  $P$  towards the safe shakedown region. Notice that although approach to the safe shakedown region is monotonic, it can require a theoretically infinite number of loading cycles with geometrically decreasing slips. This falls within the definition of shakedown adopted by Klarbring *et al.*, (2007).

#### 4.4.5 Limiting values of the loading parameter $\lambda$

If the loading parameter  $\lambda$  in Eq. (4.13) is increased, the regions excluded by the extremal constraints  $I^E$ ,  $II^E$ ,  $III^E$ ,  $IV^E$  is increased, reducing the size of the safe shakedown region. This region must be a quadrilateral for  $\lambda = 0$ , since we assume that the mean load does not permit separation at either node. Thus, there will exist some critical value  $\lambda = \lambda_1$  at which the quadrilateral defined by the extremal constraints degenerates to a triangle. At this value, the edge of the quadrilateral that is about to disappear corresponds to a constraint line that passes through the apex of the newly generated triangle, and hence three of the extremal constraint lines pass through the same point.

Values of  $\lambda$  at which this condition is satisfied can be found by enforcing the equality in any three of  $I^E$ ,  $II^E$ ,  $III^E$ ,  $IV^E$  and solving the resulting linear algebraic equations for  $v_1, v_2, \lambda$ . Since any one of the four extremal constraints may be inactive, four such values can be obtained which we label such that  $0 < \lambda_1 < \lambda_2 < \lambda_3 < \lambda_4$ . They must all

be positive, since the definition ensures that increasing  $\lambda$  reduces the admissible region. Clearly the critical value as defined above must be the lowest of the four,  $\lambda_1$ .

Increase in  $\lambda$  above  $\lambda_1$  will reduce the size of the triangular safe shakedown region and this will become null for the case illustrated in Fig. 4.14 when the extremal constraints  $I^E$ ,  $III^E$ ,  $IV^E$  intersect in a point, corresponding to the value  $\lambda_2$ . The remaining values  $\lambda_3, \lambda_4$  correspond to intersections of three constraints within a region that is inadmissible with regard to the fourth inactive constraint and hence have no physical significance. Thus, we can define the shakedown behavior of the system by solving the constraints as equalities in four groups of three, and sorting the resulting values of  $\lambda$  in ascending order. For  $0 < \lambda < \lambda_1$ , the system will always shake down. For  $\lambda_1 < \lambda < \lambda_2$  it may shake down or may reach a limit cycle, depending on the initial conditions, and for  $\lambda > \lambda_2$  it will never shakedown.

#### 4.4.6 Separation

So far, we have restricted attention to systems in which the instantaneous admissible zone is always a quadrilateral, which implies that contact is maintained throughout the transient process. However, it is possible to remove this restriction if the coefficient of friction is below the value at which the transient evolution problem can exhibit displacement discontinuities. This excludes systems that are capable of wedging. Suppose that constraint IV in Fig. 4.11 advances until the instantaneous feasible domain has the triangular form of Fig. 4.12(b). If the original operating point  $P$  lies to the left of point  $A$  in this Figure, advance of IV will move it upwards until it lies at the instantaneous intersection of III and IV. Further advance of IV will then cause separation at node 2. We could still plot the location of  $P(v_1, v_2)$  during the separation phase, but this would not be useful, since the assumption of separation at node 2 would change the equations for the reactions at node

1 and hence modify the slope and location of constraints I and II. If the safe shakedown region is a quadrilateral, there must be some subsequent time at which constraint II lies to the right of the point  $A$ , at which point separation at node 2 is no longer possible. Under the assumption of continuity of displacements, the operating point must lie exactly at the intersection between III and IV at the instant that contact is re-established. Subsequent motion of  $P$  then follows the rules already established for both nodes being in contact and in particular  $P$  will be swept to the right of  $A$  by constraint II on its path to its extreme position, thus preventing separation in any subsequent cycle. Thus, it remains true that the system will shake down if the safe shakedown region is a quadrilateral, even if separation occurs at some point during the transient process.

## 4.5 Conclusions

The evolution of nodal slip  $v_i$  for the coupled two-node system is conveniently described by a process in which the frictional constraints ‘sweep’ the instantaneous operating point  $P(v_1, v_2)$  about the  $v_1v_2$ -plane. Shakedown is possible if and only if the extremal positions of these constraints define a non-null ‘safe shakedown region’.

Critical values of the load factor  $\lambda$  on the periodic component of load can be determined by solving any three of the four frictional constraints as equalities for  $v_1, v_2, \lambda$ . Four such values are obtained and below the smallest one, the system shakes down from all initial conditions. Between the first and second root, shakedown depends on the initial condition whereas above the second root, shakedown is impossible. A similar strategy can be devised for multi-node discrete frictional systems. These results apply for coefficients of friction below that at which the incremental problem involves displacement discontinuities and/or multiple solutions.

## CHAPTER V

# Shakedown Bounds of Coupled Multi-Node Discrete Frictional Systems

### 5.1 Introduction

The methodology described in Section 4.4 could be extended to discrete systems with more than two nodes. In a  $n$  contact nodes system, all critical values of  $\lambda$  can be obtained by solving a subset of  $n + 1$  constraints as equalities for the  $n$  values of  $v_i$  and  $\lambda$ , which requires that  $n + 1$  constraint planes intersect at a point.

In this Chapter, we will first introduce the general technique for determining all the possible critical loading factors and the lower shakedown limit for an elastic frictional contact problem with  $n$  contact nodes. Next, we will develop a linear programming method to determine the upper shakedown limit,  $\lambda^{\max}$ , above which the system will not shake down, among all the possible values. Finally, both methods are demonstrated with a simple elastic block contacting on a rigid support with a friction.

### 5.2 Procedure for Determining the Lower Bound ( $\lambda^{\min}$ )

We suppose that contact is maintained at all  $n$  contact nodes for a given loading cycle, so that the normal displacement  $w_j = 0$  ( $j = 1 \sim n$ ) for all nodes, and Eq. (2.11) becomes

$$q_j = q_k^w + A_{ji}v_i ; \quad p_j = p_k^w + B_{ji}v_i \quad (5.1)$$

where,  $q_k^w$  and  $p_k^w$  are the  $k^{\text{th}}$  tangential and normal reaction forces of a given loading cycle consisting of  $m$  loading steps.

For this state to be physically admissible for a given periodic reaction force vector  $\mathbf{r}_k^w$  ( $k = 1 \sim m$ ), the Coulomb friction law demands that we satisfy the inequality Eq. (2.4) at each node,  $j$ . Therefore, substituting Eq. (5.1) into Eq. (2.4) yields

$$-fp_k^w - fB_{ji}v_i \leq q_k^w + A_{ji}v_i \leq fp_k^w + fB_{ji}v_i. \quad (5.2)$$

Further, we consider that the system is exposed to periodic external loads which cause the following reaction forces

$$\mathbf{r}_k^w(t) = \mathbf{r}_j^0 + \lambda \mathbf{r}_k^1(t). \quad (5.3)$$

where  $\mathbf{r}_j^0$  is a mean load that is independent of time  $t$  at node  $j$ ,  $\mathbf{r}_k^1(t)$  is a periodic load with zero mean value, and  $\lambda$  is a scalar load factor.

Therefore, these constraint lines in Eq. (5.2) will advance and recede in a periodic manner because of  $\mathbf{r}_k^1(t)$  at each node  $j$ , and each will experience a time (generally different for each constraint) at which the region excluded is a maximum. As long as contact is maintained at all  $n$  nodes, the instantaneous slip displacements can be characterized as a point  $P(v_1, v_2, \dots, v_n)$  in an  $n$ -dimensional space, and the admissible region at any instant in the load cycle will then be defined by a set of  $2n$  constraints, each defined by the region on one side of a hyperplane. Shakedown is possible if and only if the region defined by the extremal positions of these constraints is non-null. If such a safe shakedown space exists, the motion of the constraints generally tends to push an operating point,  $P$ , towards it, as shown in the two-dimensional case described in Section 4.4. The inequalities of these

extreme positions for  $n$  node systems can be defined as

$$\begin{aligned}
(A_{11} - fB_{11})v_1 + \cdots + (A_{1n} - fB_{1n})v_n + (-fp_k^1 + q_k^1)_{\min} \lambda &\leq fp_1^0 - q_1^0 \\
(A_{11} + fB_{11})v_1 + \cdots + (A_{1n} + fB_{1n})v_n + (fp_k^1 + q_k^1)_{\max} \lambda &\geq -fp_1^0 - q_1^0 \\
&\vdots \\
(A_{n1} - fB_{n1})v_1 + \cdots + (A_{nn} - fB_{nn})v_n + (-fp_k^1 + q_k^1)_{\min} \lambda &\leq fp_n^0 - q_n^0 \\
(A_{n1} + fB_{n1})v_1 + \cdots + (A_{nn} + fB_{nn})v_n + (fp_k^1 + q_k^1)_{\max} \lambda &\geq -fp_n^0 - q_n^0
\end{aligned} \tag{5.4}$$

from Eqs. (5.2) and (5.3). The total number of constraint lines is  $2n$  because each node has two constraint lines.

Taking equalities from Eq. (5.4), this formulation can be written in matrix form as

$$\mathbf{E}\mathbf{x} = \mathbf{b}, \tag{5.5}$$

where

$$\mathbf{E} = \begin{bmatrix} (A_{11} - fB_{11}) & \cdots & (A_{1n} - fB_{1n}) & (-fp_k^1 + q_k^1)_{\min} \\ (A_{11} + fB_{11}) & \cdots & (A_{1n} + fB_{1n}) & (fp_k^1 + q_k^1)_{\max} \\ \vdots & \vdots & \vdots & \vdots \\ (A_{n1} - fB_{n1}) & \cdots & (A_{nn} - fB_{nn}) & (-fp_k^1 + q_k^1)_{\min} \\ (A_{n1} + fB_{n1}) & \cdots & (A_{nn} + fB_{nn}) & (fp_k^1 + q_k^1)_{\max} \end{bmatrix},$$

$$\mathbf{x} = [v_1, \cdots, v_n, \lambda]^T,$$

$$\mathbf{b} = [(fp_1^0 - q_1^0), (-fp_1^0 - q_1^0), \cdots, (fp_n^0 - q_n^0), (-fp_n^0 - q_n^0)]^T.$$

Note that the matrix  $\mathbf{E}$  is  $2n$  by  $n + 1$ , the vector  $\mathbf{x}$  is  $n + 1$  by 1, and the vector  $\mathbf{b}$  is  $2n$  by 1.

To set up the matrix in Eq. (5.5), we need to find the extreme points of the reaction forces at each node, which are assumed to be  $m$  discrete loading steps for one periodic loading loop.

For this, we first extract the contact reaction forces assuming that all the nodal displacements are constrained to be zero. Once the reaction forces are obtained, we divide them into a mean load and a periodic load as in Eq. (5.3). To determine the mean load, we have to sum each component ( $q_k^w$  and  $p_k^w$ ) of the reaction forces and divide it by the

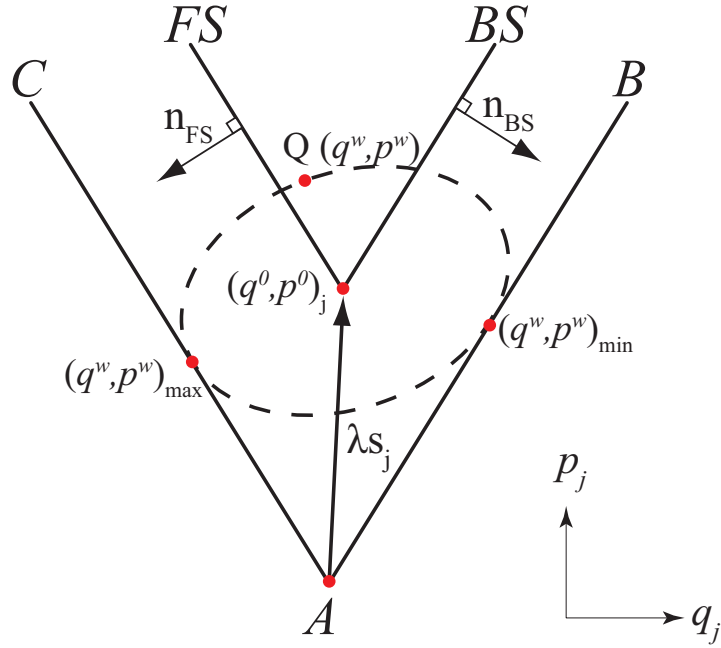


Figure 5.1: Configuration of extremal points in the given reaction loop consisting of  $m$  discrete values at node  $j$

number of discrete loading steps,  $m$ , resulting in

$$q_j^0 = \left( \sum_{k=1}^m q_k^w \right) / m, \quad p_j^0 = \left( \sum_{k=1}^m p_k^w \right) / m. \quad (5.6)$$

Hence, the periodic load at node  $j$  can be expressed in the form

$$q_k^1(t) = q_k^w(t) - q_j^0, \quad p_k^1(t) = p_k^w(t) - p_j^0, \quad k = 1 \sim m. \quad (5.7)$$

Using the given friction coefficient  $f$ , we can find the two line equations passing through the mean load,  $(q_j^0, p_j^0)$  at node  $j$ , as shown in Fig. 5.1.

These equations can be written as

$$\begin{aligned} q_j - fp_j + (fp_j^0 - q_j^0) &= 0 & (\text{B.S.}) \\ q_j + fp_j + (fp_j^0 - q_j^0) &= 0 & (\text{F.S.}) \end{aligned} \quad (5.8)$$

from Eq. (2.4). Further, we can define vectors  $\mathbf{n}_{BS} = (1, -f)$  and  $\mathbf{n}_{FS} = (1, f)$  which are perpendicular to the outer surface of each slip line, respectively. Also, let a point  $Q(q_k^w, p_k^w)$

denotes  $k^{\text{th}}$  reaction forces at node  $j$ . Given a line equation as in Eq. (5.8) and a point  $Q$  as shown in Fig. 5.1, the shortest distance of the point to the line can be formulated as

$$\begin{aligned} d(Q, \text{B.S.}) &= \text{B.S.}(Q) / \|\mathbf{n}_{\text{BS}}\| = (q_k^w - fp_k^w + (fp_j^0 - q_j^0)) / \sqrt{(1^2 + f^2)}, \\ d(Q, \text{F.S.}) &= \text{F.S.}(Q) / \|\mathbf{n}_{\text{FS}}\| = (q_k^w + fp_k^w + (fp_j^0 - q_j^0)) / \sqrt{(1^2 + f^2)}. \end{aligned} \quad (5.9)$$

By substituting every reaction force into Eq. (5.9), we can determine the extreme loading point, which is the one farthest from each slip line. Once the extremal point is determined, and the friction coefficient  $f$  is given, we can also define two line equations passing through each extremal point at each node  $j$ , which results in

$$\begin{aligned} q_j - fp_j + (fp_k^w - q_k^w)_{\min} &= 0 && \text{(line AB)} \\ q_j + fp_j + (fp_k^w - q_k^w)_{\max} &= 0. && \text{(line AC)} \end{aligned} \quad (5.10)$$

Therefore, the given reaction loop is tangential to both lines defined in Eq. (5.10). Further, we can define the vector,  $\mathbf{s}_j$ , passing through the intersection point  $A$  of both lines and the mean load. As a loading factor  $\lambda$  is increased, the trajectory of the mean load of the corresponding reaction loop, which is assumed to be tangential to both lines  $AB$  and  $AC$ , will move along the vector  $\mathbf{s}_j$ , and also the position of the extreme points will remain unchanged because of self similarity.

Once the extreme points for a reaction loop are determined, we can set up the matrix defined in Eq. (5.5). Then, we need to find all possible combinations of a subset of  $n + 1$  constraints as equalities for the  $n$  values of  $v_i$  and  $\lambda$ . Since the subset must not be repeated more than once, the number of all possible subsets can be found in the combination form,

$${}^{2n}C_{(n+1)} = \frac{(2n)!}{(n+1)!(n-1)!} \quad (5.11)$$

where  $2n$  is the number of all constraints, and  $n + 1$  is the number to be chosen, and  $!$  denotes the factorial.

Therefore, if we assign a number from 1 to  $2n$  to each row of the matrix  $\mathbf{E}$ , we can make a list consisting of the  $n + 1$  elements that correspond to each row in the matrix  $\mathbf{E}$ .

Provided that the subset of the list is determined, we can extract the corresponding rows from the matrix  $E$  that are a set of  $n + 1$  equations with  $n + 1$  unknowns. This can be written in the reduced matrix form as

$$E'x = b', \quad (5.12)$$

where the matrix  $E'$  is  $n + 1$  by  $n + 1$ , the vector  $b'$  is  $n + 1$  by 1, and the vector  $x$  is  $n + 1$  by 1, which consists of the  $n$  values of  $v_i$  and  $\lambda$ . This is the standard form of linear equations. Hence, by solving the linear equations in Eq. (5.12), we can find the  $n$  values of  $v_i$  and  $\lambda$  corresponding to a particular subset of the list.

To determine the smallest positive loading factor  $\lambda^{\min}$ , below which the system will always shake down, we repeat the same procedure throughout all possible subsets of the list, and we select the minimum positive loading factor among all possible values obtained.

### 5.3 Solution Method for Determining the Upper Bound ( $\lambda^{\max}$ )

In Section 5.2, the automated procedure for determining all critical values was described. As  $\lambda$  obtained is increased, the shape of the safe shakedown region will change at each of these critical values, and one of them will correspond to the upper shakedown limit,  $\lambda^{\max}$ , above which the system will not shake down. However, we cannot distinguish the upper limit without checking all these values obtained from the automated procedure. If contact nodes are increased, the number of values also increase rapidly as in Eq. (5.11), and it is not efficient to check them all. Therefore, it is necessary to explore a method to determine the upper bound.

We first consider a two-node problem subjected to a cyclic loading and discuss the properties at a shakedown state. Suppose that an oscillating external load is applied so that the vectors  $r_1^w$  and  $r_2^w$  track out known load loops on the two nodal reaction force diagram, as illustrated in Fig. 5.2.

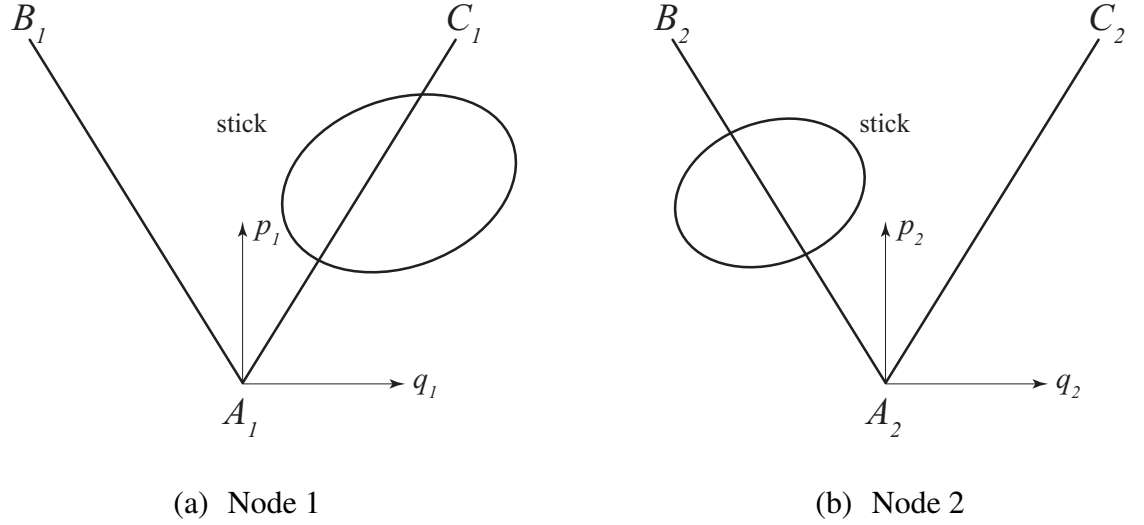


Figure 5.2: Configurations of load loops on the two nodal reaction force diagrams.

Assume that there exists a safe shakedown vector  $\tilde{\mathbf{v}} = [\tilde{v}_1, \tilde{v}_2]^T$  that makes both load loops move inside the respective stick sectors, i.e., the effect of changing  $\tilde{\mathbf{v}}$  is to cause a rigid-body motion of the load loops without change in their shape or orientation, as shown in Fig. 5.3. Therefore, given the loading factor  $\lambda$ , all reaction forces at both load loops must satisfy the stick condition in Eq. (2.4) in order to achieve a safe shakedown state, which yields

$$-fp_k^w - fB_{ji}\tilde{v}_i \leq q_k^w + A_{ji}\tilde{v}_i \leq fp_k^w + fB_{ji}\tilde{v}_i \quad (j = 1, 2; k = 1 \sim m). \quad (5.13)$$

where  $m$  is the number of loading steps at each node.

By substituting Eq. (5.3) into Eq. (5.13), we can rewrite the inequality stick conditions in the form

$$\begin{aligned} (A_{11} - fB_{11})\tilde{v}_1 + (A_{12} - fB_{12})\tilde{v}_2 + (-fp_k^1 + q_k^1)\lambda &\leq (fp_1^0 - q_1^0) \\ -(A_{11} + fB_{11})\tilde{v}_1 - (A_{12} + fB_{12})\tilde{v}_2 - (fp_k^1 + q_k^1)\lambda &\leq (fp_1^0 + q_1^0) \\ (A_{21} - fB_{21})\tilde{v}_1 + (A_{22} - fB_{22})\tilde{v}_2 + (-fp_k^1 + q_k^1)\lambda &\leq (fp_2^0 - q_2^0) \\ -(A_{21} + fB_{21})\tilde{v}_1 - (A_{22} + fB_{22})\tilde{v}_2 - (fp_k^1 + q_k^1)\lambda &\leq (fp_2^0 + q_2^0) \end{aligned} \quad (5.14)$$

where the subscripts in the formulations,  $q_j^0$  and  $p_j^0$ , denote the mean load at each node  $j$ .

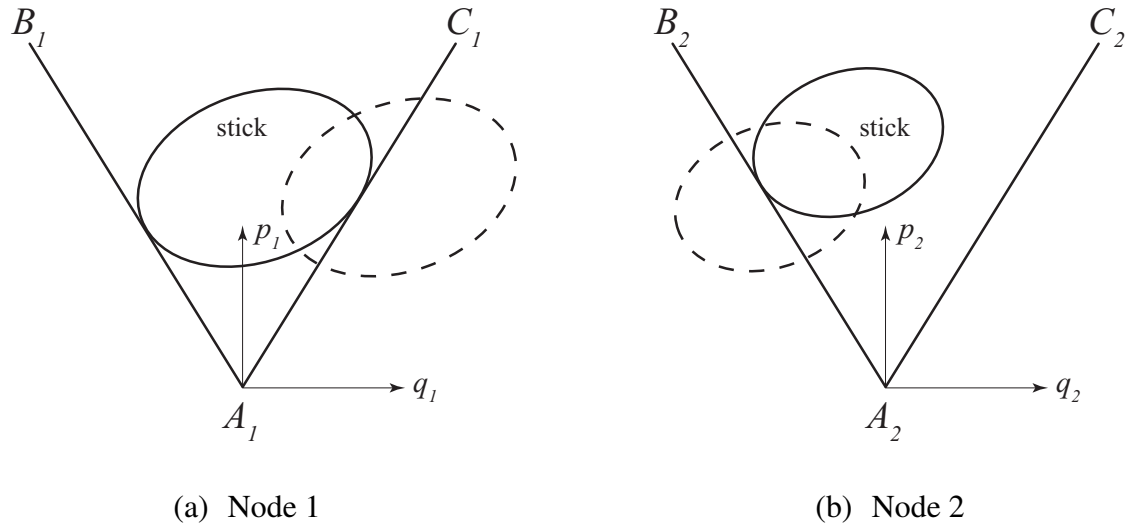


Figure 5.3: Configurations of shakedown state on the two nodal reaction force diagrams.

In Eq. (5.14) the total number of constraint is  $4m$  because each node has  $2m$  constraints. Now, provided that the loading factor  $\lambda$  is to be maximized as a variable, both a safe shakedown vector  $\tilde{v}$  and  $\lambda$  must satisfy  $4m$  inequality constraints in Eq. (5.14), each of which defines a plane separating the space  $R^3(v_1, v_2, \lambda)$  into two half spaces defining feasible and infeasible regions. The region enclosed by all constraints is feasible, and the maximum value of  $\lambda$  occurs on the boundary of the region along the  $\lambda$  axis. Therefore, we can convert this problem into a standard linear programming (LP) problem because the loading factor considered to be an objective function is linear in the design variables  $(v_1, v_2, \lambda)$ , and also the constraints are linear.

Similarly, a problem in an  $n$  contact node system,  $R^{n+1}(v_1, \dots, v_n, \lambda)$ , is to maximize the loading factor,  $\lambda$ , with the  $n$  values of  $v_i$  that place a loading loop at each node inside the stick sector defined in Eq. (5.2). In this case, each constraint defines a hyperplane that is  $n$  dimensional. The feasible region is a polytope in  $n + 1$  dimensions, and an extreme point occurs at the intersection of the  $n + 1$  hyperplanes forming the boundary of the

polytope. Also, a constraint will be active at a point if the constraint is satisfied with an equality. To convert the inequality constraints from Eqs. (5.2) and (5.3) into a standard LP problem, we can write them in LE (less than or equal) form,

$$\begin{aligned}
(A_{11} - fB_{11})v_1 + \cdots + (A_{1n} - fB_{1n})v_n + (-fp_k^1 + q_k^1)\lambda &\leq fp_1^0 - q_1^0 \\
-(A_{11} + fB_{11})v_1 + \cdots - (A_{1n} + fB_{1n})v_n - (fp_k^1 + q_k^1)\lambda &\leq fp_1^0 + q_1^0 \\
&\vdots \\
&\vdots \\
(A_{n1} - fB_{n1})v_1 + \cdots + (A_{nn} - fB_{nn})v_n + (-fp_k^1 + q_k^1)\lambda &\leq fp_n^0 - q_n^0 \\
-(A_{n1} + fB_{n1})v_1 + \cdots - (A_{nn} + fB_{n1n})v_n - (fp_k^1 + q_k^1)\lambda &\leq fp_n^0 + q_n^0
\end{aligned} \tag{5.15}$$

where  $n$  is the number of contact nodes, and  $k = 1 \sim m$ .

Further, because all inequality constraints in Eq. (5.15) are linear in the unknown variables, we can rewrite the previous formulation in matrix form, yielding

$$\begin{aligned}
&\text{maximize} && \lambda \\
&\text{subject to} && \mathbf{\Gamma}\mathbf{x} \leq \mathbf{b}
\end{aligned} \tag{5.16}$$

where

$$\begin{aligned}
\mathbf{\Gamma} &= \begin{bmatrix} (A_{11} - fB_{11}) & \cdots & (A_{1n} - fB_{1n}) & (-fp_k^1 + q_k^1) \\ (-A_{11} - fB_{11}) & \cdots & (-A_{1n} - fB_{1n}) & (-fp_k^1 - q_k^1) \\ \vdots & \vdots & \vdots & \vdots \\ (A_{n1} - fB_{n1}) & \cdots & (A_{nn} - fB_{nn}) & (-fp_k^1 + q_k^1) \\ (-A_{n1} - fB_{n1}) & \cdots & (-A_{nn} - fB_{nn}) & (-fp_k^1 - q_k^1) \end{bmatrix}, \\
\mathbf{x} &= [v_1, \cdots, v_n, \lambda]^T, \\
\mathbf{b} &= [(fp_1^0 - q_1^0), (fp_1^0 + q_1^0), \cdots, (fp_n^0 - q_n^0), (fp_n^0 + q_n^0)]^T.
\end{aligned}$$

Note that the matrix  $\mathbf{\Gamma}$  is  $2nm$  by  $n + 1$ , the vector  $\mathbf{x}$  is  $n + 1$  by 1, and the vector  $\mathbf{b}$  is  $2nm$  by 1.

To solve linear programming problems involving constraints, the simplex method developed by G. Dantzig (1947) has been widely used for numerical solution of the problems. The method provides a systematic algebraic procedure for moving from one extreme point to an adjacent one while improving the function values. To ensure the concept, we first consider a two-node system. For numerical implementation, we used the optimization toolbox within MATLAB program.

### 5.3.1 A Two-node System

A system comprises two contact nodes with three sub-matrices  $\mathbf{A}$ ,  $\mathbf{B}$ , and  $\mathbf{C}$ ,

$$\mathbf{A} = \begin{bmatrix} 243.92 & -43.91 \\ -43.91 & 262.78 \end{bmatrix}, \quad \mathbf{B} = \begin{bmatrix} 320.60 & 120.60 \\ -120.60 & 129.93 \end{bmatrix}, \quad \mathbf{C} = \begin{bmatrix} 804.04 & 80.40 \\ 80.40 & 642.46 \end{bmatrix}.$$

The both nodes remain in contact under time-varying external loads, resulting in contact nodal reactions  $\mathbf{r}_1^w$  and  $\mathbf{r}_2^w$ ,

$$\mathbf{r}_1^w(t) = \begin{Bmatrix} q_1^w(t) \\ p_1^w(t) \end{Bmatrix} = \begin{Bmatrix} 15.8 + 200\lambda \cos 2\pi(t - 0.05) \\ 588.5 + 150\lambda \sin 2\pi t \end{Bmatrix},$$

$$\mathbf{r}_2^w(t) = \begin{Bmatrix} q_2^w(t) \\ p_2^w(t) \end{Bmatrix} = \begin{Bmatrix} -400 + 700\lambda \cos 2\pi(t + 0.125) \\ 1300 + 300\lambda \sin 2\pi t \end{Bmatrix},$$

where  $\lambda$  is set at 1, and one load loop consists of  $m$  discrete steps.

### 5.3.2 Numerical Results

Using the given friction coefficient  $f = 0.35$ , the automated procedure in Section 5.2 computed the following four critical values,  $\lambda_1(= 0.6574) < \lambda_2(= 0.7391) < \lambda_3(= 1.0525) < \lambda_4(= 2.9349)$ . Therefore, the lower bound  $\lambda^{\min}$  is determined as  $\lambda_1$  with slip displacements  $v_1 = 1.5366$  and  $v_2 = 1.5936$ . Subsequently, the LP solution gave  $\lambda^{\max} = 0.7391$  with  $v_1 = -0.1564$  and  $v_2 = 1.2877$ . This value corresponds to  $\lambda_2$  obtained by the automated procedure.

To verify the accuracy of these results, we draw the admissible regions in  $v_1, v_2$  space at four different loading factors such as  $\lambda < \lambda^{\min}$ ,  $\lambda = \lambda^{\min}$ ,  $\lambda^{\min} < \lambda < \lambda^{\max}$ , and  $\lambda = \lambda^{\max}$ , respectively. At  $\lambda < \lambda^{\min}$ , a safe shakedown region enclosed by constraints shows a quadrilateral shape as in Fig. 5.4(a) so that the shakedown always occurs regardless of initial conditions. As the loading factor is increased at  $\lambda = \lambda^{\min}$ , the region is about to change from a quadrilateral to a triangle as in Fig. 5.4(b), implying that the loading factor is the minimum lower bound for the system to shake down. If the loading factor is located

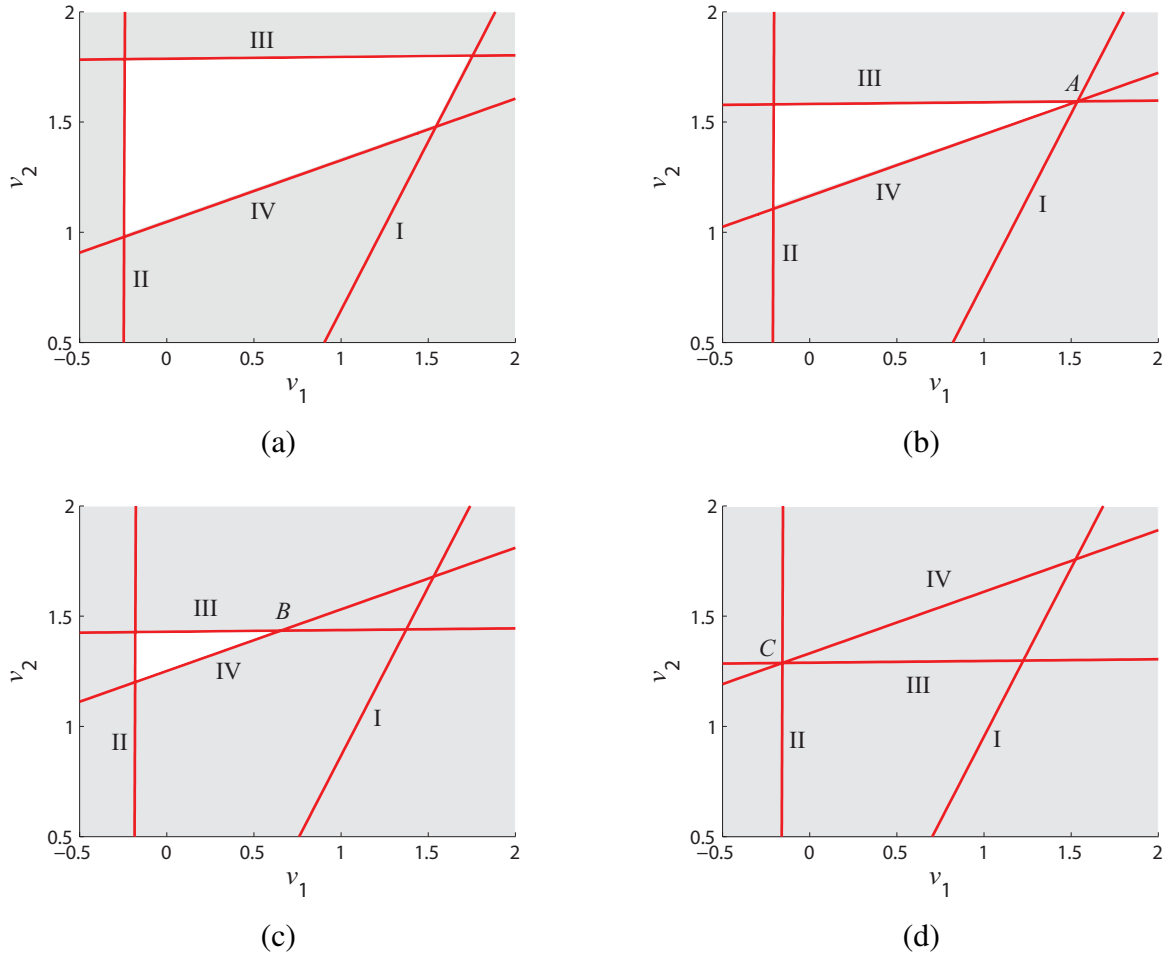


Figure 5.4: Configurations of the constraints leading to a safe shakedown region that is at  
 (a)  $\lambda < \lambda^{\min}$ , (b)  $\lambda = \lambda^{\min}$ , (c)  $\lambda^{\min} < \lambda < \lambda^{\max}$ , and (d)  $\lambda = \lambda^{\max}$ .

between  $\lambda_{\min}$  and  $\lambda_{\max}$ , the region has a complementary triangle defined in Section 4.4.4, in which cyclic slip can be found depending on the initial condition as a long term state. Finally, Fig. 5.4(d) shows the safe shakedown region shrinks to a point  $C$  at  $\lambda = \lambda^{\max}$ , above which the system will not shake down. Therefore, the results obtained from both methods agreed exactly with those expected.

## 5.4 Numerical Example for an $N$ -node System

To evaluate the robustness of the proposed methods that provide the lower and upper shakedown bounds of a multi-node system, the following example is presented.

### 5.4.1 Problem Description

The problem under consideration is illustrated in Fig. 5.5. A elastic body of height  $h$  and width  $4.5h$  has one fixed end, and the other end is contacting against a slanted rigid plane surface by the following time-varying external pressure  $p(t)$  exerted on the small strip of the upper surface;

$$p(t) = 5,000 + 1,000 \cos 10\pi(t + 0.1) .$$

We assume that the frictional problem is governed by Coulomb's law with a coefficient of friction  $f$ . Young's modulus and Poisson's ratio of the body are given by 200 GPa and 0.3, respectively. The deformation of the block is analyzed by the finite element method, and the contact surface is defined by a set of  $n(= 9)$  nodes,  $j = 1, n$ , as shown in Fig. 5.6. The normal and tangential nodal reaction forces acting on the contact surface are denoted by  $p_j$  and  $q_j$ , respectively. The problem is fully coupled in the sense that a normal reaction force induces relative tangential displacement, because the contact bodies are elastically dissimilar.

### 5.4.2 Numerical Result

Using the friction coefficient  $f = 0.4$ , the number of all possible loading factors are 43,758 as in Eq. (5.11). Fig. 5.7 shows nodal reaction force diagram at 1<sup>st</sup> and 9<sup>th</sup> nodes obtained by the automated procedure. We obtained the lower shakedown limit at  $\lambda^{\min}=0.0013$  from the automated procedure, and the upper shakedown limit  $\lambda^{\max}=1.0821$  with the corresponding safe shakedown vector  $\boldsymbol{v}$  from the LP solution method. If we use

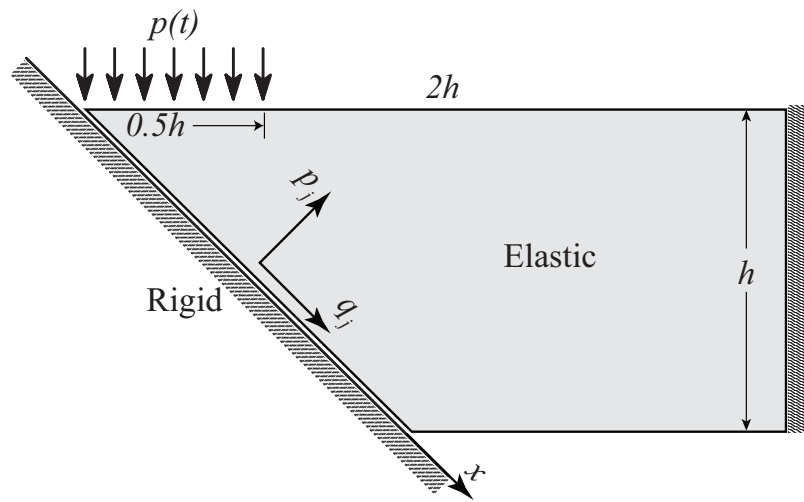


Figure 5.5: Configuration of a elastic block contacting on a rigid plane surface.

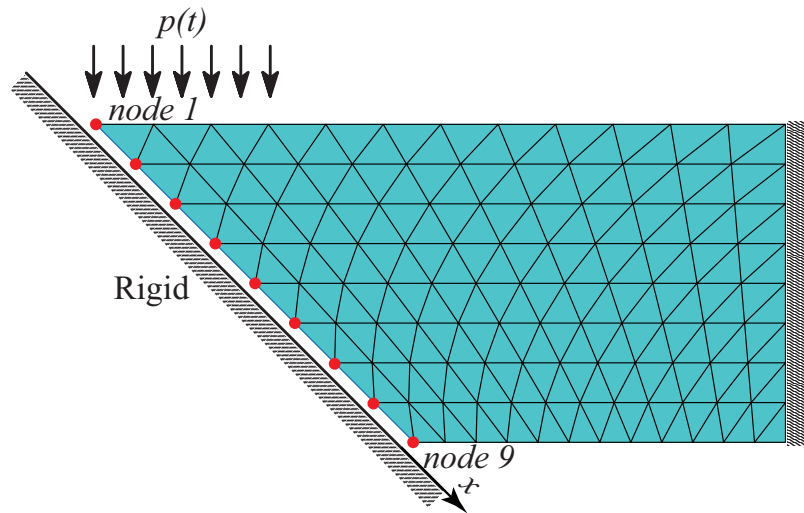
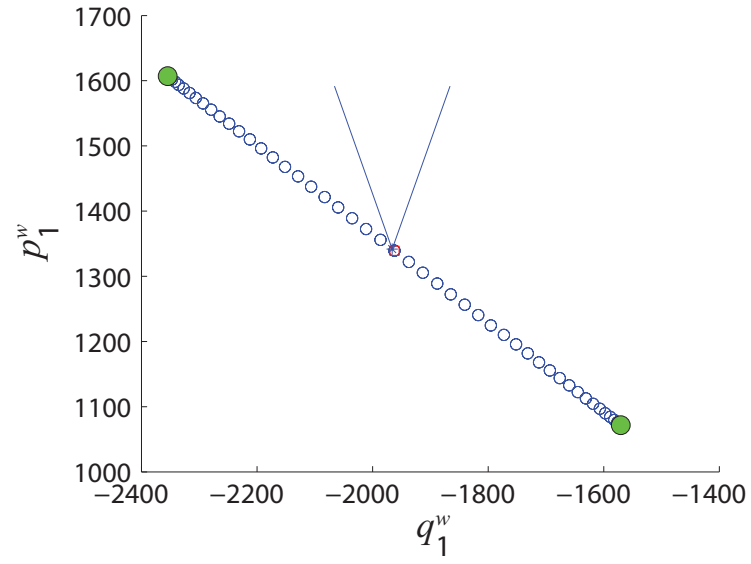
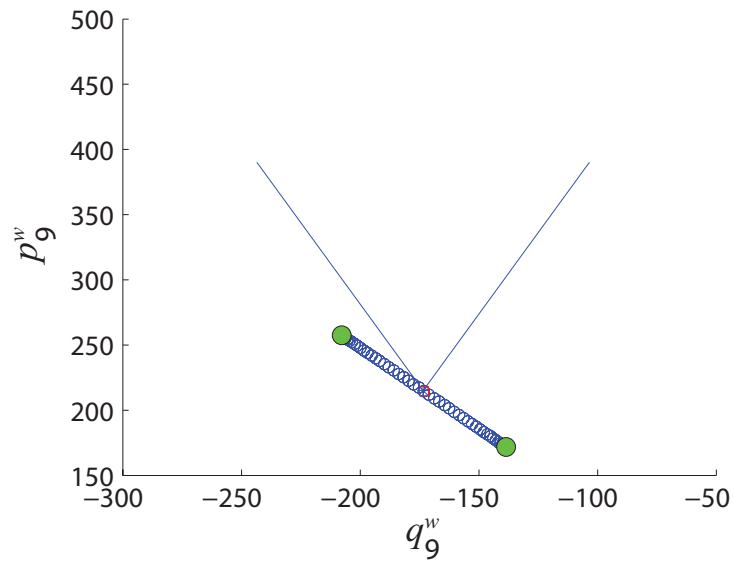


Figure 5.6: Configuration of the finite element mesh of a contact surface.



(a)



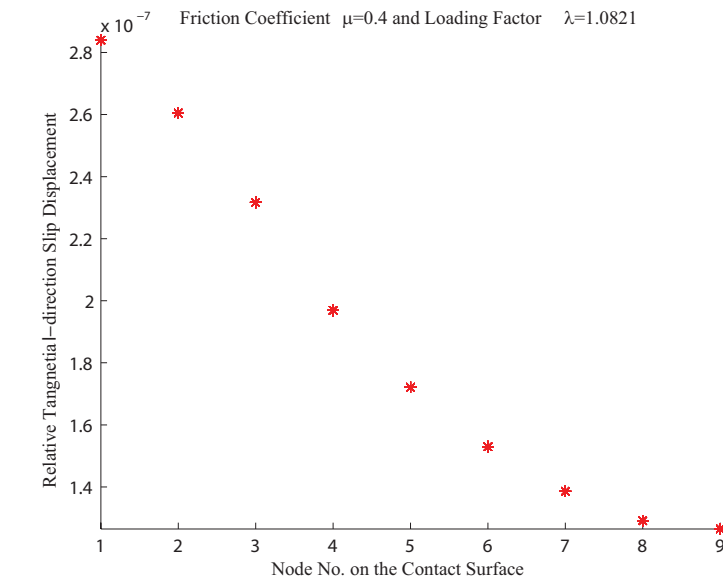
(b)

Figure 5.7: Configuration of reaction forces at (a) node 1 and (b) node 9 due to the time-varying external loading  $p(t)$ : two dots denote maximum and minimum extreme points, respectively.

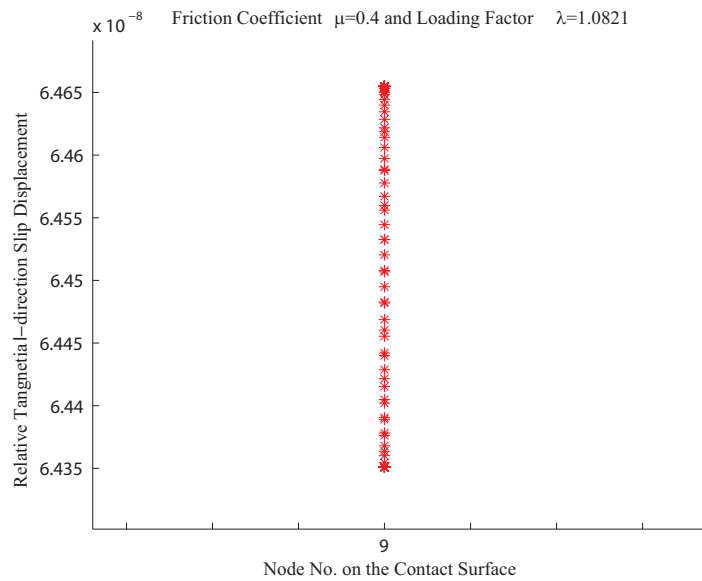
the safe shakedown vector  $v$  as initial conditions of the time evolution program at  $\lambda^{\max}$ , slips along the contact surface must cease over the whole loading cycles, as shown in Fig. 5.8(a). Otherwise, cyclic slips must occur for any other feasible initial conditions as shown in Fig. 5.8(b).

## 5.5 Conclusions

The methodology described in Section 4.4 can be extended to discrete systems with more than two nodes. We have illustrated this for the fixed end body pressed against a frictional rigid plane. Further, we introduce the linear programming method that can identify the upper shakedown limit. We showed that if the safe shakedown vector  $v$  corresponding to the vector at the upper shakedown is used as initial conditions, the system exhibits shakedown state.



(a)



(b)

Figure 5.8: Slip displacement distributions along the contact surface during the  $10^{th}$  loading cycle at the upper shakedown limit ( $\lambda = \lambda^{\max}$ ): (a) the safe shakedown vector  $\mathbf{v}$  is used as initial conditions and (b) arbitrary initial conditions except  $\mathbf{v}$  are used.

## CHAPTER VI

# Discontinuities for Elastic Quasi-static Evolution Problem

### 6.1 Introduction

As described in Section 4.2, difficulties are encountered with both existence and uniqueness of solutions for the general quasi-static elastic contact problem with Coulomb friction (Andersson and Klarbring, 2001). Cho and Barber (1998) used an analytical perturbation method to show that quasi-static slip in such conditions is always unstable in the sense that an infinitesimal perturbation from the quasi-static trajectory will grow without limit until a state change occurs either to stick or separation. They also predicted instantaneous jumps in position and state when the limiting friction condition is exceeded in one direction.

Using the  $v_1$  and  $v_2$  space described in Section 4.4, we can easily visualize the behavior of the frictional contact problem in a two-node coupled system and recognized that similarly to one node system, the quasi-static solution may also fail to define the unique state for some situations. For these cases, we will develop an analytical method to overcome friction induced instability in the context of a simple two-dimensional coupled discrete system comprising two contact nodes. In particular, we will examine whether there is a unique solution and demonstrate how to find it without using a transient dynamic approach.

## 6.2 The two-node system

### 6.2.1 Single node discontinuities in $v_1, v_2$ space

We consider the case where node 2 remains stuck and is strictly within the corresponding frictional bounds, whereas node 1 reaches the slip boundary defined by constraint I, as shown in Fig. 6.1. This corresponds to the inequality

$$q_1 \leq fp_1 \quad (6.1)$$

and at the limit of equality we have

$$q_1 = fp_1 \quad (6.2)$$

for which the flow rule from equation (2.9) is

$$\dot{v}_1 < 0 \quad (6.3)$$

Thus, when the constraint I reaches the operating point P, it must ‘push’ P to the left. This is possible if and only if the angle of inclination  $\theta$  of the line I to the vertical is between  $-\pi/2 < \theta < \pi/2$ . The angle  $\theta$  is positive provided it follows counter clockwise as shown in Fig. 6.1.

The critical condition arises when

$$A_{11} = fB_{11} \quad (6.4)$$

in Eq. (4.22).

For  $A_{11} > fB_{11}$ , regions on the right of the constraint line correspond to larger values of the left hand side of I in Eq. (4.22) and hence are inadmissible, whereas regions to the left are admissible. Thus, motion of  $v_1$  in the correct slip direction ( $\dot{v}_1 < 0$ ) takes P further into the admissible region. By contrast, for  $A_{11} < fB_{11}$ , regions to the left of the constraint line are inadmissible and hence no slip motion in the direction allowed by the flow rule is

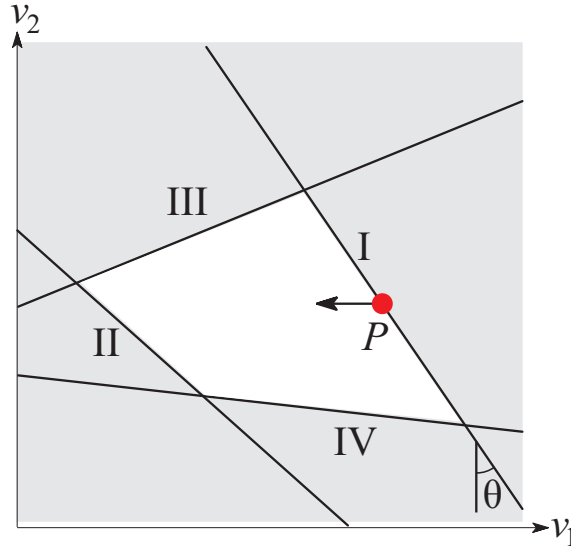


Figure 6.1: Motion of the instantaneous operating point  $P$  due to the advance of constraints I.

possible. The only remaining possibility is for the node to separate discontinuously since the reactions immediately before this transition are non-zero. We conclude that the critical coefficient of friction is

$$f_1 = \frac{A_{11}}{|B_{11}|}, \quad (6.5)$$

Similar arguments applied to constraints II,III,IV yield four critical coefficients in two equal and opposite pairs:

$$f_1, f_2, f_3, f_4 = \pm \frac{A_{11}}{|B_{11}|}, \pm \frac{A_{22}}{|B_{22}|}. \quad (6.6)$$

### 6.2.2 Both node discontinuities in $v_1, v_2$ space

Consider now the situation where the admissible region is open to infinity as in Fig. 6.2. Consider the case where constraint II advances until the only admissible region is an open triangle defined by II and III. We suppose that the coefficient of friction satisfies the condition

$$f < \min\{f_1, f_2, f_3, f_4\}, \quad (6.7)$$

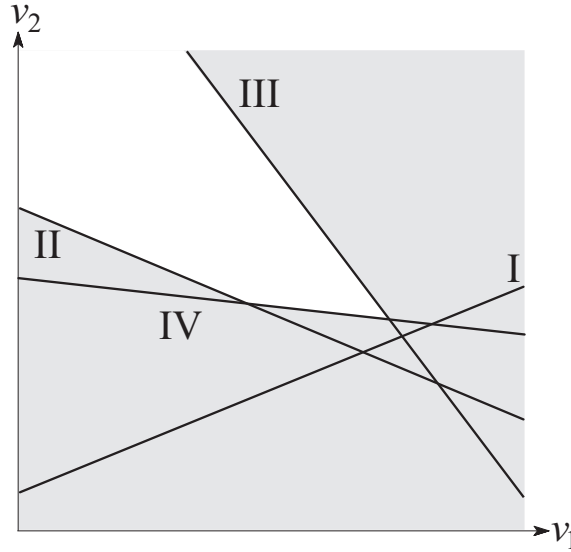


Figure 6.2: Configurations of the constraints leading to an admissible region that is a region open to infinity.

so that in particular both constraints II and III are able to move the operating point in an admissible direction when operating independently. In the case illustrated, II moves P to the right ( $\dot{v}_1 > 0$ ) and III moves P downwards ( $\dot{v}_2 < 0$ ). Suppose that we keep III fixed and advance II (the more general case leads to a similar conclusion). Once II becomes active, P will be moved to the right so as to stay on II until a situation is reached where P is at the intersection of II and III. Further advance of II or III is now impossible, since the only admissible motion is that with  $\dot{v}_1 > 0, \dot{v}_2 < 0$  and this sector is excluded by the constraints. Therefore, a discontinuous transition is the only option. The limiting coefficient of friction here is that where II and III are parallel, so

$$\det \begin{pmatrix} (A_{11} + fB_{11}) & (A_{12} + fB_{12}) \\ (A_{21} - fB_{21}) & (A_{22} - fB_{22}) \end{pmatrix} = 0, \quad (6.8)$$

or

$$A_{11}A_{22} - A_{12}A_{21} + (A_{22}B_{11} - A_{11}B_{22} + A_{12}B_{21} - A_{21}B_{12})f - (B_{11}B_{22} + B_{12}B_{21})f^2 = 0; \quad (6.9)$$

which defines two critical values of  $f$ . Notice that we need to impose an additional condition for this state to hold. Since II excludes the region to the left and III excludes that to the top, an admissible region between them will occur if and only if both lines slope upwards to the left and hence

$$A_{22} - fB_{22} > 0, \quad (6.10)$$

since we have already imposed  $A_{11} + fB_{11} > 0$  in requiring the constraint on  $f$  to be active. The corresponding condition where I and IV are parallel leads to identical equations except that  $f$  is replaced by  $-f$ . Additional conditions of the same kind can be obtained using the

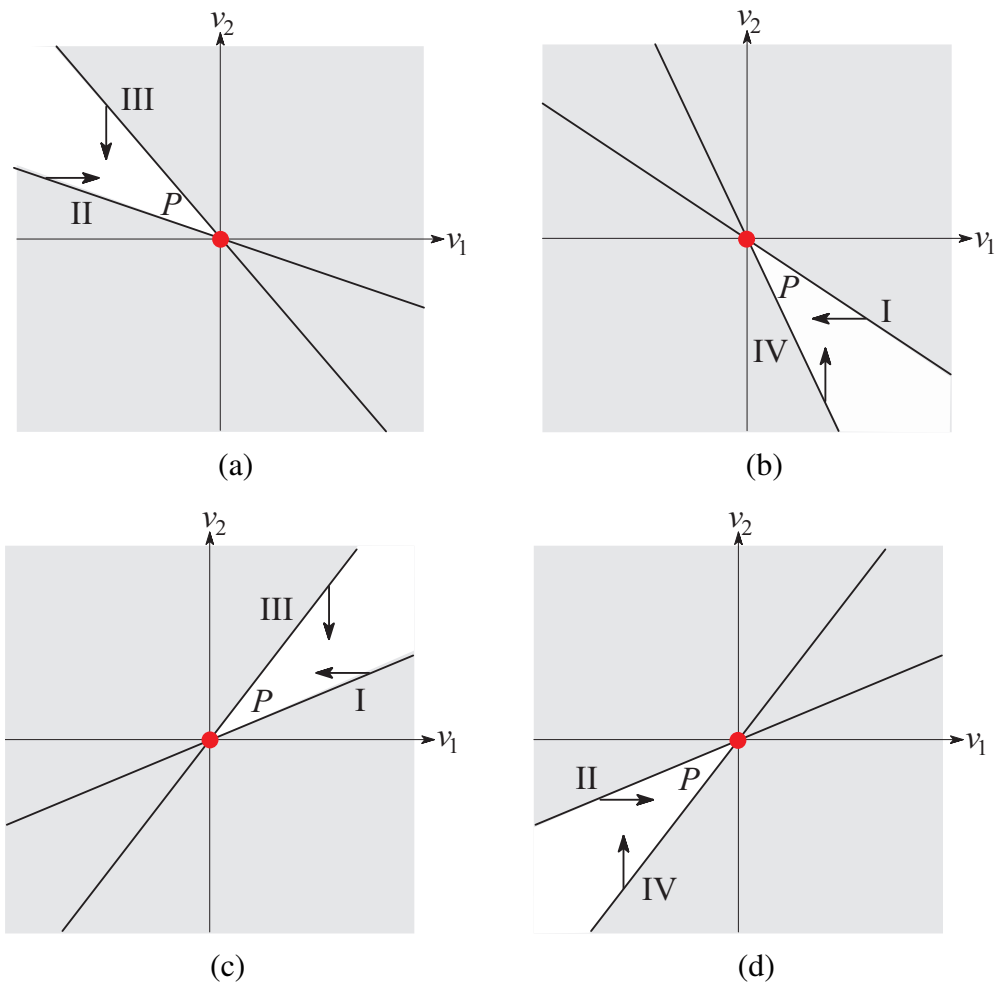


Figure 6.3: Four possible pairs in both node discontinuity.

pairs I,III and II,IV. In each case, constraints must be imposed to ensure that the limiting

case contains an admissible region, i.e.,  $A_{11} - fB_{11} > 0$  and  $A_{22} - fB_{22} > 0$  in the pair I,III. Fig. 6.3 shows four possible pairs for both node discontinuities in  $v_1, v_2$  space, assuming that there is no external loadings, i.e.,  $r^w = 0$ .

### 6.3 Perturbation analysis involving viscous damping

For the case where two-node discontinuity occurs, conditions (2.3-2.9) may fail to define a unique quasi-static evolution. In an attempt to resolve this problem, we can consider an elasto-dynamic formulation by introducing the effect of inertia or viscous damping.

We first examine whether a quasi-static evolution is stable with a viscosity term if we are not at a discontinuity point. We assume that an operating point reaches the slip boundary at node 1 defined by constraint I, remaining node 2 stuck, which yields

$$(A_{11} - fB_{11})v_1^* + q_1^w - fp_1^w = 0 . \quad (6.11)$$

where  $v_1^*$  represents the equilibrium value on the slip boundary I, and the external loadings are fixed at this time.

We now wish to examine whether a small perturbation on this equilibrium point can grow or not. By considering a small displacement perturbation  $\delta$  on the equilibrium point, Eq. (6.11) including a damping term can be written as

$$D\dot{v}_1 + (A_{11} - fB_{11})v_1 + q_1^w - fp_1^w = 0 , \quad (6.12)$$

where

$$v_1(t) = v_1^* + \delta v_1(t) .$$

Here,  $D$  represents a positive damping coefficient.

Using Eq. (6.11), Eq. (6.12) can be rewritten as

$$D\delta\dot{v}_1 + (A_{11} - fB_{11})\delta v_1 = 0 . \quad (6.13)$$

The stability of the system in backward slip depends on the homogenous solution in Eq. (6.13) that may grow or decay with time. The solution that contains one arbitrary constant  $a_1$  can be written as

$$\delta v_1(t) = a_1 e^{-bt} , \quad (6.14)$$

where

$$b = \frac{A_{11} - fB_{11}}{D} .$$

If single node discontinuity doesn't occur in a system that satisfies the condition  $A_{11} > fB_{11}$ , the perturbation in Eq. (6.14) decays with time since  $b$  is a positive value. Thus, if the operating point is not at a discontinuity point, solution for a quasi-static evolution is always stable.

In comparison, we now suppose that a quasi-static evolution algorithm reaches a discontinuity point at  $(v_1^*, v_2^*)$  for the case where both constraint II and III are unable to move further, as shown in Fig. 6.3(a), yielding

$$(A_{11} + fB_{11})v_1^* + (A_{12} + fB_{12})v_2^* + q_1^w + fp_1^w = 0 , \quad (6.15)$$

$$(A_{21} - fB_{21})v_1^* + (A_{22} - fB_{22})v_2^* + q_2^w - fp_2^w = 0 , \quad (6.16)$$

where  $(v_1^*, v_2^*)$  can be obtained by solving Eqs. (6.15 - 6.16) simultaneously, assuming that the stiffness matrix, friction coefficient and external loadings,  $\mathbf{r}^w$ , are determined at a given evolution time,  $\tau$ . At the point, a discontinuous transition is the only possible prediction. However, we may distinguish two different cases: (1) where both nodes are separated, or (2) one node is separated. The distinction depends on the external loading,  $\mathbf{r}^w$ .

### 6.3.1 Both nodes separated at discontinuity point

If both nodes are separated, reactions along the contact area must be zero. Therefore, Eq. (2.10) becomes

$$[v_1, v_2, w_1, w_2]^T = -\boldsymbol{\kappa}^{-1} [q_1^w, q_2^w, p_1^w, p_2^w]^T. \quad (6.17)$$

Since normal displacement at both nodes must be positive, i.e.,  $w_1 > 0$  and  $w_2 > 0$ , two inequality equations obtained from Eq. (6.17) constrain the feasible region of external loadings,  $\boldsymbol{r}^w$ . We can also define the feasible region of external loadings for the case where two-nodes discontinuity occurs, as in Section 6.2.2. Hence, if an overlap area exists between two feasible regions, these external loadings in the overlapped region make the two separate at the discontinuity point.

### 6.3.2 One node separated at discontinuity point

In an attempt to resolve the case where external loadings do not make the two separate, we introduce a viscous damping matrix into Eq.(2.10), yielding

$$[q_1, q_2, p_1, p_2]^T = [q_1^w, q_2^w, p_1^w, p_2^w]^T + \boldsymbol{\kappa} [v_1, v_2, w_1, w_2]^T + \boldsymbol{D} [\dot{v}_1, \dot{v}_2, \dot{w}_1, \dot{w}_2]^T, \quad (6.18)$$

where  $\boldsymbol{D}$  is a 4 by 4 damping matrix consisting of diagonal damping coefficient terms,  $D_{ii}$  ( $i = 1 \sim 4$ ).

We now wish to see whether a small perturbation at the discontinuity point,  $(v_1^*, v_2^*)$ , can grow or decay in the transient dynamic time scale,  $t$ , which should be distinct from the quasi-static evolution time scale,  $\tau$ . Note that the dynamic time scale,  $t$ , is considered to be much faster than the time in the quasi-static algorithm.

Let

$$v_1(t) = v_1^* + \delta v_1(t), \quad v_2(t) = v_2^* + \delta v_2(t) \quad (6.19)$$

where  $\delta v_i$  represents a small perturbation for each node  $i$ . After taking the derivative of Eq. (6.19) with respect to time,  $t$ , the velocities  $\dot{v}_1$  and  $\dot{v}_2$  are written as

$$\dot{v}_1(t) = \delta \dot{v}_1(t), \quad \dot{v}_2(t) = \delta \dot{v}_2(t) \quad (6.20)$$

since  $v_1^*$  and  $v_2^*$  are both constants. Thus, by substituting Eqs. (6.19 - 6.20) into the inequalities II and III in Eq. (4.22), we can express these equations as

$$D_{11}\dot{v}_1 + (A_{11} + fB_{11})v_1 + (A_{12} + fB_{12})v_2 + q_1^w + fp_1^w = 0, \quad (6.21)$$

$$D_{33}\dot{v}_2 + (A_{21} - fB_{21})v_1 + (A_{22} - fB_{22})v_2 + q_2^w - fp_2^w = 0. \quad (6.22)$$

Further, Eqs. (6.21 - 6.22) reduce to the following homogeneous equations

$$D_{11}\delta \dot{v}_1 + (A_{11} + fB_{11})\delta v_1 + (A_{12} + fB_{12})\delta v_2 = 0, \quad (6.23)$$

$$D_{22}\delta \dot{v}_2 + (A_{21} - fB_{21})\delta v_1 + (A_{22} - fB_{22})\delta v_2 = 0, \quad (6.24)$$

since Eqs. (6.15 - 6.16) become zero at the discontinuity point,  $(v_1^*, v_2^*)$ . The corresponding matrix equation is

$$\delta \dot{\mathbf{v}} = \mathbf{H} \delta \mathbf{v}. \quad (6.25)$$

where

$$\mathbf{H} = \begin{bmatrix} \frac{-(A_{11}+fB_{11})}{D_{11}} & \frac{-(A_{12}+fB_{12})}{D_{11}} \\ \frac{-(A_{21}-fB_{21})}{D_{22}} & \frac{-(A_{22}-fB_{22})}{D_{22}} \end{bmatrix}. \quad (6.26)$$

Hence, the disturbances  $\delta v_1$  and  $\delta v_2$  evolve in time, and the general solution for  $\delta \mathbf{v}$  is

$$\delta \mathbf{v}(t) = a_1 e^{\lambda_1 t} \boldsymbol{\eta}_1 + a_2 e^{\lambda_2 t} \boldsymbol{\eta}_2. \quad (6.27)$$

where  $\lambda$  is an eigenvalue representing a growth rate, and  $\boldsymbol{\eta}$  is an eigenvector with corresponding eigenvalue,  $\lambda$ . The  $\lambda$ s can be found by the characteristic equation  $\det(\mathbf{H} - \lambda \mathbf{I}) = 0$ , where  $\mathbf{I}$  is the 2 by 2 identity matrix. The characteristic equation becomes

$$\det \begin{pmatrix} H_{11} - \lambda & H_{12} \\ H_{21} & H_{22} - \lambda \end{pmatrix} = 0. \quad (6.28)$$

Expanding the determinant yields

$$\lambda^2 - \alpha\lambda + \beta = 0 \quad (6.29)$$

where  $\alpha = \text{trace}(\mathbf{H})$ ,  $\beta = \det(\mathbf{H})$ . Then,

$$\lambda_1 = \frac{\alpha - \sqrt{\alpha^2 - 4\beta}}{2}, \quad \lambda_2 = \frac{\alpha + \sqrt{\alpha^2 - 4\beta}}{2}. \quad (6.30)$$

From these equations, we can find the eigenvalues. Also, the general solution in Eq. (6.27) contains two arbitrary constants,  $a_1$  and  $a_2$ , to enable us to satisfy initial conditions on  $\delta\dot{v}_1(0)$  ( $> 0$ ) and  $\delta\dot{v}_2(0)$  ( $< 0$ ) from the velocity equation

$$\delta\dot{\mathbf{v}}(t) = a_1\lambda_1 e^{\lambda_1 t} \boldsymbol{\eta}_1 + a_2\lambda_2 e^{\lambda_2 t} \boldsymbol{\eta}_2. \quad (6.31)$$

Therefore, there are three possible scenarios for giving an infinitesimal perturbation, i.e.,

- (i) Node 1 is stick ( $\delta\dot{v}_1 = 0$ ) and node 2 is backward slip ( $\delta\dot{v}_2 < 0$ ),
- (ii) Node 1 is forward slip ( $\delta\dot{v}_1 > 0$ ) and node 2 is stick ( $\delta\dot{v}_2 = 0$ ),
- (iii) Node 1 is forward slip ( $\delta\dot{v}_1 > 0$ ) and node 2 is backward slip ( $\delta\dot{v}_2 < 0$ ).

Note that the first two cases could not give a meaningful result since the system always returns to the original discontinuity point because of its negative eigenvalue. However, if the system is perturbed slightly at both nodes, as in the third case, the system will be unstable and depart from the discontinuity point. Hence, we will consider the behavior of only the third case.

Suppose that the eigenvalues in Eq. (6.30) are real number, i.e.,  $\alpha^2 - 4\beta \geq 0$ . Note that  $\alpha$  is always negative value since we have already imposed  $A_{11} - fB_{11} > 0$  and  $A_{22} - fB_{22} > 0$ . Therefore,  $\lambda_1$  is always negative value, but the sign of  $\lambda_2$  depends only

on the trace and determinant of the matrix  $\mathbf{H}$ . Especially, the limiting case  $\lambda_2 = 0$  occurs when  $\det(\mathbf{H}) = 0$ , i.e.,

$$H_{11}H_{22} - H_{12}H_{21} = 0 . \quad (6.32)$$

Note that the limiting condition in Eq. (6.32) is the same as the condition of the limiting coefficient of friction as in Eq. (6.8).  $\lambda_2$  is a positive value when  $\det(\mathbf{H}) < 0$ . Then, an infinitesimal perturbation for  $\delta\mathbf{v}$  will grow exponentially because of second term in Eq. (6.27) until normal reaction force at either nodes become zero at a given time,  $t = t_1$ , at which a state change occurs from slip to separation. The variation of normal reactions can be computed by the following equations

$$p_1(t) = B_{11}\delta v_1 + B_{12}\delta v_2 + B_{11}v_1^* + B_{12}v_2^* + p_1^w , \quad (6.33)$$

$$p_2(t) = B_{21}\delta v_1 + B_{22}\delta v_2 + B_{21}v_1^* + B_{22}v_2^* + p_2^w . \quad (6.34)$$

Further, if we assume that normal reaction force at node 2 becomes zero earlier than at node 1, node 1 maintains forward slip state and node 2 changes from backward slip to separation state at  $t = t_1$ . Therefore, we need to set up the equations again that satisfy the Coulomb friction boundary conditions at both nodes. In order to find the system behavior for the time  $t \geq t_1$ , similar techniques can be used, as in the previous state. First, let

$$[v_1(t), v_2(t), w_1(t), w_2(t)]^T = [v_1^* + \delta v_1(t), v_2^* + \delta v_2(t), \delta w_1(t), \delta w_2(t)]^T . \quad (6.35)$$

Hence, the velocities are

$$[\dot{v}_1(t), \dot{v}_2(t), \dot{w}_1(t), \dot{w}_2(t)]^T = [\delta\dot{v}_1(t), \delta\dot{v}_2(t), \delta\dot{w}_1(t), \delta\dot{w}_2(t)]^T \quad (6.36)$$

since  $v_1^*$  and  $v_2^*$  are both constants.

By applying friction boundary conditions at node 1 ( $q_1 = -fp_1, \delta w_1(t) = 0, \delta\dot{w}_1(t) = 0$ ) and at node 2 ( $q_2 = 0, p_2 = 0$ ), and by substituting Eq. (6.36) into Eq. (6.18), the

following governing equation can be obtained

$$\begin{aligned} D_{11}\delta\dot{v}_1 + (A_{11} + fB_{11})\delta v_1 + (A_{12} + fB_{12})\delta v_2 + (B_{21} + fC_{12})\delta w_2 + r_1^* &= 0, \\ D_{22}\delta\dot{v}_2 + A_{21}\delta v_1 + A_{22}\delta v_2 + B_{22}\delta w_2 + q_2^* &= 0, \\ D_{44}\delta\dot{w}_2 + B_{21}\delta v_1 + B_{22}\delta v_2 + B_{22}\delta w_2 + p_2^* &= 0. \end{aligned} \quad (6.37)$$

where

$$\begin{aligned} r_1^* &= (A_{11} + fB_{11})v_1^* + (A_{12} + fB_{12})v_2^* + q_1^w + fp_1^w, \\ q_2^* &= A_{21}v_1^* + A_{22}v_2^* + q_2^w, \\ p_2^* &= B_{21}v_1^* + B_{22}v_2^* + p_2^w. \end{aligned} \quad (6.38)$$

Notice that  $r_1^*$  in Eq. (6.38) becomes zero from Eq. (6.15). These equations can be written in matrix form as

$$\delta\dot{\mathbf{x}} + \mathbf{G}\delta\mathbf{x} = \mathbf{P}^* \quad (6.39)$$

where

$$\begin{aligned} \delta\mathbf{x} &= [\delta v_1, \delta v_2, \delta w_2]^T, \\ \delta\dot{\mathbf{x}} &= [\delta\dot{v}_1, \delta\dot{v}_2, \delta\dot{w}_2]^T, \\ \mathbf{G} &= \begin{bmatrix} \frac{A_{11}+fB_{11}}{D_{11}} & \frac{A_{12}+fB_{12}}{D_{11}} & \frac{B_{21}+fC_{12}}{D_{11}} \\ \frac{A_{21}}{D_{22}} & \frac{A_{22}}{D_{22}} & \frac{B_{22}}{D_{22}} \\ \frac{B_{21}}{D_{44}} & \frac{B_{22}}{D_{44}} & \frac{C_{22}}{D_{44}} \end{bmatrix}, \\ \mathbf{P}^* &= [0, -q_2^*/D_{22}, -p_2^*/D_{44}]^T. \end{aligned} \quad (6.40)$$

The general solution,  $\mathbf{g}$ , for Eq. (6.39) can be written as the sum of a particular solution,  $\mathbf{g}_P(t)$  and the homogeneous solution,  $\mathbf{g}_H(t)$  which will contain three arbitrary constants to enable us to satisfy the following initial conditions,

$$\mathbf{g} = \mathbf{g}_H + \mathbf{g}_P, \quad (6.41)$$

$$\text{subjected to } \delta\mathbf{x}(t_1) = [\delta v_1(t_1), \delta v_2(t_1), 0]^T.$$

By the characteristic equation  $\det(\mathbf{G} - \lambda\mathbf{I})$ , three  $\lambda_s$  can be found, and the homogeneous solution in Eq. (6.41) is

$$\mathbf{g}_H = a_1 e^{\lambda_1 t} \boldsymbol{\eta}_1 + a_2 e^{\lambda_2 t} \boldsymbol{\eta}_2 + a_3 e^{\lambda_3 t} \boldsymbol{\eta}_3 \quad (6.42)$$

where  $a_1 \sim a_3$  are arbitrary constants,  $\lambda_1 \sim \lambda_3$  are eigenvalues, and  $\boldsymbol{\eta}_1 \sim \boldsymbol{\eta}_3$  are eigenvectors corresponding to each  $\lambda$ .

If we assume that all  $\lambda_s$  are negative value, notice that the homogeneous solution,  $\mathbf{g}_H$ , becomes zero as  $t \rightarrow \infty$  since all terms exponentially decay. Therefore, the general solution for Eq. (6.39) is determined by the following particular solution,

$$\mathbf{g} = \mathbf{g}_P = \mathbf{G}^{-1} \mathbf{P}^* \quad (6.43)$$

where superscript  $-1$  represents the matrix inverse. Furthermore, expanding the inverse matrix of  $\mathbf{G}$  in Eq. (6.43) yields

$$\mathbf{G}^{-1} = \begin{bmatrix} G_{11}D_{11} & G_{21}D_{22} & G_{31}D_{44} \\ G_{21}D_{11} & G_{22}D_{22} & G_{32}D_{44} \\ G_{31}D_{11} & G_{23}D_{22} & G_{33}D_{44} \end{bmatrix} \quad (6.44)$$

where each column includes the same damping coefficient, and the other coefficients are determined by the particular stiffness matrix and friction coefficient. By substituting Eq. (6.44) into Eq. (6.43), we can prove that the final state is not affected by the damping coefficients since these are canceled out by multiplication between  $\mathbf{G}^{-1}$  and  $\mathbf{P}^*$ . Also, notice that since the vector,  $\mathbf{P}^*$ , is determined by particular values at the point that discontinuity occurs, it is possible for us to predict the final state of the system without involving the transient dynamic analysis.

## 6.4 Numerical example

We will now investigate the behavior of a system with the following stiffness matrixes,

$$\mathbf{A} = \begin{bmatrix} 0.4276 & 0.1754 \\ 0.1754 & 0.1216 \end{bmatrix}, \quad \mathbf{B} = \begin{bmatrix} -0.1011 & -0.0220 \\ -0.0530 & 0.1082 \end{bmatrix}, \quad \mathbf{C} = \begin{bmatrix} 0.3005 & 0.0012 \\ 0.0012 & 0.5522 \end{bmatrix}. \quad (6.45)$$

From Eq. (6.6), the constraints for single-node discontinuity yield four critical coefficients,

$$f_s = \pm 1.1241, \pm 4.2290, \quad (6.46)$$

and, Eq. (6.9) yields a total of eight critical coefficients for the four pairs,

$$f_b = \pm 0.3557, \pm 0.4079, \pm 4.3009, \pm 4.9314. \quad (6.47)$$

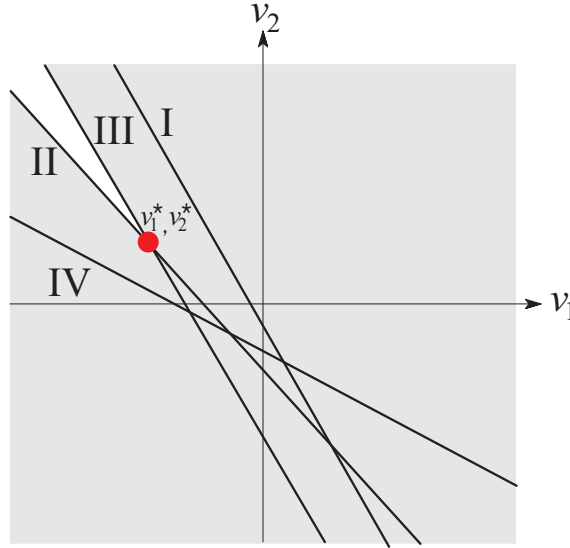


Figure 6.4: Configuration for two-node discontinuity in the pair II and III.

Therefore, the minimum critical coefficient occurs at  $f_c = 0.3557$  for two-node discontinuity in the pair II and III, and it also makes the pair II and III admissible regions,  $A_{11} + fB_{11} > 0$  and  $A_{22} + fB_{22} > 0$ .

For further investigation, we set  $f = 0.39$  for the case  $f_c < f < f_s$ . Additionally, all diagonal entries of a damping matrix,  $D$ , are set at one(1) and the others are set at zero(0). Also, external loadings are defined as

$$[q_1^w, q_2^w, p_1^w, p_2^w]^T = [2.5, 2, 1, 1]^T. \quad (6.48)$$

Note that these external loadings belong to the feasible region of two-node discontinuity, but not to the feasible region for both nodes to separate. By solving Eqs. (6.15 - 6.16) simultaneously, we can find the discontinuity point,

$$[v_1^*, v_2^*]^T = [-20.7296, 30.9087]^T, \quad (6.49)$$

and the configuration of the four constraint lines in Eq. (4.22) is illustrated in Fig. 6.4.

From Eqs. (6.18-6.24), the system matrix is

$$\delta \dot{\mathbf{v}} = \begin{bmatrix} -0.3881 & -0.1668 \\ -0.1961 & -0.0794 \end{bmatrix} \delta \mathbf{v} . \quad (6.50)$$

For the general solution in Eq. (6.27), we need first to find the eigenvalues of the matrix.

From Eq. (6.30), we can find the eigenvalues,

$$\lambda_1 = -0.4716, \quad \lambda_2 = 0.0039 . \quad (6.51)$$

Next, for a given eigenvalue  $\lambda$ , we find the eigenvectors

$$\boldsymbol{\eta}_1 = \begin{Bmatrix} -0.8943 \\ -0.4472 \end{Bmatrix}, \quad \boldsymbol{\eta}_2 = \begin{Bmatrix} 0.3914 \\ -0.9201 \end{Bmatrix} . \quad (6.52)$$

From Eq. (6.27), we can write the general solution as a linear combination of eigen-solutions,

$$\delta \mathbf{v}(t) = a_1 e^{-0.4716 t} \begin{Bmatrix} -0.8943 \\ -0.4472 \end{Bmatrix} + a_2 e^{0.0039 t} \begin{Bmatrix} 0.3914 \\ -0.9201 \end{Bmatrix} . \quad (6.53)$$

Finally, we can find  $a_1$  and  $a_2$  in order to satisfy the initial condition on  $\delta \dot{v}_1(0) > 0$  and  $\delta \dot{v}_2(0) < 0$ . At  $t = 0$ , Eq. (6.31) becomes

$$\begin{aligned} \delta \dot{v}_1(0) &= 0.4218 a_1 + 0.0015 a_2 > 0, \\ \delta \dot{v}_2(0) &= 0.2109 a_1 - 0.0036 a_2 < 0. \end{aligned} \quad (6.54)$$

Two inequalities in Eq. (6.54) constrains the feasible region for  $a_1$  and  $a_2$ , as shown in Fig. 6.5.

As time evolves, the disturbances  $\delta v_1$  and  $\delta v_2$  grow exponentially due to positive  $\lambda_2 (= 0.0039)$  until the normal pressure at node 2 from Eq. (6.33) becomes zero. At this time, the state changes from backward slip to separation at node 2, maintaining forward slip at node 1. Therefore, we need again to set up equations that satisfy the conditions on forward slip at node 1 ( $q_1 = -fp_1$  and  $\delta \dot{w}_1 = \delta w_1 = 0$ ) and separation at node 2 ( $q_2 = p_2 = 0$ ).

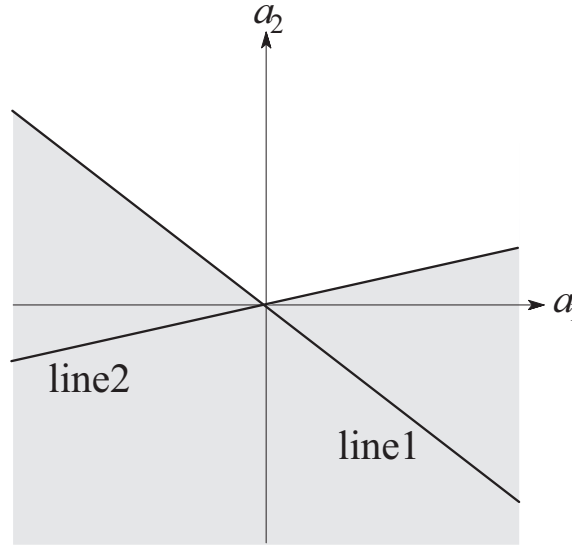


Figure 6.5: The admissible regions for  $a_1$  and  $a_2$  that satisfy initial conditions.

From Eq. (6.39), the system equations are written in matrix form as

$$\delta \dot{\mathbf{x}} + \begin{bmatrix} 0.3881/D_{11} & 0.1668/D_{11} & -0.0525/D_{11} \\ 0.1754/D_{22} & 0.1216/D_{22} & 0.1082/D_{22} \\ -0.0530/D_{44} & 0.1082/D_{44} & 0.5522/D_{44} \end{bmatrix} \delta \mathbf{x} = \begin{Bmatrix} 0 \\ -2.1236/D_{22} \\ -5.4453/D_{44} \end{Bmatrix}. \quad (6.55)$$

where entries of the damping coefficient are set at symbol. If we set the damping coefficient at 1, we can find eigenvalues from the characteristic equation,

$$\lambda_1 = -0.0112, \quad \lambda_2 = -0.4718, \quad \lambda_3 = -0.5790. \quad (6.56)$$

Note that since all eigenvalues are negative, the homogeneous solution,  $g_H$ , as in Eq. (6.42) becomes zero regardless of initial conditions as  $t \rightarrow \infty$ . Hence, the general solution,  $\mathbf{g}$ , is determined by only the particular solution,  $\mathbf{g}_P$ ,

$$\mathbf{g}_P = \begin{bmatrix} 0.3881/D_{11} & 0.1668/D_{11} & -0.0525/D_{11} \\ 0.1754/D_{22} & 0.1216/D_{22} & 0.1082/D_{22} \\ -0.0530/D_{44} & 0.1082/D_{44} & 0.5522/D_{44} \end{bmatrix}^{-1} \begin{Bmatrix} 0 \\ -2.1236/D_{22} \\ -5.4453/D_{44} \end{Bmatrix}. \quad (6.57)$$

By expanding the inverse matrix, the matrix can be written as

$$\mathbf{g}_P = \begin{bmatrix} 18.05D_{11} & -31.83D_{22} & 7.95D_{44} \\ -33.39D_{11} & 68.85D_{22} & -16.67D_{44} \\ 8.27D_{11} & -16.55D_{22} & 5.84D_{44} \end{bmatrix} \begin{Bmatrix} 0 \\ -2.1236/D_{22} \\ -5.4453/D_{44} \end{Bmatrix}. \quad (6.58)$$

From Eq. (6.58), we can conclude that the damping matrix does not influence on the final result since the corresponding damping coefficients are canceled out. Further, as  $t \rightarrow \infty$ , the final perturbations from Eq. (6.58) are

$$[\delta v_1, \delta v_2, \delta w_2]^T = [24.27, -55.42, 3.33]^T. \quad (6.59)$$

From Eq. (6.36), we can restore the final end points,

$$[v_1, v_2, w_2]^T = [v_1^* + \delta v_1, v_2^* + \delta v_2, \delta w_2]^T = [3.5459, -24.5192, 3.33]^T. \quad (6.60)$$

## 6.5 Conclusions

This investigation is to use the dynamic analysis to determine the real behavior of the system in the hope of defining a new quasi-static algorithm that captures the important features of the system trajectory in cases where the loading rate is slow in comparison with the time scale of dynamic effect. We examine whether a small perturbation on this discontinuity point can grow or not, and the system shows unstable behavior on the point. Thus, a discontinuous transition from slip to separation is the only possible solution. By tracking the dynamic trajectory satisfying the states imposed by the Coulomb friction law, we can reach the unique final state. As a result, we find that the final state is not affected by the damping coefficients because these are canceled out at the final state. We also find that the final state is determined by particular values at the discontinuity point. Therefore, it is possible for us to define the unique final state of the system without involving the transient dynamic analysis.

## CHAPTER VII

# Conclusions and Future Work

### 7.1 Conclusions

In this study, the response of frictional coupled contact problems to cyclic loading, which is governed by the Coulomb friction law, is investigated.

A time incremental algorithm, which is capable of tracking the behavior of any two-dimensional system with frictional interfaces, is devised in order to explore the response of such problems to cyclic loading. As a test example, we first consider the receding contact problem, in which a rectangular elastic body is pressed against a rigid plane by both mean and superposed oscillating loads exerted over a central strip of the upper surface. The results show that the slip and separation zones remain unchanged throughout the first loading phase, but thereafter all the zone boundaries vary during both loading and unloading periods. Therefore, Dundurs' results for receding contact problems can be extended to problems involving Coulomb's friction only as long as the loading is monotonic. The system also exhibits some degree of shakedown in the sense that the energy dissipation decreases monotonically toward a steady-state limit with each successive cycle.

A series of simulations is also performed to investigate the possible extension of Melan's theorem to frictional contacts governed by the Coulomb friction law. The previous results have established that Melan's theorem can be applied to discrete elastic systems only when

the normal contact reactions are uncoupled from the tangential slip displacements. For coupled systems, periodic loading scenarios can be devised that lead to either shakedown or cyclic slip depending on the initial condition. To gain more insight into their behavior, we explore this issue in the simplest coupled system, which involves two contact nodes. By plotting the evolution of the system on a diagram with the slip displacements at the two nodes as coordinates, we can track the evolution of the system memory graphically in slip-displacement space. The frictional inequalities define directional straight line constraints in this space that tend to sweep the operating point toward the safe shakedown condition if one exists. However, if the safe shakedown region is defined by a triangle in which two adjacent sides correspond to the extremal positions of the two frictional constraints for the same node, initial conditions leading to cyclic slip can be found. The critical value of a loading parameter at which this occurs can be determined by requiring that three of the four constraint lines intersect in a point. Below this value, shakedown occurs for all initial conditions. Also, the behavior of the system in the intermediate range, where the initial conditions are important, has been elucidated.

A similar strategy can be extended to multi-node discrete frictional systems. In the multi-node contact node system, all critical values can be obtained by solving a subset of all constraints as equalities for all values of slip displacements and loading factor, which requires that all constraint planes intersect at a point. Using this methodology, we devise the general technique for determining all the possible critical loading factors and find the lower limit among them. As the loading factor is increased, the shape of the safe shakedown region will change at each of these critical values, and one of them will correspond to the upper shakedown limit, above which the system will not shake down. However, we cannot distinguish the upper limit without checking all these values obtained from the automated procedure. To solve this difficulty, we propose a linear programming method

because constraints comprising of both loading factor and unique slip displacements are linear. The method is to maximize the loading factor with the unique vector of slip displacements that place a loading loop at each node inside the stick sector. Using the automated procedure and the linear programming method, we can determine the upper and lower limits for the system to shake down.

Finally, we study an analytical method to predict friction-induced instability in the context of a two-node system. For the case where two-node discontinuity occurs, Coulomb friction conditions may fail to define a unique solution for quasi-static evolution algorithm. In an attempt to resolve this problem, we consider an elasto-dynamic formulation by introducing the effect of viscous damping. This investigation is to use the dynamic analysis to determine the real behavior of the system in the hope of defining a new quasi-static algorithm that captures the important features of the system trajectory in cases where the loading rate is slow in comparison with the time scale of dynamic effect. We examine whether a small perturbation on this discontinuity point can grow or not, and the system shows unstable behavior on the point. Thus, a discontinuous transition from slip to separation is the only possible solution. By tracking the dynamic trajectory satisfying the states imposed by the Coulomb friction law, we can reach the unique final state. As a result, we find that the final state is not affected by the damping coefficients because these are canceled out at the final state. We also find that the final state is determined by particular values at the discontinuity point. Therefore, it is possible for us to define the unique final state of the system without involving the transient dynamic analysis.

## 7.2 Future Work

### 7.2.1 Final State Prediction in Multi-node system

In the coupled two-node system discussed in Chapter IV, the safe shakedown region is defined by a triangle for any loading factor  $\lambda$  between  $\lambda^{\min}$  and  $\lambda^{\max}$ . The results showed that the initial feasible region is divided by the vertical line passing through the common apex of two triangles, and only initial values located within one side of the feasible region reached the safe shakedown region. In contrast, for any initial conditions in the other side, the system showed the limit cycle. In this case, one node was stuck throughout the limit cycle so that the locked-in slip displacement influenced the normal tractions at each point in the loading cycle at the other node, and hence affected the amplitude of slip displacement at the other node. Therefore, depending on the initial conditions, the system may shake down or reach a limit cycle for the two-node system.

Using these findings, if we can establish how these criteria might translate to more than a coupled two-node system, we can predict the final states in coupled multi-node systems.

### 7.2.2 Uniqueness of the Limit Cycle

One parameter which is of interest in the analysis of fretting fatigue is the frictional energy dissipated in relative slip at the interface during cyclic slip, since fretting damage and wear highly correlated with the fretting fatigue.

When a system shakes down, the energy dissipation in friction per cycle goes to zero. Therefore, Melan's theorem states that this will happen if it can. This suggests that such slip will tend to reduce the energy dissipation in subsequent cycles.

For cases above the shakedown limit — i.e., where the safe shakedown region is null - we find that the system converges on a limit cycle if there is a time in the cycle when both nodes of a two-node system are slipping. This situation generalizes to a  $n$ -nodes system

if the limit cycle involves a permanent stick zone comprising  $m$  nodes, and there is a time during the cycle when  $n - m$  are all slipping. Therefore, if the system is coupled, and no nodes are permanently stuck, and if they are not all slipping at any one time, it seems likely that the system will evolve to a unique limit cycle after an infinite number of cycles. If this prediction is true for an  $n$ -node system, we can identify the frictional energy dissipation. Therefore, it is worthwhile to investigate whether there is only one true limit cycle.

## **APPENDIX**

## APPENDIX A

### Stick-Slip-Separation Behavior in One Point Model

This model was first introduced by Klarbring (1990) to illustrate the problems of uniqueness and existence that arise in frictional contact problems when the coefficient of friction is sufficiently high. Its model also helps us to understand the frictional behaviors such as stick, slip and separation.

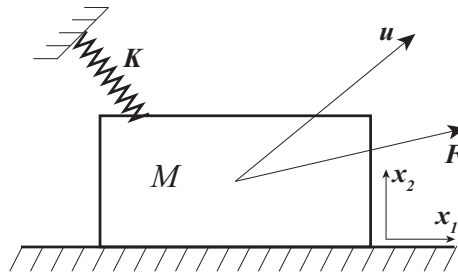


Figure A.1: The one-point model

The mass  $M$  is supported by a spring  $K$  and loaded by a force  $F$  with components  $F_1, F_2$  in direction  $x_1$  (tangential) and  $x_2$  (normal, tensile positive). The mass can make contact with a rigid plane surface under conditions of Coulomb friction with coefficient  $f$ , in which case the reaction  $R$  has components  $R_1, R_2$ . The displacement of the mass is denoted by  $u$  with components  $u_1, u_2$  and the spring is not stretched when  $u = 0$ , at which point the mass is in contact with the surface.

(a) *Possible states*

The four possible states of the system at any given time are stick, forward slip, backward slip and separation. The governing equations and inequalities for these states are

$$\begin{aligned}
 \textit{stick} & : \dot{u}_1 = 0; \quad u_2 = 0; \quad R_2 > 0; \quad -fR_2 < R_1 < fR_2. \\
 \textit{Forwardslip} & : \dot{u}_1 > 0; \quad u_2 = 0; \quad R_2 > 0; \quad R_1 = -fR_2. \\
 \textit{Backwardslip} & : \dot{u}_1 < 0; \quad u_2 = 0; \quad R_2 > 0; \quad R_1 = fR_2. \\
 \textit{Separation} & : u_2 > 0; \quad R_2 = 0; \quad R_1 = 0.
 \end{aligned} \tag{A.1}$$

Under quasi-static conditions, the mass is in equilibrium at all times and hence

$$\begin{aligned}
 F_1 + R_1 - k_{11}u_1 - k_{12}u_2 &= 0; \\
 F_2 + R_2 - k_{21}u_1 - k_{22}u_2 &= 0,
 \end{aligned} \tag{A.2}$$

where  $k_{ij}, i = 1, 2$  are the components of the stiffness matrix  $\mathbf{K}$ .

If the system is at rest, the only possibilities are stick and separation. For stick we have  $u_2 = 0$ . Using this condition in Eq. (A.2), solving for  $R_1, R_2$  and substituting in stick condition of Eq. (A.1), we find that stick is possible if and only if

$$(k_{11} + fk_{21})u_1 - fF_2 > F_1 > (k_{11} - fk_{21})u_1 + fF_2. \tag{A.3}$$

For separation,  $R_1 = R_2 = 0$ . Using this result in Eq. (A.2), solving for  $u_2$  and substituting into the inequality  $u_2 > 0$ , we find that separation is possible if and only if

$$F_1k_{21} - F_2k_{11} < 0, \tag{A.4}$$

where we have used the fact that the stiffness matrix  $\mathbf{K}$  must be positive definite and hence  $k_{22}k_{11} > k_{12}k_{21}$ .

(b) *The  $F_1 - F_2$  diagram*

The instantaneous state of the quasi-static system can be represented on a diagram with axes  $F_1, F_2$ . The applied load identifies a point on this diagram, so a given loading scenario identifies a continuous curve. For the case of mean load and superposed oscillation, this will comprise an initial segment followed by a closed curve. If we plot the

static inequalities on a diagram with axes  $F_1, F_2$  and assume (without loss of generality) that  $k_{12} = k_{21} > 0$ , we obtain the domains shown in Fig. A.2. Separation is possible only in the shaded region above the straight line  $k_{21}F_1 = k_{11}F_2$  and stick is possible in the sector beneath it. The two straight lines defining this sector always intersect on the the line  $k_{21}F_1 = k_{11}F_2$  and always have slope  $\pm 1/f$ , but the location of the vertex moves along the separation line as  $u_1$  varies.

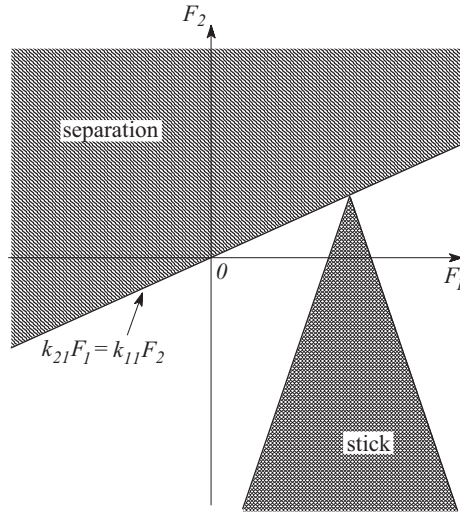


Figure A.2: The  $F_1 - F_2$  diagram

For given constant values of  $F_1, F_2$  below the separation line,  $u_1$  can adopt any value that causes the resulting point to lie within the stick sector. Fig. A.2 is plotted for the case where  $f < k_{11}/k_{21} \equiv f_{cr}$ , so there are no conditions under which both stick and separation are possible. We will consider the alternative possibility later.

(c) *Slip*

During slip, we still have  $u_2 = 0$ , so the quasi-static Eq. (A.2) take the form

$$\begin{aligned} F_1 + R_1 - k_{11}u_1 &= 0; \\ F_2 + R_2 - k_{21}u_1 &= 0, \end{aligned} \tag{A.5}$$

To impose the slip direction inequalities, we differentiate with respect to time, obtaining

$$\begin{aligned}\dot{F}_1 + \dot{R}_1 - k_{11}\dot{u}_1 &= 0; \\ \dot{F}_2 + \dot{R}_2 - k_{21}\dot{u}_1 &= 0,\end{aligned}\tag{A.6}$$

For forward slip  $R_1 = -fR_2$  and hence  $\dot{R}_1 = -f\dot{R}_2$ . Using this result in Eq. (A.6) and eliminating  $\dot{R}_2$  between the resulting equations, we then have

$$(k_{11} + fk_{21})\dot{u}_1 = f\dot{F}_2 + \dot{F}_1,\tag{A.7}$$

The forward slip inequality is therefore satisfied if  $\dot{F}_1 > -f\dot{F}_2$ . This defines the incremental loading directions indicated in Fig. (), where we attempt to cross the right hand boundary of the instantaneous stick sector. The resulting slip will lead to increasing  $u_1$  and hence will move the stick sector to the right in Fig. A.3. In effect, the sector is dragged by the operating point whenever an attempt is made to move out of the stick sector in the region below the separation line.

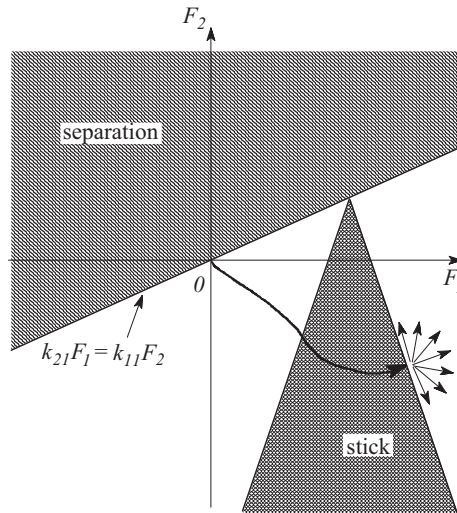


Figure A.3: Loading scenario leading to forward slip

An exactly similar analysis can be performed for backward slip and leads to the same conclusion, i.e., attempts to cross the left hand boundary of the stick sector causes negative displacement  $u_1$  and moves the stick sector so that the operating point remains on the left

boundary. We also note that if the operating point crosses the separation boundary and later crosses it again to re-enter the contact domain, the stick sector will initiate such that its apex is at the point where contact is re-established.

(d) *Oscillatory loading and shakedown*

It is then clear that a scenario leading to shakedown will look like Fig. A.4. The stick sector will move until it is just tangential to the closed curve describing the oscillatory loading on the side furthest from the origin. Shakedown then occurs if the rest of the curve lies completely within the stick sector so defined. It is also clear from this construction that shakedown will occur if and only if there exists a location for the stick sector that includes the entire closed part of the curve. Thus, Melan's theorem holds for the two-dimensional one-point model when  $f < k_{11}/k_{12}$ .

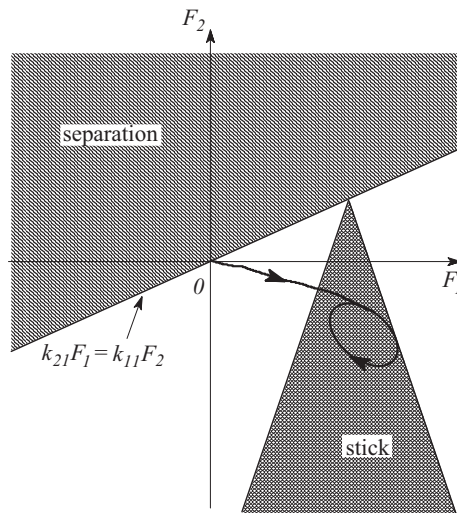


Figure A.4: Loading scenario leading to shakedown

(e) *Above the critical friction coefficient*

We now turn attention to the high friction case, where  $f > k_{11}/k_{21}$ . In this case, the domains for separation and stick take the form of Fig. A.5 and there is an overlap zone in

which both separation and stick are both possible. We know from previous studies that in this overlapping zone, the inequalities for backward slip are also satisfied under conditions of increasing load with constant direction.

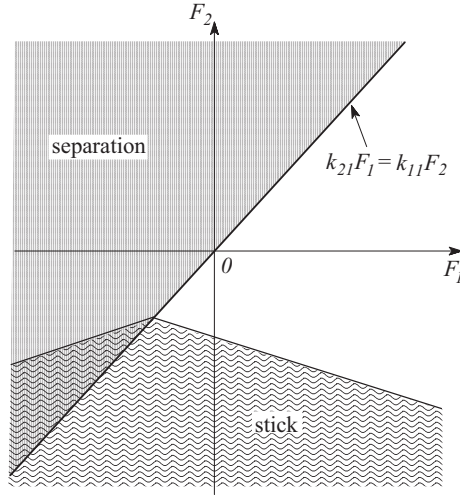


Figure A.5:  $F_1 - F_2$  diagram for  $f > f_{cr}$

An immediate conclusion from this diagram is that a state of residual stress can always be found sufficient to permit stick for any oscillatory loading scenario. If we construct any closed curve on the diagram, it can be contained within the stick sector provided we move the apex of the sector sufficiently far up the separation line. Thus, if a frictional Melan's theorem were to apply to this system, it would have to follow that the system would shake down under all conceivable oscillatory loading scenarios. This is clearly not the case however, as we will demonstrate.

(f) *Incipient slip*

Suppose we reconsider the situation when we approach the edge of the stick sector. Eq. A.5 still hold, as do Eq. A.6 and as before we eventually obtain

$$(k_{11} + f k_{21})\dot{u}_1 = f \dot{F}_2 + \dot{F}_1, \quad (\text{A.8})$$

for forward slip and by a similar argument

$$(k_{11} - fk_{21})\dot{u}_1 = -f\dot{F}_2 + \dot{F}_1, \quad (\text{A.9})$$

for backward slip.

We assume that  $k_{21} > 0$  as is implied by the slope of the separation line in in Fig. A.5, so  $k_{11} - fk_{21} > 0$  and the criterion for forward slip is the same as for  $f < f_{cr}$ . In other words, when we try to cross the right edge of the stick sector, the effect is to slip to the right, increase  $u_1$  and hence move the stick sector to the right.

However, for backward slip, we now have

$$k_{11} - fk_{21} < 0 \quad (\text{A.10})$$

and hence the backward slip criterion in Eq. A.1 requires that

$$\dot{F}_1 > f\dot{F}_2. \quad (\text{A.11})$$

This defines the directions into the stick sector rather than away from it in Fig. A.5. Thus, the system cannot back-slip when the operating point reaches the left edge of the stick sector. It also cannot remain stuck. Previous investigations suggest that it will experience a dynamic transition involving a period of separation. In particular, Cho and Barber (1998) examine the lightly damped dynamic solution under a range of conditions and develop a modified quasi-static algorithm that captures the behavior of the system in the limit where the time constant of the system becomes vanishingly small (e.g. in the limit  $M \rightarrow 0$ ). They show (in Appendix B) that any attempt to cross the boundary  $F_1 = fF_2 < 0$  from the right will cause a transition from stick to separation in which the reaction and the displacement are discontinuous. In other words, the system jumps to the separation state implied by the same point in the  $F_1 - F_2$  diagram, which involves a non-zero positive value of  $u_2$ . At the reverse transition, when the loading point again crosses the separation

line and  $u_2 \rightarrow 0$ , the system transitions either to stick or to forward slip, depending on the derivative  $dF_1/dF_2$ . To illustrate the implications for shakedown, we examine two scenarios according to this algorithm.

(i) Separation-stick cycle

Fig. A.6 shows a loading scenario that involves periods of stick and separation. We start with  $u_1 = 0$ , so the stick boundary is defined by the two dotted lines emanating from the origin. Stick persists until the loading point crosses the left boundary of the stick sector at A, at which there is a discontinuous jump to separation at finite  $u_2$ . Separation persists until B, where the transition is to stick, with a new stick sector defined by the solid lines. This time, separation occurs at C where the new stick sector is crossed, but subsequently there is no change in the location of the stick boundary and the process becomes a cyclic alternation of stick and separation.

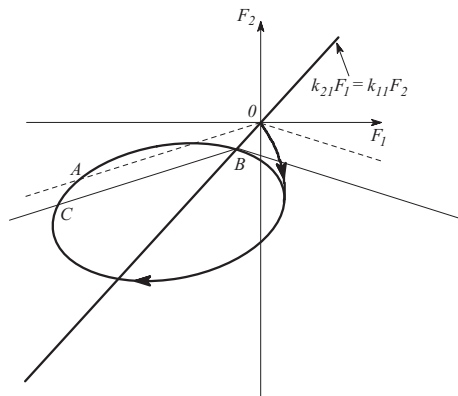


Figure A.6: Separation-stick cycle

(ii) Cyclic slip

Fig. A.7 shows a loading scenario where the system passes through periods of stick, separation and forward slip. Stick persists until point A, where there is a discontinuous transition to separation. Separation then persists until B, where contact is established with

the stick sector defined by the dotted lines. However, the loading trajectory at this point is directed into the forward slip region, so the stick sector is pushed up the separation line until the tangent point C is reached, with the sector defined by the solid lines. Stick starts at C and persists to D where there is a discontinuous transition to separation. Finally, contact is re-established at B and the cycle repeats.

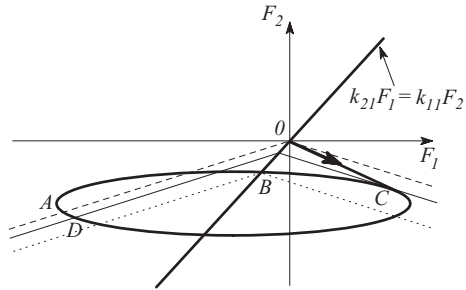


Figure A.7: Cyclic slip scenario

## **BIBLIOGRAPHY**

## BIBLIOGRAPHY

- [1] G. G. Adams. Self-excited oscillations in sliding with a constant friction coefficient — a simple model. *Transactions of the ASME. Journal of Tribology*, 118(4):819–23, 1996.
- [2] L. E. Andersson. Private communication. 2008.
- [3] L. E. Andersson and A. Klarbring. A review of the theory of static and quasi-static frictional contact problems in elasticity. *Philosophical Transactions of the Royal Society London, Series A (Mathematical, Physical and Engineering Sciences)*, 359(1789):2519–39, 2001.
- [4] N. Antoni, Q. S. Nguyen, J. L. Ligier, P. Saffre, and J. Pastor. On the cumulative microslip phenomenon. *European Journal of Mechanics, A/Solids*, 26(4):626–46, 2007.
- [5] K.E. Atkinson. *An introduction to numerical analysis*. Wiley, New York, 2nd edition, 1989.
- [6] J. R. Barber, A. Klarbring, and M. Ciavarella. Shakedown in frictional contact problems. volume PART A of *2007 Proceedings of the ASME/STLE International Joint Tribology Conference, IJTC 2007*, pages 517–519, San Diego, CA, United States, 2008. American Society of Mechanical Engineers, New York, NY 10016-5990, United States.
- [7] J.R. Barber. *Elasticity*. Kluwer, Dordrecht, 2002.
- [8] J.R. Barber and P. Hild. *On wedged configurations with Coulomb friction*. in Peter Wriggers and Udo Nackenhorst, eds., *Analysis and Simulation of Contact Problems*. Springer-Verlag, Berlin, 1985.
- [9] S. Berczynski and P. Gutowski. Identification of the dynamic models of machine tool supporting systems. part i: an algorithm of the method. *Journal of Vibration and Control*, 12(3):257–77, 2006.
- [10] A. Birinci and R. Erdol. Continuous and discontinuous contact problem for a layered composite resting on simple supports. *Structural Engineering and Mechanics*, 12(1):17–34, 2001.

- [11] G. Björkman and A. Klarbring. Shakedown and residual stresses in frictional systems. *Contact Mechanics and Wear of Rail/Wheel Systems II: Proceedings of the 2nd International Symposium*, pages 27–39, 1987.
- [12] J. Bree. Elastic-plastic behaviour of thin tubes subjected to internal pressure and intermittent high-heat fluxes with application to fast-nuclear-reactor fuel elements. *Journal of Strain Analysis*, 2(3):226–238, 1967.
- [13] L. Bureau, C. Caroli, and T. Baumberger. Elasticity and onset of frictional dissipation at a nonsliding multicontact interface. *Proceedings of the Royal Society of London, Series A (Mathematical, Physical and Engineering Sciences)*, 459(2039):2787–805, 2003.
- [14] C. Cattaneo. Sul contatto di due corpi elastici: distribuzione locale degli sforzi. *Rendiconti dell'Accademia Nazionale dei Lincei*, 27, 1938.
- [15] S. K. Chan and I. S. Tuba. A finite element method for contact problems of solid bodies. ii. application to turbine blade fastenings. *International Journal of Mechanical Sciences*, 13(7):627–39, 1971.
- [16] H. Cho and J. R. Barber. Dynamic behavior and stability of simple frictional systems. *Mathematical and Computer Modelling*, 28(4-8):37–53, 1998.
- [17] C. M. Churchman, A. M. Korsunsky, and D. A. Hills. The application of plasticity principles to friction. *Journal of Strain Analysis for Engineering Design*, 41(4):323–8, 2006.
- [18] M. Ciavarella. The generalized cattaneo partial slip plane contact problem. i. theory. *International Journal of Solids and Structures*, 35(18):2349–62, 1998.
- [19] M. Ciavarella. The generalized cattaneo partial slip plane contact problem. ii. examples. *International Journal of Solids and Structures*, 35(18):2363–78, 1998.
- [20] M. Ciavarella, A. Baldini, J. R. Barber, and A. Strozzi. Reduced dependence on loading parameters in almost conforming contacts. *International Journal of Mechanical Sciences*, 48(9):917–25, 2006.
- [21] M. Ciavarella and P. Decuzzi. The state of stress induced by the plane frictionless cylindrical contact. ii. the general case (elastic dissimilarity). *International Journal of Solids and Structures*, 38(26-27):4525–4533, 2001.
- [22] M. Ciavarella and D. A. Hills. Some observations on oscillating tangential forces and wear in general plane contacts. *European Journal of Mechanics, A/Solids*, 18(3):491–7, 1999.
- [23] M. B. Civelek and F. Erdogan. The axisymmetric double contact problem for a frictionless elastic layer. *International Journal of Solids and Structures*, 10(6):639–59, 1974.

- [24] E.G. Coker and L.N.G. Filon. *Treatise on photo-elasticity*. Cambridge University Press, 1957.
- [25] I. Comez, A. Birinci, and R. Erdol. Double receding contact problem for a rigid stamp and two elastic layers. *European Journal of Mechanics, A/Solids*, 23(2):301–309, 2004.
- [26] M. Comninou and J. Dundurs. Educational elasticity problem with friction-part ii: Unloading for strong friction and reloading. *ASME Journal of applied mechanics*, pages 47–51, 1982.
- [27] Maria Comninou and J. R. Barber. Frictional slip between a layer and a substrate due to a periodic tangential surface force. *International Journal of Solids and Structures*, 19(6):533–539, 1983.
- [28] C.A. Coulomb. The theory of simple machines (in french). *Mem. Math. Phys. Acad. Sci.*, 10:161–331, 1785.
- [29] J. S. Courtney-Pratt and E. Eisner. The effect of a tangential force on the contact of metallic bodies. *Proceedings of the Royal Society of London*, 238-A:529–550, 1957.
- [30] D. Dini and D. A. Hills. Unsymmetrical shear loading and its influence on the frictional shakedown of incomplete contacts. *Proceedings of the Institution of Mechanical Engineers, Part C (Journal of Mechanical Engineering Science)*, 218(C5):469–75, 2004.
- [31] J. Dundurs. Discussion on 'edge bonded dissimilar orthogonal elastic wedges under normal and shear loading. *Transactions of the ASME. Journal of Applied Mechanics*, 36:650–652., 1969.
- [32] J. Dundurs. Properties of elastic bodies in contact. *Modeling and Simulation, Proceedings of the Annual Pittsburgh Conference*, pages 54–66, 1975.
- [33] J. Dundurs and M. Comninou. Educational elasticity problem with friction - part i: Loading, and unloading for weak friction. *ASME, Journal of applied mechanics*, 48:841–845, 1981.
- [34] J. Dundurs and M. Comninou. Educational elasticity problem with friction - 3. general load paths. *Journal of Applied Mechanics, Transactions ASME*, 50(1):77–84, 1983.
- [35] J. Dundurs and M. Stippes. Role of elastic constants in certain contact problems. *Transactions of the ASME. Series E, Journal of Applied Mechanics*, 37(4):965–70, 1970.
- [36] S. El-Borgi, R. Abdelmoula, and L. Keer. A receding contact plane problem between a functionally graded layer and a homogeneous substrate. *International Journal of Solids and Structures*, 43(3-4):658–674, 2006.

- [37] L. N. G. Filon. Approximate solution for the bending of a beam of rectangular cross-section under any system of load. additional note. *Proceedings of the Royal Society of London*, 72:391–393, 1903.
- [38] B. Fredriksson and G. Rydholm. Shakedown in frictional system - some considerations in g. rydholm, on inequalities and shakedown in contact problems. *Diss. No. 61, Linköping Studies in Science and Technology*, pages F1–F21, 1981.
- [39] J. A. Garrido, A. Foces, and F. Paris. Bem applied to receding contact problem with friction. *Mathematical and Computer Modelling*, 15:143–154, 1994.
- [40] J. A. Garrido and A. Lorenzana. Receding contact problem involving large displacements using the bem. *Engineering Analysis with Boundary Elements*, 21(4):295–303, 1998.
- [41] M. R. Gecit. The axisymmetric double contact problem for a frictionless elastic layer indented by an elastic cylinder. *International Journal of Engineering Science*, 24(9):1571–84, 1986.
- [42] G. M. L. Gladwell. On some unbonded contact problems in plane elasticity theory. *Transactions of the ASME. Series E, Journal of Applied Mechanics*, 43(2):263–7, 1976.
- [43] L. E. Goodman and C. B. Brown. Energy dissipation in contact friction: constant normal and cyclic tangential loading. *Journal of Applied Mechanics, Transactions ASME*, 29:17–22, 1962.
- [44] L. E. Goodman and L.M. Keer. The contact stress problem for an elastic sphere indenting an elastic cavity. *International Journal of Solids and Structures*, 1:407–415, 1965.
- [45] M. T. Hanson, L. M. Keer, and T. N. Farris. Energy dissipation in non-hertzian fretting contact. *Tribology Transactions*, 32(2):147–154, 1989.
- [46] R. Hassani, P. Hild, I. R. Ionescu, and N. D. Sakki. A mixed finite element method and solution multiplicity for coulomb frictional contact. *Computer Methods in Applied Mechanics and Engineering*, 192(41-42):4517–31, 2003.
- [47] H. Hertz. Über die berührung fester elastischer köper. *Journal für die Reine und Angewandte Mathematik*, 29:156–171, 1882.
- [48] D. A. Hills and D. Nowell. *Mechanics of fretting fatigue*. Kluwer, Dordrecht, 1994.
- [49] D. A. Hills, D. Nowell, and A. Sackfield. *Mechanics of elastic contacts*. Butterworth-Heinemann Boston, 1993.
- [50] Kelly P.A. Dai D.N. Hills, D.A. and A.M. Korsunsky. Solution of crack problems — the distributed dislocation technique. *Kluwer Academic Publishers, Dordrecht, The Netherlands*, page §3.1.5., 1996.

- [51] R. M. Holt, J. Kjolaas, I. Larsen, L. Li, A. Gotusso Pillitteri, and E. F. Sonstebo. Comparison between controlled laboratory experiments and discrete particle simulations of the mechanical behaviour of rock. *International Journal of Rock Mechanics and Mining Sciences*, 42(7-8 SPEC ISS):985–995, 2005.
- [52] J. P. Hou and D. A. Hills. The effect of friction on a receding conformal contact. *Proceedings of the Institution of Mechanical Engineers, Part C: Journal of Mechanical Engineering Science*, 216(3):337–342, 2002.
- [53] J. Jäger. Half-planes without coupling under contact loading. *Archive of applied mechanics*, 67(4):247–259, 1997.
- [54] H. S. Jing and M. L. Liao. An improved finite element scheme for elastic contact problems with friction. *Computers and Structures*, 35(5):571–8, 1990.
- [55] K. L. Johnson. Surface interaction between elastically loaded bodies under tangential forces. *Proceedings of the Royal Society of London*, A230:531–548, 1955.
- [56] K. L. Johnson. Energy dissipation at spherical surfaces in contact transmitting oscillating forces. *Journal of Mechanical Engineering Science*, 3(4):362–368, 1961.
- [57] K. L. Johnson. *Contact mechanics*. Cambridge University Press, Cambridge [Cambridgeshire]; New York, 1985.
- [58] V. Kahya, T. S. Ozsahin, A. Birinci, and R. Erdol. A receding contact problem for an anisotropic elastic medium consisting of a layer and a half plane. *International Journal of Solids and Structures*, 44(17):5695–5710, 2007.
- [59] S. Karuppanan and D. A. Hills. Frictional complete contacts between elastically similar bodies subject to normal and shear load. *International Journal of Solids and Structures*, 45(17):4662–75, 2008.
- [60] J. J. Kauzlarich and J. A. Greenwood. Contact between a centrally loaded plate and a rigid or elastic base, with application to pivoted pad bearings. *Proceedings of the Institution of Mechanical Engineers, Part C: Journal of Mechanical Engineering Science*, 215(6):623–628, 2001.
- [61] L. M. Keer, N. Ahmadi, and T. Mura. Tangential loading of elastic bodies in contact. *Computers and Structures*, 19(1-2):93–101, 1984.
- [62] L. M. Keer, J. Dundurs, and K. C. Tsai. Problems involving a receding contact between a layer and a half space. *Transactions of the ASME. Series E, Journal of Applied Mechanics*, 39(4):1115–20, 1972.
- [63] L. M. Keer and T. N. Farris. Effects of finite thickness and tangential loading on development of zones of microslip in fretting. *ASLE Transactions*, 30(2):203–210, 1987.

- [64] A. Klarbring. Examples of non-uniqueness and non-existence of solutions to quasistatic contact problems with friction. *Ingenieur-Archiv*, 60(8):529–541, 1990.
- [65] A. Klarbring, M. Ciavarella, and J. R. Barber. Shakedown in elastic contact problems with coulomb friction. *International Journal of Solids and Structures*, 44(25-26):8355–8365, 2007.
- [66] S. S. Law, Z. M. Wu, and S. L. Chan. Analytical model of a slotted bolted connection element and its behaviour under dynamic load. *Journal of Sound and Vibration*, 292(3-5):777–787, 2006.
- [67] K. C. Leurer and J. Dvorkin. Viscoelasticity of precompacted unconsolidated sand with viscous cement. *Geophysics*, 71(2):31–40, 2006.
- [68] N. R. Lovrich and Rick W. Neu. Effect of mean stress on fretting fatigue of ti-6al-4v on ti-6al-4v. *Fatigue and Fracture of Engineering Materials and Structures*, 29(1):41–55, 2006.
- [69] G. Maier. Shakedown theory in perfect elastoplasticity with associated and nonassociated flow-laws: A finite element, linear programming approach. *Meccanica*, 4(3):250–260, 1969.
- [70] J. A. C. Martins, J. Guimaraes, and L. O. Faria. Dynamic surface solutions in linear elasticity and viscoelasticity with frictional boundary conditions. *Journal of Vibration and Acoustics, Transactions of the ASME*, 117(4):445–451, 1995.
- [71] J. A. C. Martins, M. D. P. Monteiro Marques, and F. Gastaldi. On an example of non-existence of solution to a quasistatic frictional contract problem. *European Journal of Mechanics, A/Solids*, 13(1):113–33, 1994.
- [72] E. Melan. Theorie statisch unbestimmter systeme aus ideal-plastischem baustoff. *sitzungsber. d. akad. d. wiss. Wien*, 2A(145):195–218, 1936.
- [73] J.E. Merwin and K. L. Johnson. An analysis of plastic deformation in rolling contact. *Proceedings of the Institution of Mechanical Engineers*, 177:676–690, 1963.
- [74] R. D. Mindlin. Compliance of elastic bodies in contact. *American Society of Mechanical Engineers – Transactions – Journal of Applied Mechanics*, 16(3):259–268, 1949.
- [75] R. D. Mindlin and H. Deresiewicz. Elastic spheres in contact under varying oblique forces. *American Society of Mechanical Engineers – Transactions – Journal of Applied Mechanics*, 20(3):327–344, 1953.
- [76] R. D. Mindlin, W.P. Mason, J.F. Osmer, and H. Deresiewicz. Effects of an oscillating tangential force on the contact surface of elastic spheres. *Proc. 1st US National Congress of Applied Mechanics*, pages 203–208, 1952.

- [77] V.I. Mossakovski. Compression of elastic bodies under conditions of adhesion. *PMM*, 27:418, 1963.
- [78] A. Mostofi and R. Gohar. Pressure distribution between closely contacting surfaces. *Journal of Mechanical Engineering Science*, 22(5):251–259, 1980.
- [79] A. Mugadu, A. Sackfield, and D. A. Hills. Analysis of a rocking and walking punch-part i: initial transient and steady state. *Transactions of the ASME. Journal of Applied Mechanics*, 71(2):225–33, 2004.
- [80] R. L. Munisamy, D. A. Hills, and D. Nowell. Static axisymmetric hertzian contacts subject to shearing forces. *Transactions of the ASME. Journal of Applied Mechanics*, 61(2):278–83, 1994.
- [81] H. Murthy, G. Harish, and T. N. Farris. Efficient modeling of fretting of blade/disk contacts including load history effects. *Transactions of the ASME. Journal of Tribology*, 126(1):56–64, 2004.
- [82] S. Nakamura. *Numerical analysis and graphic visualization with MATLAB*. Prentice Hall PTR, Upper Saddle River, N.J., 1996.
- [83] D. Nowell, D. Dini, and D. A. Hills. Recent developments in the understanding of fretting fatigue. *Engineering Fracture Mechanics*, 73(2):207–22, 2006.
- [84] D. Nowell, D. A. Hills, and A. Sackfield. Contact of dissimilar elastic cylinders under normal and tangential loading. *Journal of the Mechanics and Physics of Solids*, 36(1):59–75, 1988.
- [85] F. Paris, A. Blazquez, and J. Canas. Contact problems with nonconforming discretizations using boundary element method. *Computers and Structures*, 57(5):829–39, 1995.
- [86] A. Persson. *On the stress distribution of cylindrical elastic bodies in contact*. Dissertation, Chalmers Tekniska Hogskola, Goteborg, 1964.
- [87] M. Ratwani and F. Erdogan. On the plane contact problem for a frictionless elastic layer. *International Journal of Solids and Structures*, 9(8):921–36, 1973.
- [88] R. Saez, A. Mugadu, J. Fuenmayor, and D. A. Hills. Frictional shakedown in a complete contact. *Journal of Strain Analysis for Engineering Design*, 38(4):329–338, 2003.
- [89] D. A. Spence. Self similar solutions to adhesive contact problems with incremental loading. *Royal Society of London - Proceedings Series A*, 305(1480):55–80, 1968.
- [90] D. A. Spence. An eigenvalue problem for elastic contact with finite friction. *Proceedings of the Cambridge Philosophical Society*, 73:249–68, 1973.
- [91] D. A. Spence. The hertz contact problem with finite friction. *Journal of Elasticity*, 5(3-4):297–319, 1975.

- [92] D. A. Spence. Frictional contact with transverse shear. *Quarterly Journal of Mechanics and Applied Mathematics*, 39:233–53, 1986.
- [93] M. P. Szolwinski and T. N. Farris. Mechanics of fretting fatigue crack formation. *Wear*, 198(1-2):93–107, 1996.
- [94] K. C. Tsai, J. Dundurs, and L. M. Keer. Elastic layer pressed against a half space. volume 41 of *Trans. ASME, E, J. Appl. Mech. (USA)*, pages 703–7, Boulder, CO, USA, 1974.
- [95] J. R. Turner. The frictional unloading problem on a linear elastic half space. *Journal of the Institute of Mathematics and Its Applications*, 24(4):439–69, 1979.
- [96] J. B. Walsh. A theoretical analysis of sliding of rough surfaces. *Journal of Geophysical Research*, 108(B8):6–1, 2003.
- [97] H. P. Zhang and H. A. Makse. Jamming transition in emulsions and granular materials. *Physical Review E - Statistical, Nonlinear, and Soft Matter Physics*, 72(1):011301, 2005.